

Alma Mater Studiorum – Università di Bologna

Dottorato di Ricerca in

Bioteχνologie, Farmacologia e Tossicologia

Progetto formativo n.2 *“Farmacologia e Tossicologia”*

Ciclo XXV

Settore concorsuale di afferenza: 05/G1

Settore Scientifico disciplinare: BIO/14

***Generation and characterization of mouse models of
Small cell lung cancer and Basal cell carcinoma for the
preclinical evaluation of new therapies***

Presentata da: Margherita Ruocco

Coordinatore Dottorato

Prof. Giorgio Cantelli Forti

Relatore

Dott. Roberto Tonelli

Esame finale Aprile 2013

INDICE

1 INTRODUCTION	4
1.1 Small cell lung cancer	4
1.1.1 Etiopathogenesis and inheritance	5
1.1.2 Diagnosis and Staging	7
1.1.3 Genetics of SCLC	8
1.2 MYCN Gene	11
1.2.1 <i>MYC</i> gene family	11
1.2.2 From MYCN gene to N-Myc protein	12
1.2.3 Role of MYCN in small cell lung cancer	14
1.3 Therapeutic options and chemotherapy	15
1.3.1 Treatment of limited disease	16
1.3.2 Treatment of extensive disease	17
1.3.3 Treatment options for relapsed SCLC	18
1.3.4 Target therapies	19
1.4 Peptide Nucleic Acid	20
1.4.1 Structure and properties	21
1.4.2 PNA anti-gene	21
1.4.3 Therapeutic applications of PNA anti-gene	22
1.5 Chemotherapeutic compounds	22
1.5.1 Alkylating agents	23
1.5.2 Topoisomerasi IIa inhibitor	24
1.6 Hedgehog pathway and Basal Cell Carcinoma	25
1.6.1 Hedgehog signalling pathway	25
1.6.2 Basal cell carcinoma & Gorlin syndrome	27
1.6.3 Ultraviolet radiation and Basal cell carcinoma	29
1.6.4 In vitro model of BCC	29
1.6.5 Role of MYCN in basal cell carcinoma	30
1.6.6 Targeting therapies in BCC	30
1.6.7 EGFR signaling pathway in Basal cell carcinoma	31
1.6.8 Role of HH pathway in SCLC	33
1.7 Murine models	33
1.7.1 Tumor xenograft models	33
1.7.2 Transgenic mouse models	34
1.8 Molecular imaging	37
1.8.1 Transfection of cell lines throughout retroviral vectors	38
2 AIM OF THE STUDY	41
3 MATERIAL AND METHODS	42
3.1 Small cell lung cancer	42
3.1.1 Cell lines	42
3.1.2 RNA isolation and gene expression analysis	44
3.1.3 Protein extraction	45
3.1.4 Western Blot analysis	46
3.1.5 Fluorescence In Situ Hybridization (FISH)	47
3.1.6 In vitro treatment	47
3.1.7 PNA treatment	48
3.1.8 Generation of luciferase-positive SCLC cell lines	49
3.1.9 Establishment orthotopic xenograft models	51

3.1.10 Molecular imaging	52
3.1.11 Treatments and in vivo antitumor efficacy evaluation	52
3.1.12 Statistical Analysis	55
3.1.13 Histology and immunohistochemistry	56
3.2 Basal cell carcinoma	56
3.2.1 NEB1 cell culture	56
3.2.2 Pharmacological inhibitors	56
3.2.3 RNA isolation and gene expression analysis	57
3.2.4 Western Blot	58
3.2.5 Immunocytochemistry	58
3.2.6 Matrigel based organotypic culture	59
3.2.7 Immunohistochemistry	60
3.2.8 PTCH ^{+/-} mice colony	60
4 RESULTS	62
4.1 MYCN characterization in SCLC cell lines	64
4.2 <i>In vitro</i> chemotherapeutic treatments	65
4.3 <i>In vitro</i> anti-MYCN PNA treatment	67
4.4 MYCN-amplified SCLC xenograft orthotopic mice models	67
4.4.1 <i>In vitro</i> validation of bioluminescent signal	68
4.4.2 <i>In vivo</i> bioluminescent imaging	71
4.4.3 Mouse model validation	73
4.4.4 Ex vivo analysis of xenograft orthotopic tumor	75
4.5 <i>In vitro</i> and <i>in vivo</i> modelling of Basal cell carcinoma	75
4.5.1 Creation and characterisation of human keratinocyte cell line with stable PTCH1 suppression	77
4.5.2 Characterisation of Hedgehog signalling components in NEB1-shPTCH1 cells	
4.5.3 Non-canonical GLI1 signalling in NEB1-shPTCH1 cells	79
4.5.3 Functional studies of NEB1-shPTCH1 cells	81
4.5.4 EGFR signalling in NEB1-shPTCH1 cells	81
4.5.5 EGFR signalling and control of GLI expression in shPTCH1 cells	
4.6 EGFR signalling pathway in human and murine BCCs	87
5 DISCUSSION	90
6 REFERENCES	100

CHAPTER 1 INTRODUCTION

1.1 Small cell lung cancer

Human small-cell lung carcinoma (SCLC), accounting for approximately 15-20% of all lung cancers, is an aggressive tumor with a high propensity for early regional and distant metastases. Chemotherapy is the primary treatment option for patients with SCLC, leading to a 5 year survival of approximately 20% in limited disease (LD) and less than 5% in extensive disease (ED). Although the initial response rate to chemotherapy is very high (up to 96% for LD and up to 65% for ED), SCLC relapses after approximately 4 months in ED and 12 months in LD (Figure 1). [Govindan R. et al 2006].

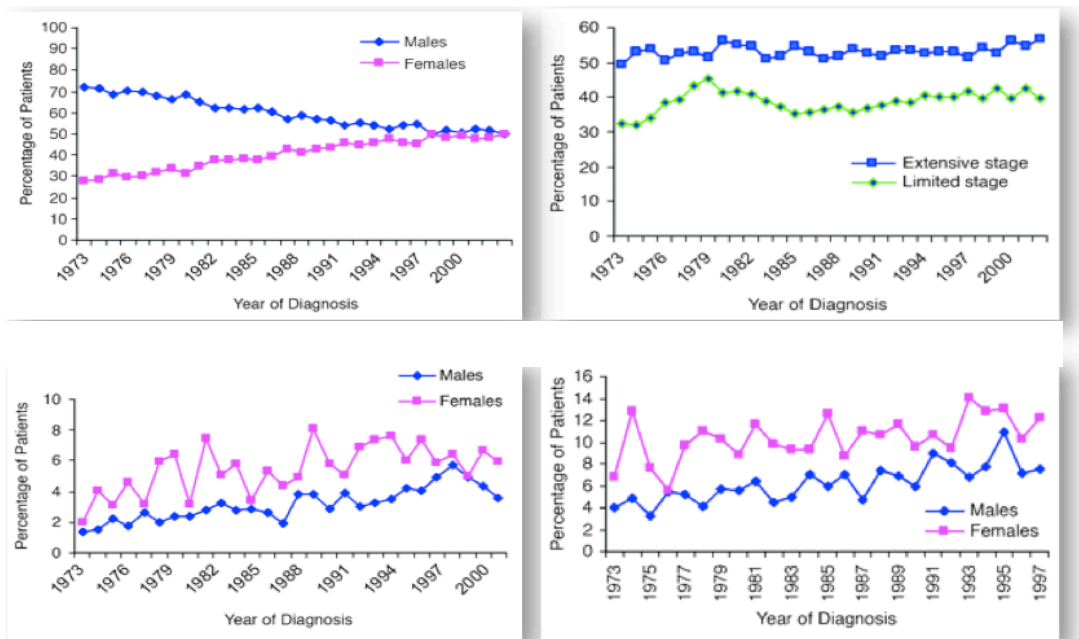


Fig.1 Govindan R. et al 2006

SCLC is strongly associated with cigarette smoking (Figure 2). [Chikako K. et al 2010]

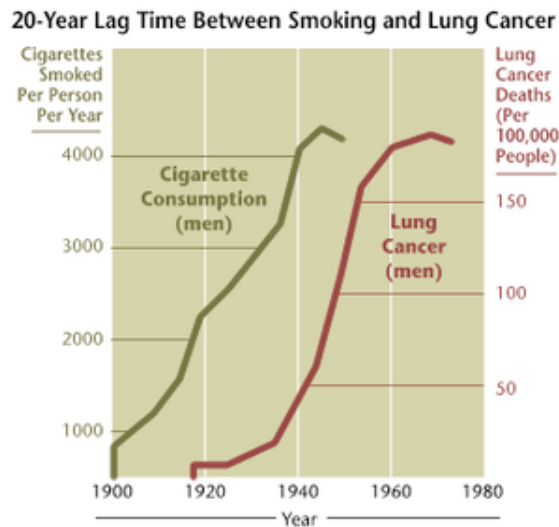


Fig.2 NIH analysis

Improving the survival rate of patient with SCLC requires a better understanding of tumor biology and the subsequent development of novel therapeutic strategies. Molecular analysis of lung cancer has provided a large amount of information on the molecular abnormalities that are more specific to SCLC. These alterations have been used as targets for new biologic therapies, such as those that focus on cell signalling and other biologic pathways involved in tumorigenesis.

1.1.1 Etiopathogenesis and inheritance

Small cell lung cancer, also known as Microcitoma, arises from cells defined as pulmonary neuroendocrine cells (PNECs). These cells, although widely distributed in organs and tissues without any neuroendocrine functions, are able to secrete hormones. They show unique morphologic features, secrete several biologic compounds and express neuroendocrine markers.

During lung development, PNECs are the first cells to form and differentiate within the primitive epithelium, reaching a peak during the neonatal period, thereafter they persist throughout life as a viable population. [Gosney JR et al 1993].

Although the origin of PNECs has not been fully determined, the endodermal origin of this cells is general accepted, since PNECs occur in immature fetal epithelium in vitro and neuroendocrine carcinomas such as SCLC seem to be derived from normal epithelium. [Ito T. et al 1997]

PNECs are distributed throughout the airway epithelium from the lobar bronchus to the alveolar duct as single cell but sometimes they form clusters called neuroepithelial bodies (NEBs). NEBs are localized only in the intrapulmonary airway. Even though their precise role is unclear the PNECs/NEBs complex represents the lung staminal niche that plays a central role in regeneration and lung carcinogenesis. [Cutz E. et al 2007]

In the healthy adult, PNEC are sparsely distributed, with approximately 1 PNEC per 2500 epithelial cells. The secretory granule-containing cells are typically tall and pyramidal in shape, extending from the basal lamina of the epithelium and possess apical microvilli projecting into the airway lumen. These microvilli function as the sensory part of the cell and upon stimulation, respond by degranulation and exocytosis of amines and neuropeptides, which exert a local paracrine and neurocrine effect on neighboring cells and activate both extrinsic and intrinsic neurons (Figure 3). [Adriansen et al. 2006; Gustafsson et al. 2008]

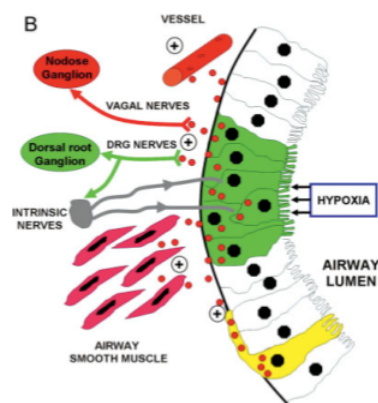


Fig. 3 Mechanism of hypoxia-induced degranulation of NEBs (green). The released dense core vesicles (red) contain signal substances including serotonin, CGRP, bombesin, calcitonin, enkephalin, somatostatin, and cholecystokinin, which activate vagal and DRG afferent neurons as well as adjacent epithelial, vascular, or smooth muscle cells. DRGs in turn activate intrinsic efferent neurons facilitating feedback signaling to the NEBs. A single pulmonary neuroendocrine cell (PNEC) (yellow) with basal extension provides paracrine influence on adjacent mucosal cells.

Although most PNECs exist as solitary cells, some are aggregated in innervated PNEC clusters referred to as neuroepithelial bodies (NEBs). Both solitary

PNECs and NEB exhibit similar phenotypes in terms of storage of adenosine triphosphate, serotonin (5-HT), and several other amines and neuropeptides in dense-core vesicles. Serotonin and other peptides (eg. bombesin, calcitonin) with growth factor-like properties are thought to play an important role in normal lung development. [Pan J. et al. 2006]

SCLC arise from bronchi, the WHO classification defines SCLCs as neuroendocrine tumors with >10 mitoses/2 mm² and small cell cytologic features. The cellularity is typically very high, with hyperchromatic nuclei, absent or very small nucleoli with scant cytoplasm, and a round or fusiform shape and a very high mitotic rate. SCLC may occur in combination with non small-cell lung cancers as well as with other LCNEC. In combination with the histologic appearance, the cell proliferation marker Ki-67 (as per the WHO classification of mitotic counts) seems to be the most useful marker to distinguish between the different subgroups of BP-NETs. A variety of peptide and amine markers including chromogranin A (CgA), neuron-specific enolase (NSE), serotonin, synaptophysin, and adrenocorticotrophic hormone (ACTH) have some utility in establishing the differential diagnosis.

Metastases are usually seen within intrathoracic lymph nodes, but distant metastases to the liver, skeleton, central nervous system (CNS), skin, and mammary glands occur.

1.1.2 Diagnosis and Staging

SCLCs do not cause any symptoms until they have spread too far to be cured, but some people with early lung cancer do have symptoms. The most common symptoms of SCLC are: cough that does not go away or gets worse; chest pain that is often worse with deep breathing, coughing, or laughing; hoarseness; coughing up blood or rust-colored sputum (spit or phlegm); shortness of breath; feeling tired or weak; infections such as bronchitis and pneumonia that don't go away or keep coming back.

When lung cancer spreads to distant organs, it may cause: weight loss and loss of appetite; bone pain (like pain in the back or hips); neurologic changes (such as headache, weakness or numbness of an arm or leg, dizziness, balance problems, or seizures).

SCLC has been staged as:

Limited disease (LD): restricted to 1 hemithorax with regional lymph node metastases, including hilar, ipsilateral, and contralateral mediastinal and ipsilateral and contralateral supraclavicular nodes. Median survival is 12-20 months with a 5-year survival of less than 5%. [Micke P. et al. 2002]

Extensive disease (ED): presence of obvious metastatic disease. Median survival is 7-12 months, with a 5-year survival less than 2%.

In a new proposal from the International Association for the Study of Lung Cancer (IASLC), however, TNM staging (Tumour, Node, Metastases) is also suggested for SCLC, and it has been recommended that it be evaluated in clinical trials.

The most common metastatic sites for SCLC are bone (19%-38%), liver (17%-34%), the adrenal glands (10%-17%), and the brain (up to 14%). [Simon C. et al. 2001]

1.1.3 Genetics of SCLC

In the past two decades, significant progress has been made in understanding the molecular and cellular pathogenesis of lung cancer. Abnormalities of proto-oncogenes, genetic and epigenetic changes of tumour suppressor genes, the role of angiogenesis, molecular abnormalities in pre-invasive respiratory lesions have recently come into focus.

The major histopathological differences between SCLC and NSCLC are due to distinct genetic alterations [Zochbauer-Muller S. 2002]. For example, RAS oncogene mutations have been detected in 15-20% of all NSCLC but never found in SCLC, whereas abnormal MYC expression, MYCN and MYCL1 in particular, is frequently observed in SCLC but is less common in NSCLC. [Meuwissen et al. 2005]

Primary chromosomal alterations

Several sites of frequent allelic loss have been identified in lung cancer [Girard L. et al. 2000]. The location of these sites was based on the determination of the minimal regions of loss that are defined by the occurrence of breakpoints (transitions between markers showing LOH and those retaining heterozygosity) surrounding regions of LOHs. These sites are likely to represent the major TSG regions that are affected in lung cancer and are therefore good indicators of critical regions of loss that warrant further investigation. It was shown previously that chromosome arms 3p have the most frequent allelic loss in SCLC (90%), in several sites, including FHIT (fragile histidine triad) locus, RASSF1 (ras effector homologue) locus, RARB (retinoic acid receptor beta) locus, FUS1 and PTEN loci.

Oncogene activation

Proto-oncogenes MYC, MYCL, MYCN are usually activated in SCLC and they represent a marker for a poor prognosis. [Johnson B.E. et al. 1996]

BCL-2 is an anti apoptotic protein expressed in 75-95% of SCLC cases [Jiang S.X. et al. 1995]. BCL-2 works against a pro-apoptotic protein BAX, a p53 target. High levels of BCL2 and low levels of BAX have been frequently found in SCLC p53^{-/-} [Brambilla E. et al. 1996]. Moreover SCLC with high expression of BCL2 are associated with a high sensitivity to chemotherapy.

Oncosuppressor deactivation

p53 is a nuclear phosphoprotein, that function as a transcription factor. The human gene is located on chromosome 17 and mouse gene on chromosome 11, it encodes a tetrameric polypeptide of 393 amino acids. p53 binds a consensus sequences on the DNA and it activates or represses the transcription of several genes. Depending on what type of genes p53 activates, that it can stimulate apoptosis or inhibit cell cycle progression or promote DNA repair or induce differentiation. Normally p53 intracellular levels are low because the protein is rapidly degraded by ubiquitin-dependent proteolysis induced by Mdm2 factor. Following stress signals p53 can be activated with a consequent increase of intracellular levels. This increase is mainly due to an increase of the stability of the protein, but we cannot exclude the presence of a

transcriptional or translational control. The stress signals that activate p53 are represented by DNA damage, chromosomal aberrations, oncogenes activities, hypoxia, shortening of telomere, lack of growth factors. [Khanna K.K. et al. 2001]

Mutations in p53 or alterations in the p53 pathway are frequent in human tumours. p53 is involved in both hereditary and sporadic tumours. Mutations in p53 are found in 50% of sporadic human cancers. These mutations affect mainly exons 5, 6, 7, 8. p53 loss of function is frequently found in SCLC.

p16^{INK4A}-cyclin D1-CDK4-RB pathway plays a central role in the cell cycle G1/S transition and alterations of one of his components is frequently found in lung cancer and in the 90% of SCLC RB protein is inactive.[Reissmann P.T. et al. 1993]

Moreover p14^{ARF} is mutated in 75% of all SCLCs.

Angiogenesis and metastasis

Recent evidence suggests that the genetic regulation of angiogenesis is also of crucial importance and that oncogenes and tumour suppressor genes can regulate it [Onn A. et al. 2003]. Vascular endothelial growth factor (VEGF) is a multifunctional cytokine that increases microvascular permeability and directly stimulates endothelial cell growth and angiogenesis. Expression of VEGF is correlated with loss of p53.[Niklinska W. et al. 2001]

Also the MMP family and their inhibitors plays a central role in metastasis and tumor associated angiogenesis.[Chambers A.F. et al. 1997; Nelson A.R. et al. 2000]

The complex E-caderin-catenin plays a central role in the architectural structure tissue maintenance [Bremnes R.M. et al. 2002]. Loss of E-caderin expression at the metastasis level is associated with a poor outcome.[Hirata T. et al. 2001; Kalogeraki A. et al. 2003]

1.2 MYCN Gene

1.2.1 MYC gene family

MYC genes are frequently involved in human cancers. The family of proto-oncogenes *MYC* is composed of a group of transcription factors belonging to the class *basic-helix-loop-helix-zipper* (bHLHZ) [Eilers M. et al. 1991]. The Myc proteins family is involved in the regulation of proliferation and cell cycle, in the processes that lead to differentiation and to apoptosis, in genomic instability and neoplastic transformation [Grandori C. et al. 2000; Nesbit C.E. et al. 1999]. Most studies on *MYC genes* are focused on three members (*c-MYC*, *MYCN* and *L-MYC*), which, when activated, appear to be important in the development of various human cancers. *c-MYC* was the first of the three to be discovered through its homology with *v-MYC*, the transforming gene of the MC29 virus of avian myelocytomatosis [Vennstrom B. et al. 1982]. *MYCN* and *L-MYC* were subsequently identified through their homology with *v-MYC* amplicons in the cells, respectively, of neuroblastoma and small cell lung cancer [Schwab M. et al. 1983; Nau M.M. et al. 1985]. The *MYCN* oncogene, in particular, was identified in 1983, in neuroblastoma cell lines with DMs (double minute chromatin bodies) and / or HSRs (homogeneously staining regions) [Schwab M. et al. 1983; Kohl N.E. et al. 1983]. In situ hybridization allowed us to locate human *MYCN* on the short arm of human *MYCN* distal chromosome 2, region 2p 23-24. Only the second and third exons of the gene are translated and they lead to the formation of the protein. Other genes, at least three, belong to this family: *S-MYC*, *B-MYC* and *P-MYC*. The *MYC* genes can be activated through different mechanisms such as gene amplification [Dalla-Favera R. et al. 1982], chromosomal translocation [Magrath I. et al. 1990], proviral insertion [Payne G.S. et al. 1982], retroviral transduction [Neil J.C. et al. 1987] and other processes not yet known. The members of this family play a key role in activating and controlling gene expression: in fact, they have the same structural motifs of many transcriptional factors, like oncoproteins *v-Fos* and *v-Jun*, leucine-zipper motifs are set in the C-terminus of the protein where, due to their α -helices, they are able to wrap the DNA [Landschulz W.H. et al. 1988]. Before the C-terminus, there is a *helix-loop-helix* domain, already identified in several transcription factors, such as proteins E12 and E47 [Murre C. et al. 1989]. The

proteins also contain a stretch of basic amino acids upstream of helix-loop-helix motif, called "basic region", previously identified in the myogenic transcription factor MyoD, which is the region involved in sequence-specific DNA binding [Davis R.L. et al. 1990]. Considering all these structures *MYC* gene family contains a motif of bZIP- bHLH able to interact with DNA in which the bZIP and bHLH domains lie in adjacent positions separated by only a basic domain "b". Unlike normal bHLH domains, it allows fusion of that structure to hang the DNA through the basic regions of bHLH motif, while any dimerization (Myc-Max) of protein monomers are guaranteed by the bZIP motif (Figure 4).

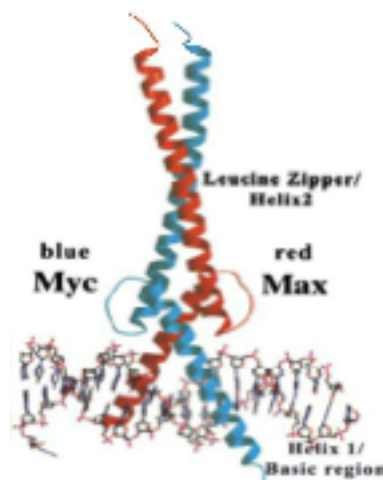


Fig. 4 Structure of a bZIP-bHLH motif: Myc-Max heterodimer and the binding with DNA.

1.2.2 From *MYCN* gene to N-Myc protein

The post-transcriptional regulation of *MYCN* is influenced by a ribosomal internalization signal located at mRNA 5'-UTR, which amplifies the translation initiation and determines the redistribution in the cytoplasm [Jopling C.L. et al. 2001]. The N-Myc degradation in neuroblastoma is ATP dependent and it is mediated by the 26S proteasome in the nucleus; degradation can however be done by the employee via calpain [Bonvini P. et al. 1998].

MYCN is as a classic dominant oncogene. The forced expression of *MYCN* can transform normal cells, usually in cooperation with RAS oncogene [Yancopoulos G.D. et al. 1985; Schwab M. et al. 1985; Small M.B. et al 1987]. The over-expression of *MYCN* can release the embryonic fibroblasts from senescence

[Schwab M. et al. 1988], the addition of an RNA antisense MYCN in neuroblastoma cell lines that over-express MYCN can reduce the proliferation or induce differentiation and / or apoptosis [Negroni A. et al. 1991; Schmidt M.L. et al. 1994]. Moreover, the over-expression of human MYCN in the neuroectoderm of the transgenic TH-MYCN mouse produces, in a dose-dependent way, neuroblastoma resembling tumors [Weiss W.A. et al. 1997].

N-Myc protein is a nuclear phosphoprotein with a short half-life (30-50 min) and it shows regions of high homology (overall 38% amino acid identity) with c-Myc. N-Myc, like all the Myc family proteins, has three specific amino acid sequences [Pession A. et al. 2005]:

- a globular domain of transactivation in N-terminus, containing the Myc Boxes I (MBI) and II (MBII);
- an unstructured intermediate region;
- a C-terminus domain containing a basic region (BR), which is involved in the recognition and specific binding to DNA.

Myc forms complexes with DNA only at very high concentrations, indicating that these interactions may not be physiologically significant. It is possible that Myc required interaction with a second protein to play its role as a transcription factor. This was subsequently identified in a small protein called Max [Blackwood E.M. et al. 1991].

Max is a ubiquitous nuclear protein with a long half-life, and like Myc, contains the helix-loop-helix and leucine-zipper basic motif. Max binds to itself and to other transcription factors through its leucine zipper to form homo- and heterodimers respectively. Max itself lacks a transactivation domain so that Max homodimers have a repressive function. In contrast, Myc contains a transactivation domain but cannot homodimerize. However Myc can heterodimerize with Max to form heterodimers that can both bind DNA and transactivate. The transcriptionally active Max/Myc dimer promotes cell proliferation as well as apoptosis. [Amati B. et al. 1994]

This complex binds specifically to a palindromic nucleotide sequence CACGTG on DNA, called E-box [Solomon D.L. et al. 1993]; another binding site between

on DNA is an asymmetric sequence CATGTG. Other transcription factors such as USF, TFE3 and TFEB binds to these sequences. This leads to a great series of transcriptional activation of genes that promote cell growth. [Grandori C. et al. 1997]

Despite the structural and functional homology, the expression of c-Myc and N-Myc is very different: c-Myc is ubiquitous expressed in proliferating cells, while N-myc has a pattern of expression quite restricted [Strieder V. et al. 2002]. Development studies on mouse show that N-myc is mainly expressed during the early stages of differentiation: at birth it's still expressed in brain, kidney, intestines, heart and lungs, but it is subsequently down-regulated and in the adult mouse its expression occurs mainly in the early development of B lymphocytes [Wakamatsu et al. 1997; Strieder V. et al. 2002].

The transcript of N-myc is rather complex: it begins in different sites that can be grouped under the control of two promoters; the multiplicity of start sites to start combines with alternative splicing to generate two forms of mRNA. The mRNAs have different 5' leader sequences but identical structure. Both forms of mRNA are unstable with a half-life of 15 min. They encode the two N-myc proteins of 65 and 67 kD. [Stanton L.W. et al. 1987]

1.2.3 Role of *MYCN* in small cell lung cancer

MYCN amplification was found first in human neuroblastoma in 1983 by Schwab and colleagues. Following studies have confirmed that the presence of more than 10 copies of *MYCN* gene per haploid genome is an unfavorable prognostic marker, independent from other parameters. 25-30% of primary untreated NB shows the amplification of *MYCN*, which is associated with advanced disease, rapid progression and poor prognosis [Sansone R. et al. 1991]. The reason of this association is still uncertain. There is also a direct correlation between the levels of N-Myc protein and the aggressiveness of this tumour. The *MYCN* amplification was identified as a single genetic factor which adds a prognostic significant information to clinical variables such as age and stage, infact, currently the status of *MYCN* is the only genetic variable of cancer used as a criterion for stratification of treatment in clinical trials of NB [Berthold F. et al. 1997]. In 1997 Weiss W.A. and his group showed that *MYCN*

contributes to the genesis of neuroblastoma with the generation of a transgenic mice that over-express MYCN in neuro-ectodermal cells and for this they develop neuroblastoma.

The amplification of MYCN is associated with the development of several pediatric tumors, as well as NB: glioblastoma (< 5%), medulloblastoma (5-15%); and other adult solid tumors: melanoma of neuroectoderm tumor, astrocytoma, retinoblastoma (10-20%) and cell lung cancer (10%). In general, overexpression of the MYC family oncogenes is a frequent molecular alteration in SCLC, occurring in 18-31% of SCLCs, and more common in chemo-refractory disease. [Wistuba et al. 2001]

Kim and colleagues in 2006 identified novel alterations in SCLC performing comparative genomic hybridization on a set of 24 SCLC cell lines, using cDNA microarrays representing 22000 human genes (providing an average mapping resolution of <70kb). They identified DNA amplifications corresponding to oncogenes known to be amplified in SCLC, including MYC (8q24), MYCN (2p24) and MYCL1 (1p34). Their findings support a role of altered apoptotic balance in the pathogenesis of SCLC, and suggest that MYC family genes might affect oncogenesis through distinct sets of targets, in particular implicating the importance of transcriptional repression. [Kim YH. et al. 2006]

1.3 Therapeutic options and chemotherapy

SCLC is distinguished from the other forms of lung cancer by its aggressive clinical course, with widespread metastases at diagnosis, the frequent occurrence of para-neoplastic syndromes [Lally BE. et al 2007], and its sensitivity to both chemotherapy and radiotherapy; Small cell lung cancer (SCLC) now represents only 13% of all newly diagnosed lung cancers, annual incidence of SCLC has been decreasing over the past 30 years. [Puglisi M. et al. 2010]

As already mentioned SCLC can be staged in limited disease and extensive disease.

1.3.1 Treatment of limited disease

The survival of patients with LD-SCLC has improved over the past 20 years, with a 5-year survival rate of 13.9% compared with 6% before 2000 [Puglisi M. et al. 2010]. The positive outcome in LD seems to be multifactorial, with better staging, platinum-based chemotherapy and the use of prophylactic cranial irradiation (PCI) all exerting an effect. The addition of TRT to chemotherapy, both sequentially and, more recently, concomitantly, significantly reduces the risk of intrathoracic failures, resulting in improvements in long-term survival in this population.

The function of surgery has never been fully developed because of the apparent failure of this treatment modality in two randomized trials reported in 1976 and 1994. Both trials did not show any survival advantage for surgery alone or in combination with TRT, compared with radiotherapy alone [Fox W. et al. 1973; Lad T et al. 1994]. A recent review of these data suggests that the 'intention to treat' results may have misrepresented the effect of surgery, as not all patients randomized to surgery and included in the analyses actually underwent a complete resection. Infact, only 48% and 77% of patients, respectively, did so, meaning that the impact of surgery may have been underestimated [Lim E. et al. 2008].

Other published prospective series also suggest that surgery, after induction chemotherapy, can achieve high local control rates in early stage SCLC (stage I – III) with favorable long-term survival results. To validate this hypothesis, a number of randomized trials have recently been designed to compare surgery, in combination with chemotherapy or chemo-radiotherapy, with the current standard of treatment with chemo-radiotherapy using modern staging methods.

Combined modality therapy with chemotherapy and thoracic irradiation is the current accepted standard for patients with LD- SCLC (NCCN, 2008). There are a number of unresolved issues in the delivery of chemotherapy and radical radiotherapy in LD-SCLC including timing of TRT, early vs late, concomitant or sequential, total dose and fractionation schedule. Many trials have addressed the timing issues, but they have differed in trial design as well as the

chemotherapy regimen used as reviewed recently by Socinski and Stinchcombe (2007).

Etoposide (EP) remains the only chemotherapy that can be delivered at full dose in combination with radiotherapy in LD-SCLC.

1.3.2 Treatment of extensive disease

Chemotherapy is the main treatment for ED-SCLC. Treatments in the past including oral Etoposide, standard and high-dose regimens have been extensively reviewed by the authors in an earlier publication [Popat and O'Brien, 2005]. Combination therapy with EP is considered the standard first-line regimen, but a randomized Phase III trial failed to prove a definitive survival benefit for EP compared with the cyclophosphamide, doxorubicin and vincristine regimen (CAV).

A study conducted by the Japan Clinical Oncology Group showed a significant survival benefit for irinotecan and cisplatin combination vs EP, but a second study in US patients of the same agents failed to show any significant difference.[Okamoto H. et al.2007]

The GC chemotherapy (gemcitabine plus carboplatin) achieved survival rate, response rate and time to progression equivalent to EP. The two regimens had a different toxicity profile. The GC regimen is useful, particularly in patients with mixed small cell and non-small cell tumours, and for those for whom alopecia is a real problem.

To summarize these results, all the recent randomized trials using later generation cytotoxics have not had a significant impact on standard care for SCLC, failing to identify a new platinum-based combination over the established platinum etoposide.

Author	Staging	Patients (n)	Experimental regimen		Standard regimen	Outcomes		
			Schedule	Schedule		Overall survival (months)	RR	
Noda et al (2002)	ED	154	irinotecan/ cisplatin	I: 60 mg/m ² days 1, 8, 15 P: 60 mg/m ² day 1; q4w I: 65 mg/m ² days 1-8 P: 30 mg/m ² days 1, 8; q3w	E: 100 mg/m ² days 1, 2, 3 P: 80 mg/m ² day 1; q3w E: 120 mg/m ² days 1, 2, 3 P: 60 mg/m ² day 1; q3w	12.8 vs 9.4 months	+ve	+ve
Hanna et al (2006a)	ED	331				9.3 vs 10.2 months	NS	NS
Lara et al (2009)	ED	645				9.9 vs 9.1 months	NS	NS
Hermes et al (2008)	ED	220	irinotecan/ carboplatin	I: 1.75 mg/m ² day 1 Ca: AUC 4 day 1; q3w	E: 120 mg/m ² orally days 1-5 Ca: AUC 4 day 1; q3w	8.5 vs 7.1 months	+ve	/
Socinski et al (2009)	ED	733	Pemetrexed/ carboplatin	Pe: 500 mg/m ² day 1 Ca: AUC 5 day 1; q3w	E: 100 mg/m ² days 1, 2, 3 Ca: AUC 5 day 1; q3w	7.29 vs 9.56 months	-ve	-ve
Niell et al (2005)	ED	587	Paclitaxel/ etoposide/ cisplatin	Pa: 1.75 mg/m ² day 1 E: 80 mg/m ² days 1-3 P: 80 mg/m ² day 1; q3w	E: 80 mg/m ² days 1, 2, 3 P: 80 mg/m ² day 1; q3w	10.6 vs 9.9 months	NS	+ve
Mavroudis et al (2001)	ED, LD	133		Pa: 1.75 mg/m ² day 1 E: 80 mg/m ² days 1-4 P: 80 mg/m ² day 2; q3w	E: 120 mg/m ² days 1, 2, 3 P: 80 mg/m ² day 1; q3w	9.5 vs 10.5 months	NS	NS
Hoegener et al (2008)	ED	795	Topotecan/ cisplatin	T: 1 mg/m ² days 1-5 P: 75 mg/m ² day 1; q3w	E: 100 mg/m ² days 1, 2, 3 P: 75 mg/m ² day 1; q3w	10.3 vs 9.4 months	Non-inferior	+ve
Eckardt et al (2006)	ED	784		T: 1.7 mg/m ² oral days 1-5 P: 60 mg/m ² day 5; q3w	E: 100 mg/m ² days 1, 2, 3 P: 80 mg/m ² day 1; q3w	39.3 vs 40.3 weeks	Non-inferior	NS
Lee et al (2009)	ED, LD, poor prognoses	241	Gemcitabine/ carboplatin	G: 1200 mg/m ² days 1, 8 Ca: AUC 5 day 1; q3w	E: 120 mg/m ² day 1; 100 mg/m ² bid orally days 2, 3 P: 60 mg/m ² day 1; q3w	8 vs 8.1 months	Non-inferior	NS

Abbreviations: P = cisplatin; Ca = carboplatin; E = etoposide; I = irinotecan; Pe = pemetrexed; Pa = paclitaxel; T = topotecan; G = gemcitabine; RR = response rate; NS = not significant; AUC = area under the curve; ED = extensive disease; LD = limited disease; SCLC = small cell lung cancer.

Table 1 Phase II/III studies of combination chemotherapy in patients with ED-SCLC

1.3.3 Treatment options for relapsed SCLC

Despite high initial response rates to chemotherapy, SCLC usually recurs within 1 year after treatment.

On the basis of retrospective data, distinction has been made between (1) sensitive patients, that is those with a response to first-line therapy and a treatment-free interval of at least 90 days, (2) resistant patients, that is relapse within 90 days and (3) refractory patients, that is no response to first-line treatment. [Fischer B., Arcaro A. 2008]

Single-agent Topotecan is currently the only approved drug for the treatment of patients with SCLC who have failed or relapsed after first-line chemotherapy. Topotecan is available in both intravenous and oral formulations and randomized studies have suggested that both have similar clinical activity in SCLC. A randomized Phase III trial has shown significant benefit with oral topotecan plus best supportive care vs best supportive care only in relapsed patients unsuitable for intravenous regimens [Gralla RJ et al. 2004]. There are several ongoing trials for this stage.

1.3.4 Target therapies

During the last decades, target therapies have been developed by several pharmaceutical companies, but only few clinical trials have obtained encouraging results.

Ongoing trials are focusing on molecules against the proliferative, antiapoptotic and angiogenic pathways.

Ras/Raf inhibitors. The ras family genes have been identified as potential targets for therapeutic intervention because of somatic mutations in different human cancers. They are mutated in non-small cell lung cancer (NSCLC) approximately 20% of the time. The enzyme farnesyl transferase is involved in post-translational modification of the ras proteins by covalently linking a farnesyl group to the ras protein. This permits the ras protein to be translocated to the surface membrane, allowing the protein to be involved in signalling for increased proliferation and inhibition of apoptosis. The class of farnesyl transferase inhibitors is designed to block farnesylation and prevent the mature ras signalling and thus inhibit cell proliferation and facilitate apoptosis. Multiple agents that inhibit farnesylation have been developed, and two farnesyl transferase inhibitors have been tested in patients with lung cancer in three Phase II trials. R115777 has been studied in patients with NSCLC and in patients with relapsed small cell lung cancer (SCLC) after chemotherapy. There has been a single trial of L-778,123 in patients with untreated NSCLC [Seep-Lorenzino et al. 1995]. There were no objective responses among the 22 patients with relapsed SCLC treated with R115777. [Jonson BE. et al. 2004]

C-kit pathway inhibitors. More than 70% of SCLC cell lines and tumor specimens co-express Kit and its ligand SCF, leading to the hypothesis that this co-expression constitutes an autocrine growth loop. A study by Krystal and coll. showed that Imatinib, a tyrosine kinase inhibitor c-KIT and PDGFR specific, arrests SCLC cell line growth [Kristal GW. et al 2000]. This study led to several clinical trials with no significant results.[Shneider BJ. et al 2006; Spigel DR. et al. 2007]

IGF1R/PIK3/AKT1/FRAP1. Evidence suggests that the PI3K/Akt pathway (mTOR) may be important in proliferative and anti-apoptotic signalling in SCLC.

This may be responsible for the chemo-resistance to Imatinib [Tsurutani J. et al. 2005]. A new IGF1R inhibitor, NVP-ADW742, enhances SCLC cell lines chemotherapy sensitivity [Krystal GW. et al. 2005] and monoclonal antibodies are currently being studied in clinical trials to be used in combination with chemotherapy and other target therapies.

Anti-angiogenic treatments Currently, only Bevacizumab has demonstrated an overall survival in extensive SCLC, but clinical trials are still ongoing.

Immunotherapy: The BEC2/BCG (Bacillus Calmette-Guérin) vaccine was studied extensively in SCLC over the past decade and ultimately failed to achieve a significant benefit in OS. Ipilimumab is currently the subject of a phase III clinical trial to determine whether blockade of CTLA-4 in patients with extensive-stage SCLC enhances antitumor T-cell.

1.4 Peptide Nucleic Acid

1.4.1 Structure and properties

The PNAs are synthetic analogs of nucleic acids, in which the normal phosphodiester backbone is replaced by a pseudo-peptide chain composed of monomers of N-(2-aminoethyl) glycine.[Nielsen P.E. et al. 1991]

The PNA binds sequence-specific DNA and RNA according to the rules of Watson-Crick pairing.[Egholm, M. et al. 1994]

The PNAs are achiral and non-ionic molecules; PNA oligomers also show greater specificity in binding to complementary DNAs, with a PNA/DNA base mismatch being more destabilizing than a similar mismatch in a DNA/DNA duplex. PNAs are not easily recognized by either nucleases or proteases, so they are not degraded in cells and are extremely stable in biological fluids. [Demidov V.V. 1994]

The compounds are neutral and therefore have a low solubility in water compared to DNA. The neutral PNA molecules have a tendency to form aggregates in the nucleotide sequence-dependent manner. The solubility of PNA is also linked to the length of the oligomer and the purine relationship:

pyrimidine [Hyrup B. et al. 1996]. Some modifications, including the incorporation of positively charged lysine residues, can improve solubility. To increase the solubility in water, negative charges can also be introduced, especially in the PNA-DNA chimeras.

The concentration of a PNA oligomer is determined by measuring the absorbance at 260 nm at 80°C [Kuhn H. et al. 1998]. At this temperature, the nitrogen bases are considered completely detached and the disruption of π system by the peptide skeleton takes less important.

PNAs bind preferentially to the complementary sequences; more weakly to those containing a mismatch. [Nielsen P.E. et al. 1993]

1.4.2 PNA anti-gene

The PNA interferes with gene expression through two mechanisms [Ray A. et al. 2000]:

- anti-gene strategy: through inhibition of transcription by binding to DNA;
- anti-sense strategy: through inhibition of translation by binding to mRNA.

The anti-gene strategy has the advantage, compared with antisense, to block the gene of interest even before it is transcribed: this allows to be used at lower concentrations and shows a stronger inhibitory and prolonged over time compared to antisense. [Pession A. et al. 2005]

1.4.3 Therapeutic applications of PNA anti-gene

The effectiveness of PNA anti-gene has been tested in different cell lines of neuroblastoma. Sun and colleagues have shown that these third-generation antisense conjugated to somatostatin analogs (SSA), are able to penetrate the nuclear area, to selectively inhibit the expression of MYCN in IMR-32 lines and stopping the growth. [Sun L. et al. 2002]

Other studies showed the inhibition of E μ enhancer regions responsible of the over-expression of c-MYC in Burkitt lymphoma lines (BL) [Cutron G. et al. 2003], and the inhibition of c-MYC through PNA strategy in prostate carcinoma

cells. [Boffa L.C. et al. 2000] The inhibition usually leads to cellular cycle arrest and decrease of cell growth.

PNA conjugated to specific nuclear localization sequences (NLS) define the most evident effects in MYCN amplified neuroblastoma cell lines compared to not-amplified.

These encouraging results obtained from *in vitro* studies must be followed by testing *in vivo* the PNAs.

1.5 Chemotherapy compounds

The chemotherapy drugs identify all those drugs whose chemical structure and physical properties are useful in the treatment against the majority of tumors.

They may be synthetic or produced by strains of microorganisms, show selective toxicity to infectious agents and cancer cells and absence (or reduced) toxicity to normal cells of human organism.

The chemotherapeutic agents cause cell death through different mechanism.. Anti-neoplastic agents are divided into specific categories based on their mechanism of action. In the following paragraphs we summarize features of two classes in particular: alkylating agents and inhibitors of topoisomerase II.

1.5.1 Alkylating agents

Alkylating agents can become strong electrophiles, thus interacting with nucleophilic groups (phosphate groups, amino, sulfhydryl, hydroxyl, carboxyl, imidazole) alkylating proteins and nucleic acids. Crucial importance has the cytotoxic effect related to the association of these drugs with DNA. The reaction that leads to the formation of stable drug-DNA complex (and / or protein) is schematically divided into two phases: 1) activation and 2) nucleophilic attack.

In the activation phase, cellular metabolic processes activate the alkylating agent to form an interim net positive charge. Once activated, the compound is able to interact with a number of groups which have a high electron density (phase nucleophilic attack).

The main target of the alkylating agent is DNA; the chemical structure determines the degree of alkylation of various nucleophilic groups found in the nucleic acid molecule. In addition, both the structure and the charge of alkylating agents affect the specificity sequence of alkylation.

The alkylation of DNA bases leads to various physiological changes such as base-pairing errors and subsequent mutations during replication; chemical injury and subsequent excision of bases, formation of covalent bonds within a filament and / or between filaments of DNA matched, stable ties with the associated proteins. Besides altering the functions of nucleic acids, the chemical alteration of cellular proteins leads to changes in different enzymatic functions, including those responsible for DNA repair.

These agents do not distinguish between cells into cell cycle and in quiescent cells (G0 phase), however, they are more toxic to rapidly proliferating cells. They are used to treat, in combination with other compounds, a wide variety of solid tumors and lymph.

Cisplatin and Carboplatin

Cisplatin and Carboplatin are platinum-based drugs that are widely used in cancer chemotherapy.

Cisplatin has a structure consisting of two labile ligands, two chlorides, and two inert binders, two amines; both in *cis* position. It acts interfering with all cell cycle phases binding the DNA. The most frequent bound is the intrastrand crosslink between two adjacent guanine. [Wang D. et al. 2005; Gonzales V.M. et al. 2001]

Carboplatin has instead a motif CBDC (bidentate cyclobutane dicarboxylate), which gives more stability to the compound (Figure 5). It shares with cisplatin the same mechanism of action.



Fig. 5 Structures of cisplatin and carboplatin.

Other interactions, however, have to be taken into consideration: mitochondrial DNA, actin (shift in composition), phospholipids and phosphatidylserine. The cross-link format involves a folding of the DNA, with exposure of the minor groove to the hooking of different proteins.

Cisplatin and Carboplatin are extremely potent anti-neoplastic compounds and they are usually used in the treatment of small cell lung cancer, non-small cell lung cancer, ovarian cancer, metastatic testicular cancer in combination with bleomycin vinblastine, and ovarian cancer in combination with cyclophosphamide. Cisplatin is the first line therapy for small cell lung cancer but can be substituted with carboplatin. Indeed, Carboplatin has less nephrotoxicity, neurotoxicity, ototoxicity and emetogenesis and more stability than cisplatin.

1.5.2 Topoisomerasi IIa inhibitor

Etoposide (VP-16)

Etoposide is a semisynthetic derivate of the vegetal alkaloid podophyllotoxin responsible for inhibition of an essential enzyme for structural maintaining of DNA: mouse isomerase II α (α Topo2). It acts by forming a ternary complex DNA-drug Top2- α and disrupting the normal role of this enzyme on nucleic acid. [Li TK. et al. 2001]

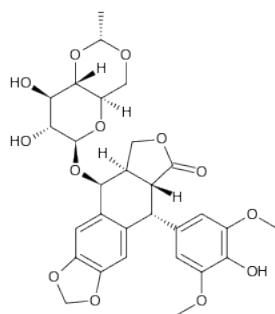


Fig.6 Etoposide structure.

The drug inhibits the enzyme through steric hindrance (direct entry to the cleavage site that the enzyme has generated), triggering the following Fas-FasL apoptotic cascade [Beck et al. 2001]. Its activity is directly proportional to the concentration of ATP.

Etoposide also involves inhibition of Topoisomerase I through an indirect mechanism: the drug, binding to Top2 α , triggers the apoptotic cascade through deregulation of BCL-2, an important anti-apoptotic factor, hence activation of effector caspases (9-3), alteration of mitochondrial potential and the formation of toxic oxygen reactive inducing the block of Topoisomerase I. The blockade of this enzyme only requires further trigger the apoptotic cascade that amplifies the cytotoxic effect of the etoposide. [Sordet et al. 2004]

The drug is used as a chemotherapeutic agent, single or in combination with others, in various forms of cancer: Ewing's sarcoma, small cell lung cancer, testicular cancer, lymphoma, non-lymphocytic leukemia and glioblastoma multiform, and neuroblastoma. The most common adverse effects are: low blood pressure, alopecia, diarrhea, leukopenia and anemia.

1.6 Hedgehog pathway and Basal Cell Carcinoma

The Hedgehog signalling pathway regulates embryonic development and may be aberrantly activated in a wide variety of human cancers [Wicking C. et al. 2001]. Efforts to target pathogenic HH signalling have steadily progressed from the lab to the clinic, and the recent approval of the HH inhibitor Vismodegib for patients with advanced BCC represents an important milestone [Von Hoff DD. et al. 2009]. On the other hand, HH pathway antagonists have failed to show significant clinical activity in other solid tumours.

1.6.1 Hedgehog signalling pathway

The Hedgehog (HH) signalling pathway is required for the control of cell growth, proliferation and differentiation. The pathway is most active during embryogenesis but is also important for regulating the cell cycle in adult cells [Altaba A. et al. 2001; Beachy P. et al. 2004]. HH signalling is controlled by the three HH ligands: Desert (DHH), Indian (IHH) and Sonic (SHH), which is most

relevant to skin. As SHH ligands bind to the PTCH1 transmembrane receptor, another transmembrane protein Smoothed (SMO) accumulates on the cell membrane where it is phosphorylated and activated [Denef N. et al 2000]. Upon activation, SMO causes the dissociation of Suppressor of Fused (SUFU), a negative regulator of the HH signalling pathway resulting in activation of GLI transcription factors, although it is unclear how the signal is transduced between SMO and SUFU (Figure 7). [Donovan J. et al 2009]

Of the three GLI transcription factors all are activators however, GLI-2 and GLI-3 can have repressive functions. GLI-1 is the most prominent of the three and its over expression has been observed in many different types of cancers. [Ruiz i Altaba A. et al 2002]

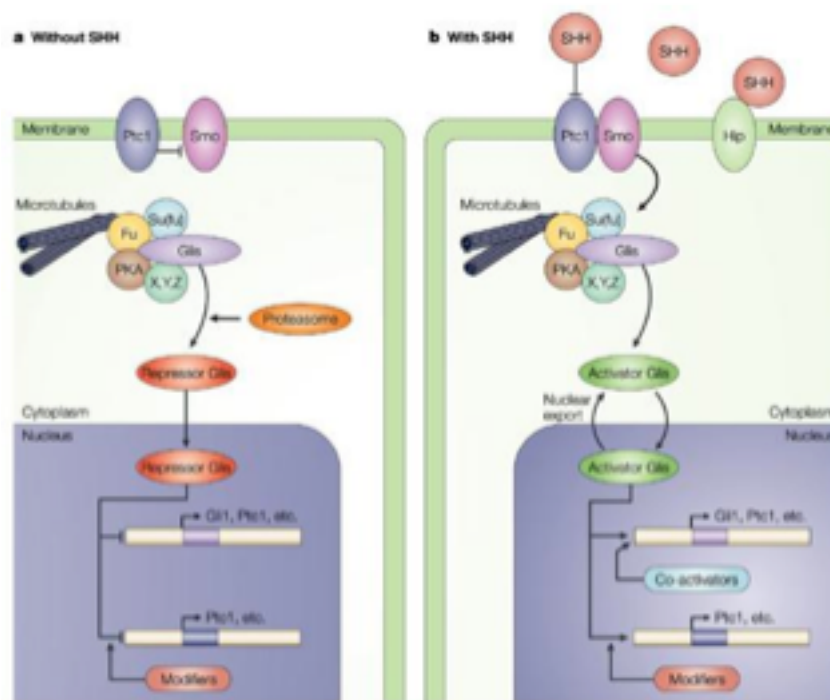


Fig.7 The hedgehog signalling pathway

As a result of mutations of PTCH1 as seen in BCC, SMO is no longer repressed resulting in activation of the downstream signalling cascade. PTCH1 loss of heterozygosity or loss of function mutations have been observed in 30-70% of sporadic BCCs [Saran A. et al 2009]. Activating mutations have also been identified in SMO, although these are much less prevalent in BCCs. [Xie J. et al 1998]

The HH signalling cascade results in activation of the GLI transcription factors which are thought to increase cell proliferation and inhibit both differentiation and apoptosis. A positive feedback mechanism has been reported between GLI-1 and GLI-2 which implies that GLI-2 also plays a role in the formation of BCCs. GLI-2 was shown to activate proliferation in keratinocytes while repressing epidermal differentiation [Regl G. et al. 2002]. HH signalling has also been linked to Notch [Adolphe C. et al. 2006], TGF- β [Cretnik M. et al 2009] and Wnt/ β -catenin pathways. [Adolphe C. et al. 2006]

1.6.2 Basal cell carcinoma & Gorlin syndrome

Basal cell carcinoma (BCC) is the most common skin cancer in the world with BCCs accounting for 70% of all skin cancer [Mancuso M. et al. 2004]. BCC is the most common malignancy in Caucasians with approximately 3 in 10 developing the disease within their lifetime and an annual increase in worldwide incidence of 10% [Crowson et al 2006]. The prevalence of BCC varies depending on geographical location where the incidence is greater in countries with greater sunlight exposure.

There are three subtypes of BCCs, identifiable by their histology: superficial, nodular and morpheic. Morpheic is the most aggressive and nodular the most common (Crowson, 2006) (Figure 8). Superficial BCCs appear as ulcers on the surface of the skin and histologically, they form a mass of cells below the epidermis. These extend from the dermis to the papillary dermis and have an increased risk of reoccurring if they are not fully removed (Saldanha et al., 2003).

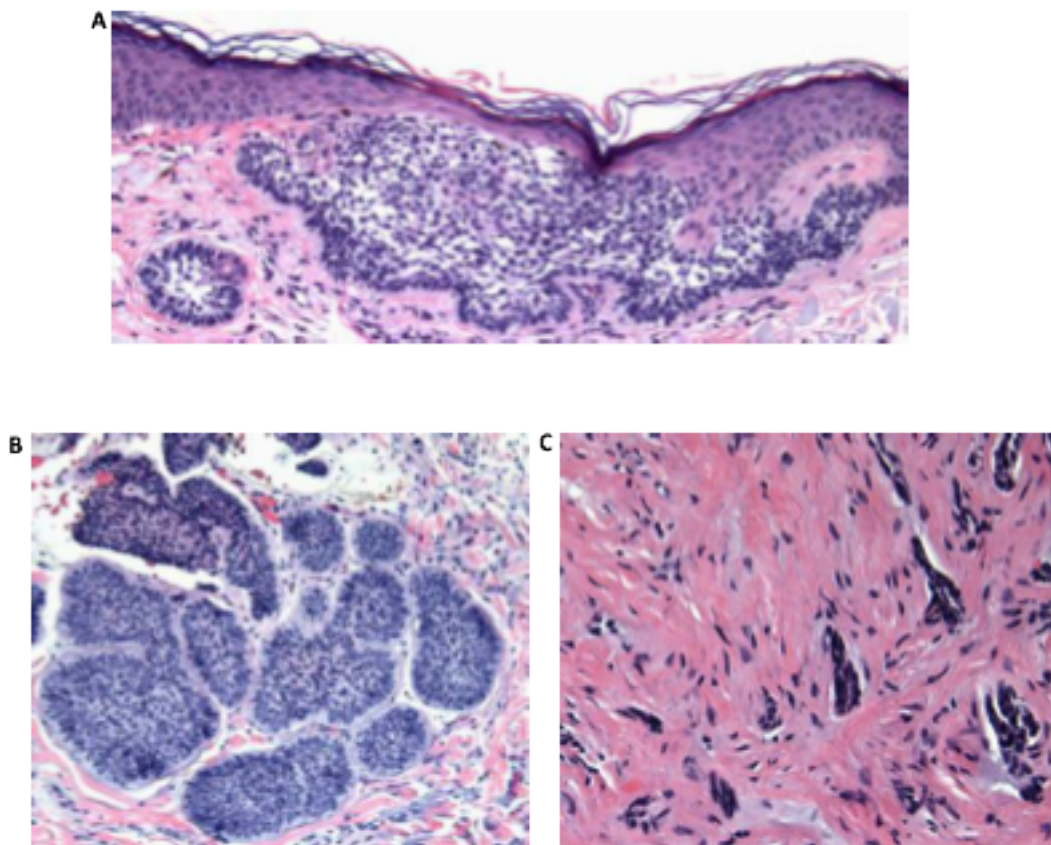


Fig.8 BCC histology Histological section of [A] superficial, [B] nodular and [C] morpheic BCC (Crowson, 2006).

Although the majority of BCCs arise sporadically, several cases are attributable to the basal nevus syndrome, also known as Gorlin syndrome, an autosomal dominantly inherited disorder characterized by the occurrence of multiple BCCs and of extracutaneous tumors, that was first described by Professor Robert J Gorlin in 1960 [Gorlin RJ. et al. 1960]. Genetic studies on patients with BCNS have led to the identification of inactivating mutations located on chromosome 9p22, specifically in the human homologue of the *Drosophila* gene *Ptch1*, as the genetic defect underlying this syndrome [Jonhson RL. et al. 1996; Hanh H. et al. 1996]. The same loss of function mutations were found in sporadic BCCs from patients without BCNS [Gailani ME. et al. 1997]. The activation of Hedgehog signalling was then confirmed by the increased expression of the GLI-1 transcription factor. [Ghali L. et al. 1999]

BCCs very rarely metastasize but they are locally aggressive and 5-9% may have multiple recurrences [Marcil I. et al 2000]. Moreover they can cause significant scarring and disfigurement. This is mainly on the head or neck

however, it is potentially more damaging if located around the eyes. Surgery is curative for most patients; other common treatments include cryotherapy and radiotherapy while Imiquimod and photodynamic therapy (PDT) are more recent forms [Lien MH. et 2011]. Imiquimod based creams are applied to the tumour to cause an inflammatory response to destroy the lesion. 74% of patients reported complete remission of the tumours; however, this is only used to treat superficial BCCs. PDT involves applying a photosensitive drug to the tumour and upon activation of the drug by light, oxygen radicals are released that induce cell death with a cure rate reported to be 79%. However, for those few that develop locally advanced or metastatic BCC, there was no effective treatment. Then at the beginning of 2012, GDC-0449, a Genentech molecule, received the FDA approval. GDC-0449 is a SMO antagonist, that has shown a 50% response in metastatic tumours and 60% in advanced local tumours.

1.6.3 Ultraviolet radiation and Basal cell carcinoma

The p53 tumour suppressor gene plays an important role in cellular regulation. Its functions include cell cycle arrest, DNA damage repair and initiation of apoptosis. It is well documented that half of all BCCs have mutations of the TP53 gene [Soleti et al., 2009; Rady et al., 1992] with BCCs most commonly developing on sun exposed skin. The frequency of BCCs was shown to increase with patient age, which implies that longer exposure to UV light may cause mutations of p53. CC to TT or C to T transitions at di-pyrimidine sites of the p53 gene were found in UV exposed tumours resulting in the loss of function of the protein [Mancuso et al., 2004; D'Errico et al., 1997; Deneff et al., 2000; Zhang et al., 2001]. Due to this, the cells are unable to repair DNA damage caused by UV exposure and may not undergo apoptosis. Indeed, p53 knockout mice have been shown to develop BBC-like tumours significantly earlier than wild type mice after UV irradiation.[Kim et al., 2002]

1.6.4 *In vitro* model of BCC

During my 10 months work experience at the Blizard Institute of Queen Mary University in London I have assisted Dr.Muhammad M.Rahman to create an *in vitro* model of BCC by suppressing PTCH1 expression in human keratinocytes using RNAi; this model has been used to determine the extent and nature of HH

signalling in human BCC (including control of the GLI transcription factors) as well as to determine how PTCH1 interacts with other major signalling pathways, particularly those that may influence the formation and progression of this common skin tumour.

1.6.5 Role of MYCN in basal cell carcinoma

Studies on medulloblastoma, a primitive neuroectodermal childhood malignant brain tumour arising from cerebellar granule neuron precursors, identified *NMYC* as a direct target gene of the Shh pathway, suggesting that N-Myc protein is an important downstream mediator of Shh-induced proliferation and tumourigenesis.[Heine VM. et al. 2010]

In their work, Freier and colleagues performed immunohistochemistry (IHC) and fluorescence in situ hybridisation (FISH) on 273 BCC specimens to assess the expression of N-Myc protein and gene copy numbers of the *NMYC* gene locus in a representative BCC tumour collection. High N-Myc protein expression was detected in 72.7% (160/220) of all BCC specimens. Strong N-Myc immunopositivity was more frequently found in infiltrative BCCs compared to nodular/superficial BCCs ($p=0.005$), and in BCCs of the head compared to BCCs of other anatomic localizations ($p=0.021$). The prevalence of *NMYC* copy number gains was 17.5% (37/211), including three tumours with nodular differentiation that exhibited a distinct high-level amplification of the *NMYC* locus. These data indicate that high expression of the Shh downstream mediator, N-Myc, is a frequent event in BCC, predominantly in more aggressive subtypes. [Freier K. et al. 2005]

1.6.6 Targeting therapies in BCC

Half a dozen pharmaceutical companies have embarked on Hedgehog Inhibitor (HHI) development, and BCCs that are not curable by local therapies are potential targets for trials of HHIs. The leading molecule has been Cyclopamine [Binns et al. 1963]. Cyclopamine was discovered when pregnant sheep that were eating the *Veratrum californicum* species of lily containing Cyclopamine, would carry embryos with holoprosencephaly (HPE). HPE is a developmental disorder where the midline of the face does not develop resulting in a cyclopic eye which has been linked to HH signalling as Cyclopamine was shown to

specifically inhibit SMO [Chen et al. 2002; Taipale J. et al. 2000]. SHH-/- knockout mice have also been reported to develop HPE. Cyclopamine has been shown to inhibit human medulloblastoma growth which has led to the proposal for HH antagonists as a valid treatment however non-canonical HH signalling and the development of BCC through this mode of signalling has important therapeutic implications. Due to the low affinity of Cyclopamine, synthetic derivatives have been developed such as BMS-833923 (Bristol-Myers Squibb), CUR-61414, HhAntag-691, IPI-926, MK4101, SANT1, SANT4 and Cyclopamine- KAAD.

The most encouraging results have been achieved by using the Genetech compound GDC-0449 Vismodegib, trade name ERIVEDGE. This compound has been approved by FDA in January 2012 after a phase II trial (Erivance BCC) conducted to fully evaluate the efficacy and safety of Vismodegib in patients with locally advanced or metastatic Basal cell carcinoma. In 33 patients with metastatic BCC, the independently assessed response rate was 30% (95% confidence interval [CI], 16 to 48; P=0.001). In 63 patients with locally advanced basal-cell carcinoma, the independently assessed response rate was 43% (95% CI, 31 to 56; P<0.001), with complete responses in 13 patients (21%). The median duration of response was 7.6 months in both cohorts. [Van Hoff D.D. et al . 2008; Tang YJ. et al. 2012]

The drug is also undergoing clinical trials for metastatic colonrectal cancer, small cell lung cancer, advanced stomach cancer, pancreatic cancer, medulloblastoma and chondrosarcoma.

The targeting of other HH components such as GLI with GANT58 and GANT61 are undergoing various phases of development.

1.6.7 EGFR signaling pathway in Basal cell carcinoma

Several studies suggest that HH can cooperate with EGFR signalling as the over expression of SHH in HaCaT immortalized keratinocytes that were grown in organotypic culture, induced a basal phenotype and promoted invasion of the cells into the collagen matrix. SHH expression was shown to increase the phosphorylation of EGFR, JNK and Raf as well as increase Matrix Metalloproteinase-9 (MMP-9) which has been implicated in cell invasion and tumour aggression. [Tai et al., 2008]

The epidermal growth factor receptor (EGFR) is the cell-surface receptor for members of the epidermal growth-factor family (EGF-family) of extracellular protein ligands [Herbst RS. et al. 2004]. Mutations affecting EGFR expression or activity could result in cancer.[Zhang H, et al. 2007].

Epidermal growth factor and its receptor was discovered by Stanley Cohen of Vanderbilt University. Cohen shared the 1986 Nobel Prize in Medicine with Rita Levi-Montalcini for their discovery of growth factors.

The binding activates several pathways principally the MAPK, Akt and JNK pathways, leading to DNA synthesis and cell proliferation [Oda K. et al. 2005]. Such proteins modulate phenotypes such as cell migration, adhesion and proliferation. Activation of the receptor is important for the innate immune response in human skin.

Studies have shown that EGFR signalling modulates the expression of GLI target genes in N/Tert human immortalised keratinocytes [Kasper et al., 2006]. 19 genes were found to be induced synergistically by GLI1 and EGF treatment also; GLI1 target genes were shown to be modulated by EGFR signalling through MEK/ERK pathways.

Studies have also identified that HH and EGFR synergy can induce oncogenic transformation which is mediated through EGFR activation of RAS/RAF/MEK/ERK. EGFR/MEK/ERK pathways are able to induce JUN signalling which is essential for oncogenic transformation. EGFR/MEK/ERK pathways also increase GLI1 and GLI2 expression. In mouse cells where BCCs develop as a result of activated HH signalling, inhibiting both EGFR and GLI signalling shows a reduction of BCC growth and therefore presents a potential therapeutic opportunity [Schnidar et al. 2009].

In contrast, Neill group has previously shown that the over expression of GLI1 in N/Tert cells reduces EGFR expression and that compact colony formation (a characteristic of BCC tumour formation) is associated with repressed ERK activity [Neill et al., 2008]. Lately we performed staining of a panel of BCCs that revealed no pERK expression in 13/14 tumours whereas pERK was expressed in the epidermis suggesting that its loss is important for tumour formation.

1.6.8 Role of HH pathway in SCLC

In 2009 BMS started a clinical trial to determine the maximum tolerated dose (MTD) of BMS-833923 administered in combination with carboplatin and etoposide followed by BMS-833923 alone in subjects with extensive-stage Small Cell Lung Cancer (SCLC). The trial is still ongoing [Tang JY. et al. 2012] There are infact several scientific evidences of HH involvement in SCLC. Park and colleagues found that Hedgehog is activated in SCLC cells independently of the lung microenviroment. They found that treatment with Cyclopamine, a Smo inhibitor, decreased the survival of SCLC cells in low serum and also decreased GLI1 mRNA levels. [Park KS. et al. 2011]

1.7 Murine models

Animal models of cancer provide an alternative means to determine the causes of and treatments for malignancy, thus representing a resource of immense potential for cancer medicine. The models described here identify what is the next step after an *in vitro* testing and the analysis of a molecule in a biological system more complex than cellular, more human-like.

The mouse (*mus musculus*) is among the most used species for preclinical studies; this is mainly due to its size, lifelenght, molecular and physiological similarities with man.[Frese KK. et al 2007]

1.7.1 Tumor xenograft models

The xenograft model is obtained through the injection of tumor cells in nude mouse and Severe Combined Immunodeficiency (SCID) mouse: these animals have deficits in the immune system and mainly in the lymphoid component. Nude mouse does not present thymus and for this reason is immunodeficiency in T-lymphoid cell and presents total loss of hair; the SCID mice present genetic alterations, these are reflected in lack of lymphoid B cells, T cells and natural killer cells (NK).

The term *xeno* means "external", infact it involves transplantation of cells, tissues or organs between different species of living beings. This technique differs from allo-transplantation, where donor and recipient belong to the same species.

Xenograft models can be divided into: 1) Ectopic xenograft models and 2) Orthotopic xenograft models. In the ectopic model transplant is made under the skin; in the orthotopic, instead, transplantation is in the same anatomical location where usually the tumor arises.

The orthotopic is largely considered more predictive of the clinical outcome. Studies are, indeed, closest to those observed in a clinical, vastly reducing false positives associated with an experimental drug. Moreover they are less expensive than transgenic models, with lower latency and suitable for all types of cancer. [Killion KK. et al 1999; Sharpless NE. et al. 2006]

1.7.2 Transgenic mouse models

The term transgenic was coined in 1981 by Gordon and Ruddle to describe an animal whose genome is introduced into an exogenous gene; in the 80s the term was extended to the experiments of "gene-targeting", a method used to insert genes into specific points of the genome and production of chimeric and knockout mice, in which one or more genes are selectively removed from the genome. Today transgenic animals are called the animals that have undergone any type of genetic specific modification.

The use of transgenic mice to study specific genes that cause the onset of determinate cancers is the best approach in spite of the use of xenograft animals. This choice depends by several reasons: the similarity of the histological tumor; the tumor is not usually immunogenic, but it develops in a immunocompetent mouse; the tumor develops spontaneous, and also it can present metastasis; it is possible to study a wide range of cancers.

SCLC transgenic mouse model

It has been very challenging to create a transgenic mouse model of SCLC. The issues were the cell of origin and its neuroendocrine features and several aberrational genetic patterns that are involved in this tumor.

So far Berns and colleagues created the best suitable mouse model of SCLC starting from the findings that high mutation frequencies of tumor suppressor genes Rb1 and Trp53 have been observed in human SCLCs. Introduction of both Rb1 and Trp53 lesions into pulmonary epithelial cells via mouse germ line

mutations is precluded by the embryonic lethality of Rb1 null mutants. They therefore decided to use the Cre-loxP system for introducing Rb1 and Trp53 mutations somatically in a broad range of lung epithelial cells. In a relative short time-span after lung epithelial cells were infected with Adeno-Cre virus [Lyons SK. et al. 2003], they observed small foci of NE cell proliferation in airways, and in these, both alleles of Rb1 and Trp53 were inactivated. These lesions progressed to dysplasia and histologically malignant lung tumors, displaying NE differentiation and SCLC morphology. These tumors, accordingly designated mouse small cell lung carcinomas (MSCLCs), were highly proliferative, invasive, and had a marked capacity to metastasize to liver, brain, adrenal gland, bone, and ovaries. Taken together, histopathology, immunophenotype, and patterns of growth and dissemination of MSCLC are indeed strikingly similar to human SCLC.[Meuwissen et al. 2001; Berns A. et al. 2005]

BCC mouse model

The identification of the pivotal role of HH signalling in BCC carcinogenesis stimulated the engineering of several models in which HH signalling could be manipulated and BCCs could be produced, some of which carry inactivating mutations in genes encoding inhibitors of HH signalling, and some of which carry activated mutants or overexpressed wild-type positive regulators of this pathway. These models have allowed studies of interventions — chemoprevention and chemotherapy — as well as more basic investigations into BCC tumorigenesis.

The first lesson derived from the models is that deregulated HH signalling is indeed crucial to BCC carcinogenesis. Thus, either constitutive or conditional overexpression of Gli1 [Nilsson M. et al. 2000] or of Gli2 [Grachtchouk M. et al. 2000] in keratinocytes can produce BCC-like proliferations in the skin. Similarly, expression of SMO carrying the activating mutations identified in human BCCs also can produce murine BCCs [Xie J. et al. 1999]. Furthermore, Ptch1^{+/-} mice develop BCCs, and those BCCs often have deletion of the wild-type copy of Ptch1 as well as upregulation of HH signalling [Aszterbaum M. et al. 1999]. Similarly, mice carrying one inactivated, mutant allele of the HH suppressor Sufu are also susceptible to BCC development [Svard, J. et al.2006]. Thus, mice carrying mutations in genes that encode at least four different components

of the HH signalling machinery develop BCCs, or at least skin tumours resembling BCCs.

Another lesson is that it seems that the degree of activation of HH signalling is correlated with the histological appearance — the stronger the activation, the more the tumours resemble human BCCs [Grachtchouk, V. et al. 2003].

As already reported, p53 loss of function is frequently found in human BCCs and in murine BCC-like lesions. This was shown first by the development of medulloblastomas in almost 100% of *Ptch1*^{+/-};*Trp53*^{-/-} mice as opposed to an incidence of less than 10% in *Ptch1*^{+/-} mice that have wild-type p53 [Wetmore C. et al. 2001]. Similarly, Epstein and coll. found that *Ptch1*^{+/-} mice in which p53 is deleted conditionally in K14-expressing keratinocytes have a marked enhancement of BCC carcinogenesis [Aszterbaum M. et al. 1999]. Therefore, the high incidence of p53 mutations in human BCCs is probably not simply caused by the fact that BCCs usually arise in sun-exposed skin, but rather reflects the ability of p53 loss to contribute to the development of BCCs and perhaps to that of other HH-driven tumours as well.

Finally, results of pharmacological interventions in the *Ptch1*^{+/-} mouse seem so far to correlate well with results of the same interventions in humans. For example, topical application of the retinoid tazarotene, a retinoic acid receptor- β/γ ligand that is widely used for treatment of acne, (see later) inhibits BCC development in the *Ptch1*^{+/-} mouse and has clear anti-BCC efficacy in humans. Similarly, we have found that systemic non-steroidal anti-inflammatory drugs, such as celecoxib, weakly inhibit BCC carcinogenesis in both human and mouse *PTCH1*^{+/-} individuals.

Gene	BCC as a result of overexpression (transgenic)	BCC as a result of knockout
<i>Shh</i>	Yes	No
<i>Ptch1</i>	No	Yes
<i>Smo</i>	Yes	No
<i>Sufu</i>	No	Yes
<i>Gli1</i>	Yes	No
<i>Gli2</i>	Yes	No

Table 2 Occurrence of basal cell carcinoma (BCC) in mouse models

For our immunohistochemical analysis, in particular, we have used tissues from mice lacking one *Ptc1* allele (*Ptc1*^{neo67/+}), derived by gene targeting of 129Sv embryonic stem cells and maintained on the outbred CD1 strain background, X-ray irradiated at the estimated time of the second anagen, active growth phase of hair follicles, [i.e., 35 days (n = 60)] or of the second telogen, resting phase of hair follicles, [i.e., 60 days (n = 56)]. [Mancuso M. et al. 2004]

1.8 Molecular imaging

Bioluminescence imaging (BLI) is increasingly being used to provide quantitative and more rapid assessment of drug efficacy in preclinical oncology research. BLI of firefly luciferase (*Photinus pyralis*; FLuc) activity provides a cost-effective and extremely sensitive method for imaging fundamental biological processes in vitro and in vivo [6-8]. In vivo BLI is an excellent method to gain a dynamic, longitudinal profile of engraftment. Luciferase oxidizes luciferin in the presence of adenosine tri-phosphate (ATP) and oxygen to form an electronically excited oxy-luciferin species. Visible light is emitted following the relaxation of excited oxy-luciferin to its ground state [Sadikot R. et al. 2005]. Because this light can be transmitted through mammalian tissues, it is possible to use bioluminescence for non invasive and quantitative monitoring of tumors burden.

In nature there are different bioluminescent systems characterized by a specific enzyme system. The most used bioluminescent system in scientific research is the North American firefly luciferase, but several clones of luciferase were identified from jellyfish (*Aequorea*), from the sea pansy (*Renilla*), from corals (*Tenille*) and from various bacteria as *Vibrio fischeri* and *V. harveyi*.

Luciferase is an excellent marker for gene expression because it lacks post-translational modifications and has a half-life ($t_{1/2}$) *in vivo* of about 3 hours.

The spectrum of light is between 530 and 640 nm with an emission peak at 562 nm. This emission spectrum, coupled to the optical properties of tissue, allows light to penetrate through several centimeters of tissue. In this way it is possible to detect light emitted from the internal organs of small mammals that express the luciferase as reporter gene. The photons are detected by a special Charge Coupled Device (CCD) camera that convert photons into electrons. The CCD

camera spatially encoding the intensity of the incident photons into electrical charge patterns to generate an image. This camera is controlled by a computer for image acquisition and analysis.

The BLI is widely used in cancer research for identifying metastasis and to measure the proliferation of tumor cells that express luciferase. Some studies done using HeLa luminescent cells injected into the tail vein of immunodeficient mice have demonstrated the utility of BLI in the early detection of lung metastases. Similarly, other studies have shown that bioluminescence is a powerful methodology for understanding the pathogenesis of the disease *in vivo*. It has been shown that the detection of tumor cells in internal organs by BLI has a sensitivity at least equal to that of positron emission tomography (PET). Moreover BLI does not require toxic and radioactive tracers, only administration of D-luciferin, non-toxic even in newborn pups. [Dohlen G. et al. 2008]

1.8.1 Transfection of cell lines throughout retroviral vectors

Recombined retroviruses have been widely used to obtain stable expression of heterologous genes in the mammalian cells. The most commonly studied and used retroviruses are those belonging to the Retroviridae subclass. This retrovirus typology is modified and it has lost its replicative capacity because it does not present some genes express within the wild type strain. They allow the stable integration of transgenes within the eukaryotic cells genome. [Blesh A. et al. 2003]

Retroviruses are viruses whose genome consists in a single-stranded RNA of around 10 Kb of size with a region ψ for the packaging. It includes three essential genes, *gag*, *pol*, *env*. They codify respectively for the core proteins, the inverse transcriptase and the capsid.

Long Terminal Repeats (LTR) are placed to each edges and these sequences are implied in the integration phase. LTRs are divided in three regions: U3, R and U5. The 5' R is defined as the initial signal sequence for the transcription phase in the 5' LTR, whereas the U3 region contains both the promoter and the enhancer element. Moreover, the U3 region contains the signal of polyadenylation. During the retro-transcription, the U3 region at the 3' LTR and

the U5 region at the 5' LTR of the viral RNA are duplicated (Figure 9). Once the cell is infected, the RNA is retro-transcribed in a double DNA filament that enters in the nucleus and it is integrated in the genome of the host cell, expressing in this way the viral proteins. Simple retroviruses such as MLV are unable to cross the nuclear membrane and the infection is restricted to cells in mitosis, when the nuclear membrane is dissolving.

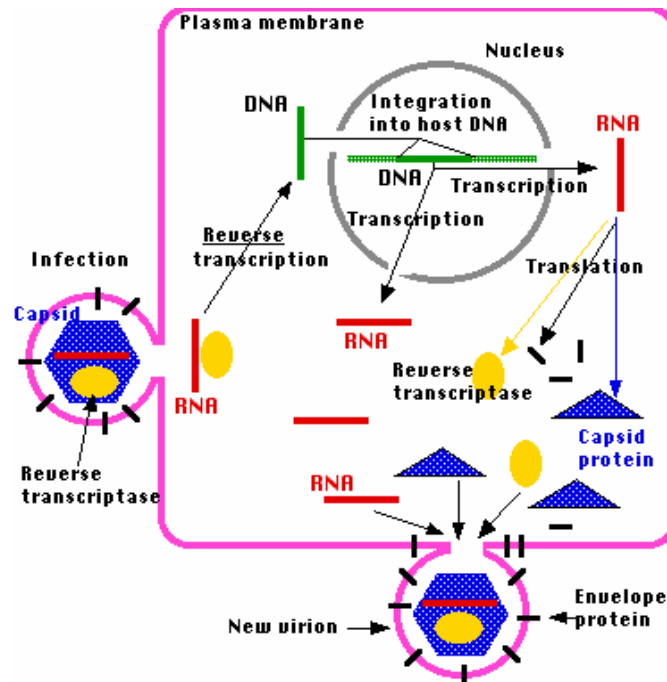


Fig.9 Life cycle of retrovirus.

The most common retroviral vectors are derived from MLV (Moloney Murine Leukaemia Virus), an amphotropic virus able to infect both human and murine cells.

In these vectors, viral genes are replaced by the transgene of interest, which is inserted between the LTRs downstream packaging signal and the promoter. They can also be added with marker genes (such as neomycin) and alternative promoters of viral origin.

The gag, pol and env coding regions are separated into distinct transcriptional units to decrease the risk of production of wild-type virus through recombination, and added to cell lines that are called packaging cells. The packaging cells are able to generate a complete virion, but empty because they do not contain the sequence ψ and cannot package the viral genome in the virion. The viral vector instead contains the transgene downstream of ψ , and thus, if inserted into a

packaging line, it produces a viral progeny which virion is provided by the packaging line and the genome is the recombinant viral vector containing the transgene .

The range of cells that can be infected by recombinant retroviruses thus produced, depends on the type of envelope protein in the virion. We can distinguish ectotropic retrovirus, which can only infect cells of rodents and anfortropic retrovirus, which infects almost all mammalian cells.

The choice of vector system is highly dependent on target cells. Generally, vectors derived from MLV are easier to produce and, to date, are available in a wide range of packaging cells. However, infection by these viruses is extremely low in quiescent cells or low growth rate and therefore should be used only in cells with high growth rates such as tumor cells.

CHAPTER 2

AIM OF THE STUDY

Human small cell lung cancer (SCLC) accounting for approximately 15-20% of all lung cancers, is an aggressive tumor with high propensity for early regional and distant metastases. Chemotherapy is the primary treatment option, leading to a 5 year survival of approximately 20% in LD and less than 5% in ED. Although the initial tumor rate response to chemotherapy is very high, SCLC relapses after approximately 4 months in ED and 12 months in LD.

Basal cell carcinoma (BCC) is the most prevalent cancer in the Western world, and its incidence is increasing worldwide. This type of cancer rarely metastasizes and the death rate is extraordinary low. Surgery is curative for most of the patients, but for those that develop locally advanced or metastatic BCC there is currently no effective treatment. Moreover surgery is expensive, in total the cost of care for non-melanoma skin cancers is the fifth highest for all cancers in US.

Both types of cancer have been deeply investigated and several genetic alterations have been found. These alterations could become targets for new pharmacological therapies.

New drug must be investigated through preclinical and clinical studies. Especially, prediction of human tumor response based on preclinical data could reduce the failure rates of subsequent new anticancer drugs clinical development.

Therefore, the aims of the study were the following:

1- To create and characterize a novel BLI xenograft orthotopic mouse model of SCLC to evaluate the tumor onset and progression and the efficacy of new pharmacological strategies.

2- To compare an in vitro model with a transgenic mouse model of BCC and to investigate and delineate the canonical Hedgehog signaling pathway and its connections with other molecular pathways. Thus may lead to potential new therapies, less invasive than surgery.

CHAPTER 3

MATERIALS AND METHODS

3.1 Small cell lung cancer

3.1.1 Cell lines

In Table 1, all the SCLC cell lines that have been characterized for MYC family genes. After this characterization the most representative have been chosen for *in vitro* proliferation assays, chemotherapeutic treatments and orthotopic mouse model.

Three of the members of the MYC family, *MYC*, *NMYC* and *LMYC*, have been shown to be amplified in tumors and tumor cell lines from patients with small cell lung cancer.[Johnson BE. et al. 1996]

CELL LINE	MEDIUM	CHARACTERISTICS
H69	RPMI 1640 + FBS 10%, L-glutammin 1% and antibiotics, penicillin and streptomycin 1%	Small round cells growing in medium- large aggregates. Source: Lungs Expression of myb, fes, fms, raf, ras mRNA c-met and p53 mutations
H526	RPMI 1640 + FBS 10%, L-glutammin 1% and antibiotics, penicillin and streptomycin 1%	Small round cells growing in medium- large aggregates. Source: Lungs Expression of myb, fes, fms, raf, ras and c- kit mRNA
N592	RPMI 1640 + FBS 10%, L-glutammin 1% and antibiotics, penicillin and streptomycin 1%	Small round cells growing in medium- large aggregates.
GLC14	RPMI 1640 + FBS 10%, L-glutammin 1% and antibiotics, penicillin and streptomycin 1%	Small round cells growing in aggregates. Source: Supraclavicular node biopsy before the start of chemotherapy

H378	RPMI 1640 + FBS 10%, L-glutammin 1% and antibiotics, penicillin and streptomycin 1%	Small round cells growing in aggregates. Source: metastatic site, pleural effusion.
H1618	HITES + FBS 10%, L- glutammin 1% and antibiotics, penicillin and streptomycin 1%	Small round cells growing in aggregates. Source: metastatic site, bone marrow.
H510	RPMI 1640 + FBS 10%, L-glutammin 1% and antibiotics, penicillin and streptomycin 1%	Small round cells growing in aggregates.
H510A	RPMI 1640 + Ham's F12 (1:1) + FBS 10%, L- glutammin 1% and antibiotics, penicillin and streptomycin 1%	Adherent cells. Source: metastatic site, adrenal gland.
H82	RPMI 1640 (w/o phenolred) + FBS 10%, L-glutammin 1% and antibiotics, penicillin and streptomycin 1%	Small round cells growing in medium- large aggregates.
DMS-79	RPMI 1640 + FBS 10%, L-glutammin 1% and antibiotics, penicillin and streptomycin 1%	Small round cells growing in medium- large aggregates. Expression of v-fes, c-raf1, H-ras, K-ras and N-ras, and SHH proteins. After treatment they produce ectopic ACTH.
H146	RPMI 1640 + FBS 10%, L-glutammin 1% and antibiotics, penicillin and streptomycin 1%	Small round cells growing in medium- large aggregates. Expression of myc, myb, fms, raf, ras
GLC16	RPMI 1640 + FBS 10%, L-glutammin 1% and antibiotics, penicillin and streptomycin 1%	Small round cells growing in medium- large aggregates. Source: Supraclavicular node biopsy after chemotherapy
GLC19	RPMI 1640 + FBS 10%, L-glutammin 1% and antibiotics, penicillin and streptomycin 1%	Small round cells growing in medium- large aggregates. Source: Supraclavicular node biopsy after second reinduction therapy for relapsed SCLC

Cell lines were subcultured at 37°C / 5% CO₂ weekly.

The generation of luciferase positive SCLC-cell lines required Phoenix cell line (Phoenix Retroviral Expression System, Orbigen). Cell culture was maintained in DMEM medium (SIGMA-ALDRICH, Milwaukee, WI) supplemented with 10% FBS (Euroclone, Pero, Milano, Italy), 1% L-glutamine 2mM (GIBCO-Invitrogen, Carlsbad, CA), 1% streptomycin/penicillin antibiotics (GIBCO-Invitrogen, Carlsbad, CA).

3.1.2 RNA isolation and gene expression analysis

Total RNA was extracted from 2x10⁶ SCLC cell lines and from 30 mg of frozen tissues according RNAspin Mini RNA Isolation Kit (GE Healthcare, UK): after homogenization, add 350 µl Buffer RA1 and 3.5 µl β-mercapto-ethanol to the samples. To clear the lysate filter it with a RNAspin Mini Filter unit. Centrifuge 1 min at 11000 x g, add 350 µl 70% ethanol, mix the samples and load them into a RNAspin Mini column. After 30 sec at 8000 x g, add 350 µl Membrane Desalting Buffer, centrifuge for 1 min at 11000 x g to dry the membrane. Centrifuge for 1 min at 11000 x g, digest DNA with 95 µl of DNase reaction mixture, incubate for 15 min at room temperature. Wash the membrane with 200 µl Buffer RA2, centrifuge 11000 x g for 1min, add 600 µl Buffer RA3, centrifuge 11000 x g for 1 min, add 250 µl Buffer RA3, centrifuge 11000 x g for 2 min. Elute the RNA in 40 µl H₂O RNase-free. Each RNA sample was quantified twice with the NanoDrop ND-1000 spectrophotometer (NanoDrop Technologies, Wilmington, DE). The 2 µg RNA (final volume of 10 µl) was reverse transcribed using Superscript II RNaseH (Invitrogen): add 1 µl dNTP 10 mM and 1 µl oligo dT to 10 µl of sample, incubate the mix for 5 min at 65°C and for 1 min in ice. Add 4 µl Buffer 5x, 2 µl DTT 0.1M, 1 µl RNase OUT to the sample, incubate at 42°C for 2 min, add 1 µl of Superscript II (50U), incubate at 42°C for 50 min and at 70°C for 15 min. Quantitative PCR analysis was performed to confirm MYCN over expression and to analyse the efficacy of the PNA treatments. We used LightCycler® 480 Roche, according to the manufacture's instruction and SYBR Green I Master (Roche Applied Science, Mannheim, Germany). The real-time

quantitative PCR was performed added to 10 ng cDNA (4 μ l final volume), 10 μ l Fast Star SYBRGreen MasterMix 2x (Roche), 0.6 μ l primers forward and reverse 10 nM and water to final reaction volume of 20 μ l. PCR reaction conditions were 2 min at 50°C, 10 min at 95°C, for 50 cycles: 15 sec at 95°C, 60 sec at 60°C. Each sample was amplified in triplicate. $\Delta\Delta$ Ct calculations were used to determine the level of expression of target genes relative to reference control and to a calibrator (untreated samples or normal tissue).

The primer sequences for analyse MYCN over expression in SCLC tumors, SCLC cell lines and to test the efficacy of PNA treatment are:

- MYCN forward: 5'-CGA CCA CAA GGC CCT CAG T-3'
- MYCN reverse: 5'-TGA CCA CGT CGA TTT CTT CCT-3'
- MYC forward: 5'-CAC CTG AGA CTG AAA CCG TAC AA-3'
- MYC reverse: 5'-CTT CTG CAA ATC TGG ATG GC-3'
- MYCL forward: 5'-CAA GCG ACT CGG AGA ATG AA-3'
- MYCL reverse: 5'-GCA TGG AGA TGT GGA AAT GCT T-3'
- ATPs forward: 5'-TCA CCC ACA CTG TGC CCA TCT ACG A-3'
- ATPs reverse: 5'-CAG CGG AAC CGC TCA TTG CCA ATG G-3'
- β -ACT forward: 5'-TCA CCC ACA CTG TGC CCA TCT ACG A-3'
- β -ACT reverse: 5'-CAG CGG AAG CGC TCA TTG CCA ATG G-3'

3.1.3 Protein extraction

The N-myc protein was assessed in total protein extracts. The total proteins were extracted resuspending the pellet of cells or homogenized tissues in RIPA buffer (ROCHE) lysing solution added with 4 Protease Inhibitors (Aprotinin, Leupeptine, Phenylmethanesulfonyl fluoride, Sodium Orthovanadate SIGMA) in a 1:200 rate. con l'aggiunta di quattro inibitori delle proteasi in rapporto 1:200. After 10 min of incubation on ice, the sample was centrifuged at 15000 x g for 3 min at 4°C and the supernatant was collected containing total cellular proteins.

Protein were quantified with BCA method [Smith PK. et al. 1985] and the standard curve was constructed using known amounts of BSA protein (Bovine Serum albumin), by NanoDrop ND-1000 spectrophotometer (NanoDrop Technologies, Wilmington, DE).

3.1.4 Western Blot analysis

Proteins were separated by one-dimensional gel electrophoresis in denaturing conditions (SDS-PAGE: Sodium Dodecyl Sulphate - Polyacrylamide Gel Electrophore). The samples, containing 100 micrograms of proteins were solubilized by incubation at 95°C for 5 min after the addition of 2X Laemmli sample buffer (125 mM Tris pH 7, 4% SDS, 20% glycerol, 10% β -mercaptoethanol and bromophenol blue 0.004%) and water to a volume of about 20 μ l. Following the preparation of Separating gel 7-10% (7-10% acrylamide, 375 mM Tris pH 8.8, 0.1% SDS, 0.1% APS, TEMED 0.1%) and 4% stacking gel (4% acrylamide, 125 mM Tris pH 6.8, 0.1% SDS, 0.1% APS, TEMED 0.1%), the samples were loaded in gel electrophoresis and run at 160 V for about 60-90 min in electrophoresis buffer (125 mM Tris, 0.96 M glycine and 0.5% SDS) with a molecular weight marker, SeeBlue Plus2 Pre-Stained Standard (Invitrogen).

Proteins were separated by SDS-PAGE and they were transferred to PVDF membrane (polyvinylidene fluoride, Hybond-P, Amersham Biosciences) by western blot using the Bio-Rad wet system (Mini Trans-Blot Cell). The membrane was activated in methanol for 10 sec and then rebalanced in water for 5 min. Sponges and filters, before use, were soaked in transfer buffer (25 mM Tris, 192 mM glycine, methanol 10%), and then were assembled filter-sponge-gel-membrane-filter-sponge and the transfer was performed in transfer buffer at 250 mA for 2 hours. The membrane was subjected to successive incubation of 1 hour at room temperature with blocking solution (PBS, Tween 0.2% and 5% milk), and subsequential over-night incubation with the primary antibody: mouse monoclonal N-myc IgG (NCM II 100, Calbiochem) or mouse monoclonal $\beta\beta$ -actin (Calbiochem). After 3 washes in PBS and Tween 0.2%, incubated with corresponding secondary antibody Sheep anti-mouse IgG-HRP (horseradish peroxidase) (Amersham Biosciences). All antibodies were diluted in PBS+Tween 0.2% and 3.5% BSA (1:200 N-Myc and 1:10000 N-Myc anti-mouse).

The membrane was washed 3 times in PBS and 0.2% Tween for 5 min and was incubated for 1-2 min in the dark with the ECL detection solution (Amersham Biosciences). The survey was carried out to ChemiDoc (Biorad), using the program QuantityOne.

3.1.5 Fluorescence In Situ Hybridization (FISH)

FISH analysis was performed on fixed SCLC cells and on paraffin embedded tissue to confirm MYCN amplification. The tissue slides were treated with Paraffin Pre Treatment Kit from Abbott Molecular Inc (Des Plaines IL 60018 USA) and FISH analysis was performed according to the protocols recommended by the manufacturer (Vysis Inc., Downers Grove, IL, USA). Specific locus probe for MYCN (LSI-N-MYC(2p24), Vysis) and centromeric probe for chromosome 2 (CEP2(2p11.1-q11.1), Vysis) were used. Hybridization signals were analysed on a Olympus BX51 microscope coupled to a Cytovision Ultra system (Applied Imaging, Sunderland, UK).

3.1.6 *In vitro* treatment

To assess the cytotoxic and proliferative effects of chemotherapeutic drugs, on H69, H526 and GLC14 cell lines, at 72 hours, I used the Adenosine TriPhosphate monitoring system based on firefly (*Photinus pyralis*) luciferase (ATPlite™ Perkin Elmer, Waltham, MA, USA). The experiments were performed on 96-well microplate adding 50 µl of mammalian cell lysis solution to a 100 µl cell suspension. After 5 min in an orbital shaker at 700 rpm, I added substrate solution containing luciferase and D-luciferin. After 5 min in an orbital shaker and 10 min at dark the emitted light was measured with Infinite F200, TECAN. The measured luminescence is proportional to the ATP concentration. ATP is a marker for cell viability because it is present in all metabolically active cells and the concentration declines rapidly when the cells undergo necrosis or apoptosis. (ATPLT-0408 / REV. F). Each experiment was performed at least four times. The concentration range used is shown in the table below.

	Stock solutions[µM]	Range [µM]
Cisplatin (CDDP)	3300	400 – 200 – 100 – 50 – 25
Carboplatin (CBDCA)	2690	600 – 300 – 150 – 75 – 37,5
Etoposide (VP-16)	33900	140 – 70 – 35 – 17,5 – 8,75

After this, we performed new experiments to obtain the EC50 for each drug.

The dilutions range this time was:

	H69	N592	GLC14
CDDP	40 μ M	400 μ M	400 μ M
	4 μ M	200 μ M	200 μ M
	0,4 μ M	100 μ M	100 μ M
	0,0004 μ M	50 μ M	50 μ M
	0,000004 μ M	25 μ M	25 μ M
CBDCA	600 μ M	600 μ M	600 μ M
	300 μ M	300 μ M	300 μ M
	150 μ M	150 μ M	150 μ M
	75 μ M	75 μ M	75 μ M
	37,5 μ M	37,5 μ M	37,5 μ M
VP-16	140 μ M	140 μ M	140 μ M
	70 μ M	70 μ M	70 μ M
	35 μ M	2,8 μ M	35 μ M
	17,5 μ M	0,028 μ M	17,5 μ M
	8,75 μ M	0,00028 μ M	8,75 μ M
		0,000028 μ M	

Cisplatin/Etoposide combination treatment

Cisplatin in combination with etoposide is now considered to be the standard first-line treatment of SCLC. The main goal is to achieve better results with lower doses of the two drugs and to improve their toxicological profile.

After the EC50 evaluation of each drug we performed a combination experiment using H69 cell line treated with CDDP and VP-16 at the same time.

EC50 1/2 of each drug has been added and citotoxic effect evaluated via ATPlite.

3.1.7 PNA treatment

The PNA was designed as homologous to a unique sequence of the noncoding (antisense) strand in exon 2 of MYCN (bp 1,650-1,665: 5'-ATGCCGGGCATG ATCT-3'; Genbank accession no. M13241). This PNA antigene (PNAs), which is

complementary to a unique sequence in the DNA strand, was designed to directly inhibit mRNA synthesis. To test the specificity of the activity of this PNAs, a mismatched PNA (PNAmt) was also designed containing a 3-base substitution (5'-GTGCCGAGCATGGTCT-3'). Specificity was verified using the BLAST homology program. All the PNA molecules were covalently linked to their COOH terminus with a nuclear localization signal (NLS) peptide (PKKKRKV) to mediate transfer across the nuclear membrane [Tonelli R. et al . 2005]. Synthesis, purification and characterisation of the PNAs and PNAmt was made by our laboratory as described.[Pession A. et al. 2004]

PNAs-NLS was added at concentrations of 2.5, 5, 10 μ M on H69 cell line growth in Optimem added with 0.25% of FBS. Cells were harvested and analysed at 24, 48 and 72 hours after treatment.

3.1.8 Generation of luciferase-positive SCLC cell lines

The pMMP-LucNeo vector (Figure 10), a generous gift from Prof. A. Kung (Harvard University, Boston) was used to transform in XL1 E.coli competent cells (Agilent Technologies, Stratagene, La Jolla, CA).



Fig.10 pMMP-LucNeo vector

One microgram of plasmid DNA was used to transform E. coli with heat shock at 42°C for 30 sec, bacteria were grown overnight at 37°C in LB medium composed of 5 g bacto-yeast extract, 10 g bacto-tryptone, 10 g NaCl, 1 ml ampiciline 1 mg/ml and 1 l water. The plasmid DNA was extracted and purified with QIAfilterPlasmid Maxi Kit (QIAGEN, Duesseldorf, Germany), the DNA was quantified using NanoDrop ND-1000 (NanoDrop Technologies, Wilmington, DE).

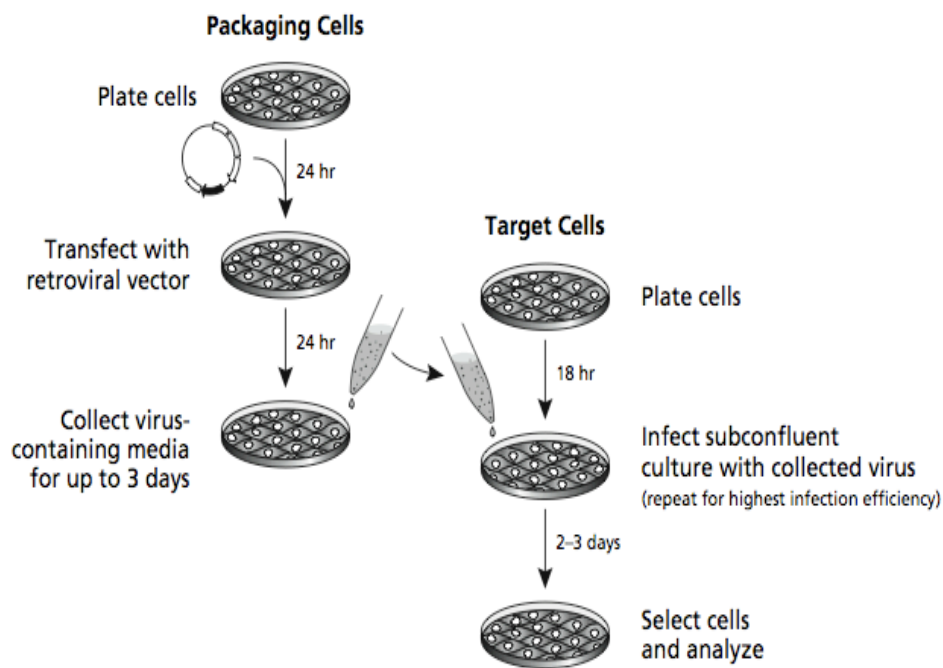
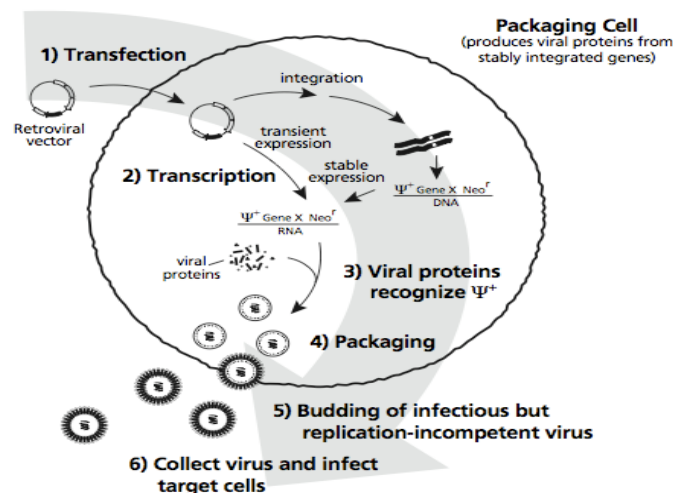


Fig.11 Transfection scheme

For each of the four SCLC cell line selected (H69, H526, DMS79 and GLC14), Phoenix packaging cells were seeded 2.8×10^5 cell/well in a six wells plate, the day after the cells were transfected with 5 μ g plasmid DNA and 10 μ l Lipofectamine 2000 reagent (Invitrogen, Carlsbad, CA) in 1 ml of DMEM for 5 hours at 37°C. After the incubation 1 ml DMEM with 20% FBS was added and the day after the medium was changed. 1ml of medium contained retroviral vector particles, produced in the Phoenix packaging cell line, were filtered and introduced into SCLC cell lines with Polybrene 8 μ g/ml (Millipore, Billerica, MA)

and 5 ml fresh medium. 5×10^5 cells of H69, H526, DMS79 and GLC14 were seeded 12 hours before the infection (Figure 11).

After transduction, the SCLC cell lines were selected with 1 mg/ml G418 (GIBCO-Invitrogen, Carlsbad, CA) for 14 days, then stable transfectants Luciferase expression in 105 live intact cells was examined using Luciferase Assay Reagent (Promega, Madison, WI) and measured with a spectral scanning multimodal plate reader (Varioskan Flash, Thermo Scientific, Waltham, MA) in the 560-670 nm range of absorbance. Six different dilution (106, 105, 104, 103, 102, 10) of luciferase positive SCLC live intact cells were analysed on the LB 981 (Berthold Technologies) after added of 100 μ l of D-Luciferin Steady- Glo[®] Luciferase Assay System (Promega, Madison, WI).



3.1.9 Establishment orthotopic xenograft models

All experiments involving animals were reviewed and approved by the Bioethical Committee of Bologna University, Italy and by Italian Ministry of Health. Animals were kept under pathogen free conditions, with ad libitum access to food. Orthotopic xenograft models were established by injection of 1.5×10^6 H69 and H526 in 20 μ l NaCl solution. 6-week-old NOD/SCID mice (Charles River Laboratories, France) were anesthetized with 0.3 mg/kg body weight Zoletil 100 and Atropine Sulphate 1mg/ml, and injected in the pulmonary parenchyma through the ribs of the mice. No mice died as a result of this treatment. General physical status of the animals were recorded daily, and mice

were killed by cervical dislocation after being anesthetized with 0.3 mg/kg body weight Zoletil 100 (Virbac S.r.l., Carros Cedex, France), when showing signs of poor health. The cancer progression was monitored every 7 days for a total of 5 weeks. The tumour presence was confirmed in each models with Bioluminescence Imaging analysis and histology.

3.1.10 Molecular imaging

Mice anesthetized with 0.5 mg/kg body weight Zoletil 100 (Virbac S.r.l., Carros Cedex, France) in association with Atropine sulfate were i.p. injected with 150 mg/kg D-luciferin (Synchem OHG, Felsberg, Germany) dissolved in PBS, and were imaged with the low-light imager system LB981 (Pharmaceutical Sciences, S.Orsola-Malpighi Hospital, University of Bologna, Italy). To investigate the kinetics of the *in vivo* reactions, mice inoculated 14 days prior with H69-Luc cells were imaged for 20 min with sequential 1-min exposure. Mice were imaged for 20 min with sequential 1-min exposure during imaging sessions conducted immediately after i.p. injection of D-luciferin. The collected images were used to generate kinetics plot for luciferase, which were used to determine the optimal temporal windows for subsequent experiments.

Mice inoculated with H69-Luc cells were placed in supine positions inside the instrument and imaged for 3 min, beginning at 8 min after the luciferin injection. For each acquisition, the bioluminescent signal from the ROI was depicted as a pseudocolor image superimposed on a greyscale photographic image. The Winlight software version 2.9 of the low-light imager system LB981 (Berthold technologies, Wildbad, Germany) was used to analyze the BLI data. The luminescent signals were calculated as photon flux per second (ph/s) considering a ROI 2246 mm².

3.1.11 Treatments and *in vivo* antitumor efficacy evaluation

To validate our mouse model we used the same antitumoral agents given in clinic. Our goal is to evaluate the tumor regression in mouse and to correlate this regression with the human pathology course.

From man to mouse model

It is not possible to extrapolate the animal dose only by scaling down from human dose (HED), It is necessary to apply a formula named body surface area (BSA) normalization method [Reagan-Shaw S. et al. 2008]:

$$\text{Animal Dose (mg/kg)} = \text{Human Dose (mg/kg)} * (\text{Human } k_m / \text{Animal } k_m)$$

To convert the usual clinic mg/m² into the mg/kg, we can use the km values in table below [<http://dtp.nci.nih.gov>]:

Species	Weight (kg)	BSA (m ²)	K _m factor
Human			
Adult	60	1.6	37
Child	20	0.8	25
Baboon	12	0.6	20
Dog	10	0.5	20
Monkey	3	0.24	12
Rabbit	1.8	0.15	12
Guinea pig	0.4	0.05	8
Rat	0.15	0.025	6
Hamster	0.08	0.02	5
Mouse	0.02	0.007	3

Tab. Representative Surface Area (BSA) to weight ratios (km) for various species

Alternatively, the table below gives approximated factors for converting doses expressed in terms of mg/kg from one species to an equivalent surface area dose expressed as mg/kg in other species tabulated.

		To				
		Mouse 20g	Rat 150g	Monkey 3kg	Dog 8 kg	Man 60 kg
From	Mouse	1	1/2	1/4	1/6	1/12
	Rat	2	1	1/2	1/4	1/7
	Monkey	4	2	1	3/5	1/3
	Dog	6	4	2/3	1	1/2
	Man	12	7	3	2	1

To express a mg/m² dose in any given species as the equivalent mg/kg dose, divide the dose by the appropriate km factor.

Species	Weight (kg)	BSA (m ²)	K _m factor
Human			
Adult	60	1.6	37
Child	20	0.8	25
Baboon	12	0.6	20
Dog	10	0.5	20
Monkey	3	0.24	12
Rabbit	1.8	0.15	12
Guinea pig	0.4	0.05	8
Rat	0.15	0.025	6
Hamster	0.08	0.02	5
Mouse	0.02	0.007	3

In vivo treatments

In clinic the standard protocol to treat SCLC is an association between Cisplatin (CDDP) and Etoposide (VP-16). The treatment schedule is the following: VP16 110 mg/m² for three days and CDDP 60mg/m² only the first day [Puglisi M. et al. 2010]. The translated regimens exceeded the MTD currently found in literature [Houghton PJ. et al. 2010] so we decided to set the regimens as:

Etoposide 12 mg/kg day 1, 2, 3(First week); 15 mg/kg day 1, 2, 3

Cisplatin 3.5 mg/kg day 1(First week); 4.5 mg/kg day 1

The treatments started after 15 days from the first positive signal and was 4 weeks long. Etoposide and cisplatin were obtained from Hospital Drug Repository. The drugs were dissolved in physiological saline. As placebo control 5 mice were treated only with physiological saline.[Nemati F. et al. 2000]

Tumor regression evaluation after treatment

Tumor regression was evaluated by BLI. Weekly mice received an intraperitoneal injection of 150 mg/kg D-luciferin from Gold Biotechnology (St. Louis,MO,USA) and placed in the light-tight chamber of a cooled CCD camera system LB981 (Berthold technologies, Wildbad, Germany) under Zoletil anaesthesia. Photographic and luminescent images were acquired 8 min after D-luciferin injection in supine position for 3 minutes. The Winlight software version 2.9 of the low-light imager system LB981 (Berthold technologies, Wildbad, Germany) was used to analyze the BLI data. The luminescent signals were calculated as photon flux per second (ph/s) considering a ROI of 2246 mm².

3.1.12 Statistical Analysis

Both in vitro and in vivo data were presented as means \pm Standard Error Mean (SEM). In vitro data were from at least three independent experiments.

For the Xenograft mouse models the bioluminescence intensity relative to the tumor progression was reported as mean \pm SEM (standard error of mean) considering the photon flux (ph/s) as the sum of prone signals for each mouse after background subtraction.

3.1.13 Histology and immunohistochemistry

Each small cell lung cancer sample was divided into two parts. A piece was frozen in liquid nitrogen and it was kept at -80°C for molecular analysis and an other piece was fixed in formalin for histological analysis.

Murine tissues were fixed in 4% formalin, dehydrated, embedded in paraffin, cut into 4 μm sections and stained with hematoxylin an eosin (H&E) methods. Bone marrow and peripheral blood were evaluated with May-Grunwald-Giemsa staining. For H&E staining, tissue sections were subjected to subsequent incubations in toluene, 100% ethanol, 95% ethanol, 70% ethanol, distilled water, hematoxylin, distilled water, eosin, distilled water, 70% ethanol, 95% ethanol, 100% ethanol and toluene. After coverslip application, slides were observed by light microscopy. . For May-Grunwald-Giemsa staining, the slides with blood smears were subjected to subsequent incubation with May-Grunwald for 3 min, washing in water, incubation with Giemsa for 7 min, washing in distilled water. After coverslip application samples were observed by light microscopy.

SCLC tissue sections were processed for immunohistochemistry. Sections were subjected to subsequent incubations in xilene, 100% ethanol, methanol and 0,3% hydrogen peroxide, 96% ethanol, 70% ethanol, distilled water and then incubation in citrate buffer in pressure cooker. The sections were washed with 1x PBS, incubated with goat serum for 15 min at room temperature, washed with 1x PBS and incubated with 1:50 anti-N-Myc primary antibody (Oncogene) over night. The day after the slides were washed in 1x PBS and they were incubated with anti-mouse secondary antibody (DAKO, Evison) for 20 min. After wash in 1xPBS, they were developed with a 5% Di-Amino-Benzidine

chromogen in TAI Buffer pH 7.6 with 3% hydrogen peroxide. After wash in 1x PBS slides were subjected to subsequent incubations in distilled water, hematoxylin, distilled water, 70% ethanol, 95% ethanol, 100% ethanol and toluene. After coverslip application, slides were observed by light microscopy.

3.2 Basal cell carcinoma

3.2.1 NEB1 cell culture

The PTCH knockdown models were generated by M.Rahaman, as a part of his PhD course, using NEB1 cells which originate from epidermal keratinocytes and are immortalised using HPV16 [Morley et al. 2003]. NEB1 cells were retrovirally transduced with PTCH1 shRNA constructs termed 29A and 189A that target exons 3 and 24 respectively. A non-targeting scramble control vector was used to create a control cell line.

Scramble control non-targeting sequence: GCGCGATATATAGAATACG

29A target sequence exon 3: AAGGTGCTAATGTCCTGACCA

189A target sequence exon 24: AAGGAAGGATGTAAAGTGGTA

NEB1 cells were cultured in keratinocyte growth medium (KGM) consisting of Alpha MEM and heat inactivated foetal bovine serum (Lonza, Slough, UK), L-glutamine and penicillin/streptomycin (PAA Laboratories, Somerset, UK). The KGM supplement was made up of epidermal growth factor (EGF), hydrocortisone, insulin (bovine pancreas), adenine and cholera toxin (Sigma, Poole, UK). Cells were incubated at 37°C in 5% CO₂. Cells were passaged at 70% confluence, detached using Trypsin-EDTA

3.2.2 Pharmacological inhibitors

To investigate Hedgehog pathway and its connection with other pathways and their role in BCC aetiology, NEBs cell line were treated with several pharmacological inhibitors.

Inhibitor	Target	Company	Details
AG1478 (658552)	EGFR	Merck	Cell permeable, reversible, competitive inhibitor
Cyclopamine-KAAD (239804)	SMO	Merck	Cell permeable, competitive inhibitor
SANT1 (559303)	SMO	Merck	Cell permeable, competitive inhibitor
UO126 (662005)	MEK	Merck	Cell permeable, non-competitive inhibitor

3.2.3 RNA isolation and gene expression analysis

RNA isolation and gene expression analysis was performed as already reported in paragraph 3.1.2. The primer sequences designed to analyse selected gene overexpressions in BCC *in vitro* model were:

GENE	FORWARD PRIMER	REVERSE PRIMER	T°
DUSP6	CCGCAGGAGCTATACGAGTC	TTGAGCTTCTTGAGCAGCAG	60
EGFR	TCAAATTGTGCCGAACAAGA	ATCTGACATTGGGGTTCCAG	57
ELK	GAAGCCATTCCTTTGTCTGC	CCCTATTGAAAAGCCCCATT	60
FOS	GGAATTAACCTGGTGCTGGA	TCAGACCACCTCAACAATGC	60
GAPDH	GTGAACCATGAGAAGTATGACA	CATGAGTCCTTCCACGATACC	60
GLI1	GAAGACCTCTCCAGCTTGGA	GGCTGACAGTATAGGCAGAG	60
GLI2	TGGCCGCTTCAGATGACAGATGTTG	CGTTAGCCGAATGTCAGCCGTGAAG	58
JUN	ACAGAGCATGACCCTGAACC	CCACCATGCCTGCCCGTTG	60
PTCH1	ACTCGCCAGAAGATTGGAGA	TCCAATTTCCACTGCCTGTT	58
SMO	GGCTGCTGAGTGAGAAG	CTGGTTGAAGAAGTCGTAGAAG	58

3.2.4 Western Blot

Western Blot was performed as already reported in paragraph 3.1.3 and 3.1.4. We used the following primary antibodies (diluted 1:1000):

Antibody	Company	Type	Size(kDa)
EGFR	Santa Cruz	Goat polyclonal	170
ERK	Cell Signalling	Rabbit polyclonal	42, 44
GLI1 C18	Abcam	Rabbit polyclonal	27
GLI1 H300	Santa Cruz	Rabbit monoclonal	45
MEK	Cell signalling	Rabbit monoclonal	45
pEGFR Y845	Santa Cruz	Rabbit polyclonal	170
pEGFR Y1173	Santa Cruz	Goat polyclonal	170
pERK E10	Cell Signalling	Mouse monoclonal	42, 44
pERK 20G11	Cell Signalling	Rabbit monoclonal	42, 44
pMEK	Cell Signalling	Rabbit polyclonal	45
PTCH C20	Santa Cruz	Goat polyclonal	140
SMO C17	Santa Cruz	Goat polyclonal	85

3.2.5 Immunocytochemistry

Immunocytochemistry staining was used to determine the cellular localisation of proteins. Cells were initially seeded in 12 well plates on top of 18mm diameter glass cover slips (VWR International Ltd, Leicestershire, UK). The cells were washed twice with PBS before being fixed with 4% paraformaldehyde for 15 minutes. Cells were then washed with PBS three times and permeabilised in triton X-100 (Sigma, Poole, UK) for 10 minutes. The cells were then blocked in 3% BSA (Fisher Scientific, Leicestershire, UK) for 30 minutes followed by the addition of the primary antibody diluted 1:1000 in 3% BSA for 1 hour. Following three PBS washed for 5 minutes, a fluorescence dye labelled secondary antibody diluted to 1:800 in PBS was added and incubated for 1 hour while being protected by light. Alexa 488 and Alexa 568 secondary antibodies (Invitrogen, Paisley, UK) emit green and red fluorescence respectively. The cells

can also be stained for another antibody with an alternate secondary staining colour for co-localisation for example in which case, the primary and secondary antibody incubations were repeated. After three PBS washes, the nuclei of the cells were stained with 0.1 µg/ml of DAPI for 5 minutes before a final wash in PBS. Coverslips were mounted onto microscope slides using Vectashield fluorescence mounting medium (Vector Laboratories Ltd, Peterborough, UK) and stored at 4°C away from light. The slides were viewed and images taken on the Zeiss LSM 510 Meta Confocal Microscope.

Images taken by the confocal microscope were quantified using Image J software [Collins 2007]. Images were edited to only show the fluorescence channel of the protein of interest and then converted to greyscale. Cells were selected and analysed based on the intensity of pixels taking into account the size of the cell. The relative density was then calculated which indicates the intensity of staining.

3.2.6 Matrigel based organotypic culture

The Matrigel organotypic culture provides a base for an artificial skin model. A dermis layer is created using Matrigel, collagen and fibroblasts. Keratinocytes are then seeded on top of the 'dermis' layer and cultured with an air liquid interface where the fibroblasts grow in culture media but not the keratinocytes. This to an extent mimics the skin in vitro.

One day prior to the experiment, Matrigel (BD Pharmingen, NJ, USA) is taken from -20°C storage and allowed to defrost overnight at 4°C while on ice. On the day of the experiment, a mix is made up of 350 µl of Matrigel, 350 µl of Rat tail Collagen type 1 (Millipore, Watford, UK), 100 µl KGM media, 100 µl of FBS per gel. At this point, the mix is acidic therefore 1 M NaOH is added drop by drop until the solution changes from yellow to pink. 500,000 fibroblasts re-suspended in 100 µl are added to the mix and all components are gently mixed in a 50 ml falcon tube avoiding any bubble formation. 1 ml of the mix is dispensed into the well of a 24 well plate and left in the incubator at 37°C, 5% (v/v) CO₂ for 2 hours. Once the gel has set, 1 ml of KGM media is added to the top of the gel and incubated overnight.

The 1 ml of media was then removed from the gel and a 4.7 I.D x 8 mm cloning ring (Fisher Scientific, Leicestershire, UK) is pressed onto the gel within the well. This dislodges the gel from the walls of the well plate and provides an enclosed space to add 500,000 NEB1 cells resuspended in 500 μ l of KGM media. This ensures that the NEB1 cells settle and grow on the surface of the gel. The gel is incubated overnight at 37°C, 5% (v/v) CO₂.

Stainless steel wire gauze that is sculpted to provide a raised platform is placed within a 6 well plate. A single Cyclopore 0.4 μ m polycarbonate membrane with a 13 mm diameter (Whatman, Kent, UK) is placed on top of the gauze. The ring is removed from the gel and placed directly on the membrane. 4.5 ml of KGM media is added to the well ensuring that there are no bubbles underneath the gauze and that the media does not drown the gel. This allows the dermis part of the gel to receive media from the bottom while the NEB1 cells on the top do not. The organotypic model is incubated for 28 days or more with weekly media changes. At the end of the experiment, gels were either snap frozen or embedded in wax for histological sectioning.

3.2.7 Immunohistochemistry

To further investigate the activity of EGFR pathway in BCC, we performed immunohistological studies on human BCC and murine BCC. Mouse BCC tissues were kindly provided by Dr. Mancuso. In their laboratory in Rome, Dr Mancuso and colleagues created a Ptch^{+/-} mouse model that after X-ray irradiation during the telogen phase develop BCC-like tumors. If irradiated during the anagen phase of the hair cycle they develop more aggressive-infiltrative tumors. We used these tissues to perform classic immunohistochemical analysis as already reported in paragraph, using antibodies already listed in tab.

3.2.8 PTCH +/- mice colony

All the experiments involving animals were reviewed and approved by the Bioethical Committee of Bologna University, Italy and by Italian Ministry of Health. Animals were kept under pathogen free conditions, with ad libitum access to food. Ptch ^{+/-} mice were generated by M.P Scott and E.H. Epstein (Stanford University) and purchased from Jackson Laboratory (Bar Harbor, ME)

[88]. They were C57BL/6 and DBA/2J F1 hybrids, and were heterozygous for a deletion of exons 1 and 2 and insertion of the *lacZ* and *neo* genes. Genomic DNA was isolated from mouse-tail tips harvested when animals were 17 days old. The lysis buffer used is constituted of Tris 1 M pH8.5, EDTA 0.5 M pH8, NaCl 5 M, SDS 10% and water. Each tail tip was incubated over-night in agitation in 500 µl lysis buffer and 2.25 µl proteinase K(Sigma). The suspension was put in 500 µl iso-propanol, gently mixed and DNA tail was picked and put in 100 µl Elution Buffer over-night at 37°C. Each DNA sample was quantified twice with the NanoDrop ND-1000 spectrophotometer (NanoDrop Technologies, Wilmington, DE). The genotypes of *Ptch* +/- transgenic mice were determined by qualitative PCR analysis using primers: *PTCH* mutR CAC GGG TAG CCA ACG CTA TGT C; *PTCH* mutF GCC CTG AAT GAA CTG CAG GAC G; *PTCH* wtR CTG CGG CAA GTT TTT GGT TG; *PTCH* wtF AGG GCT TCT CGT TGG CTA CAA G. PCR reaction contained 300 ng gDNA, Buffer II 1x (Applied Biosystem, Roche), 0.2 mM dNTPs, 2 mM MgCl₂, 1 µM primer reverse and forward, 0.03 U/uL Taq DNA polymerase (Euroclone). We used PTC-225 Peltier Thermal Cycler (MJ Research) and PCR reaction conditions were 1.5 min at 94°C, for 35 cycles: 30 sec at 94°C, 1 min at 69°C, 45 sec at 72°C; final step of 2 min at 72°C. We analysed the PCR product on a 1% Agarose gel with GelRed in TBE 0.5x

CHAPTER 4

RESULTS

4.1 MYCN characterization in SCLC cell lines

H69, H526 and H82 were already been characterized in our lab, and to picture the complete panorama of this aggressive neoplasia, we analysed other ten cell lines, which carried different features.

I first evaluated the expression of Myc family genes (MYC, MYCN and MYCL), SCLC markers.

As reported in Figure 12, H69, H526, N592 and GLC14 showed MYCN overexpression at the expense of lower expression of MYC and MYCL. All the other cell lines, as well, overexpress preferably only one of the three genes.

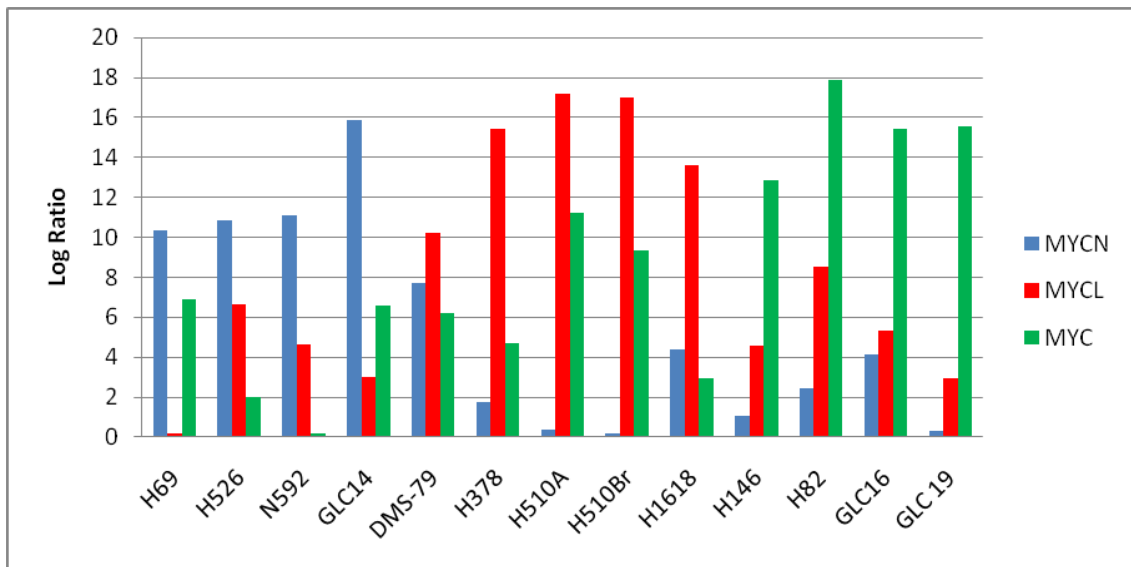


Fig.12 Myc family genes mRNA expression in different SCLC cell lines

NMYC overexpression was correlated with N-Myc protein in the same cell lines, after Western Blot analysis (Figure 13).

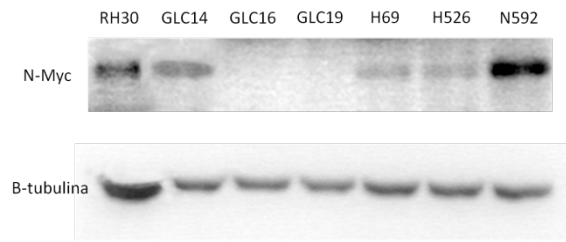


Fig. 13 Western Blot analysis of RH30, GLC14, GLC16, GLC19, H69, H526, N592

The presence of MYCN amplification was also confirmed by FISH from all the four cell lines.

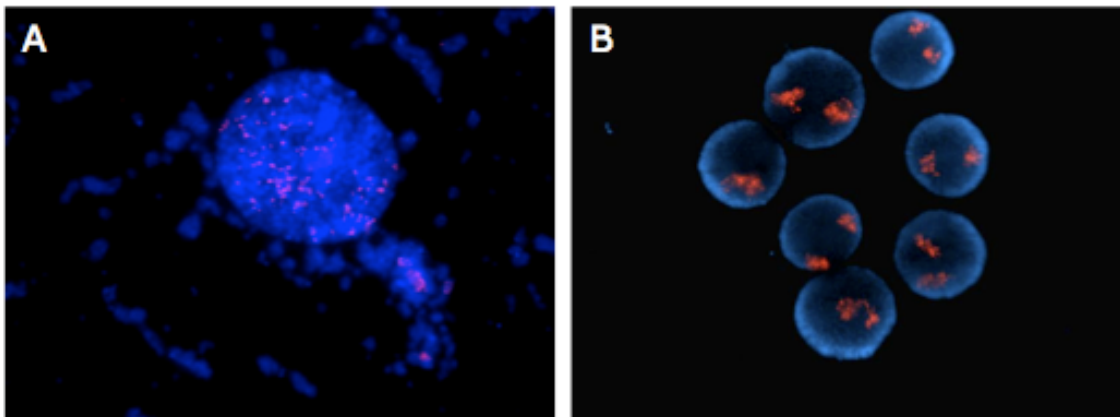


Fig.14 FISH of MYCN probe to nuclei of SCLC cell lines H69 (A) and H526 (B)

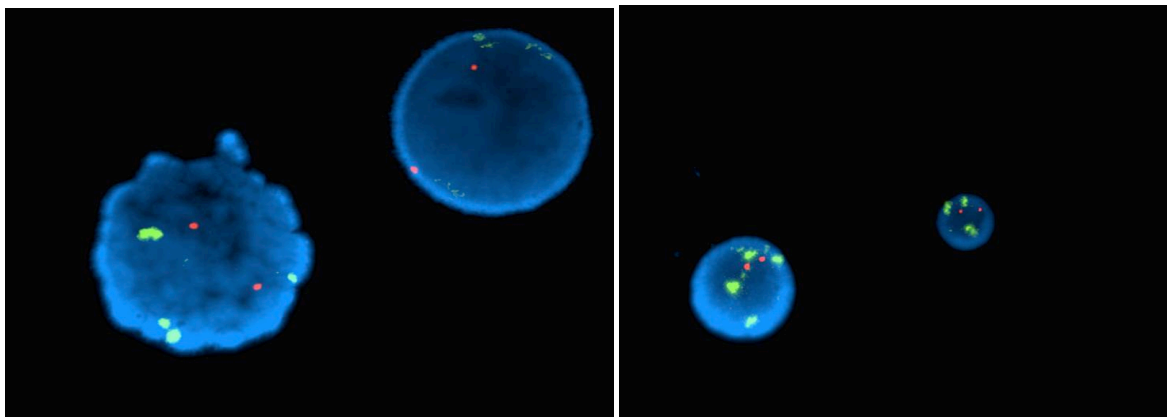


Fig.15 FISH of MYCN probe to nuclei of SCLC cell line N592

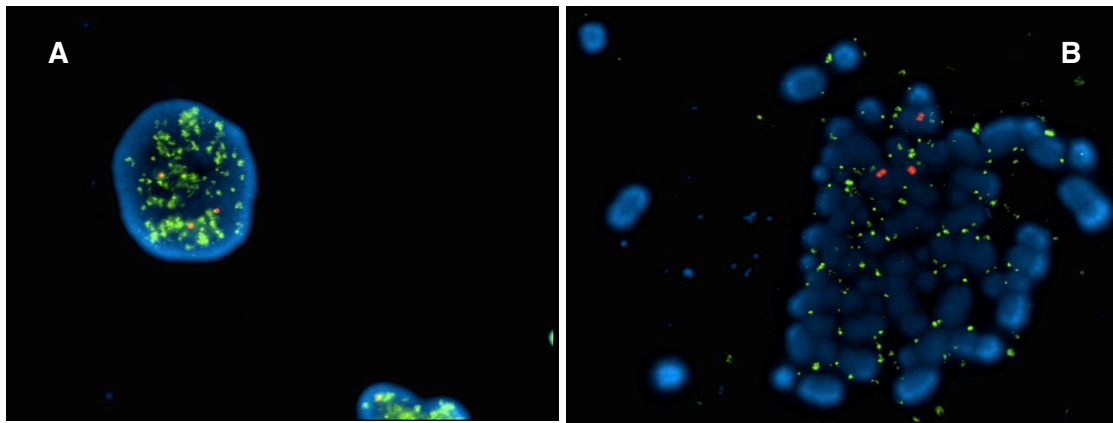


Fig.16 FISH of MYCN probe to interphase (A) and metaphase (B) nuclei of SCLC cell line GLC14

H69 and H526 have been characterized previously in my lab, and they showed MYCN amplification (Figure 14A-B: Green probe represents MYCN gene). The amplification of MYCN gene was, then, verified by FISH in two other SCLC cell lines. In particular, GLC14 derived from a patient before chemotherapy treatment. The N592 cell line shows the duplication of chromosome 2 and the presence of green signal concentrated in well-defined areas suggests the presence of HSR(Homologous Staining Region) (Figure 15: "gene specific" probe = green signal; centromeric probe for chromosome 2 = red signal).

FISH analysis of GLC14 cell line shows the triplication and quadruplication of chromosome 2 and an abundant amplification of MYCN gene. Moreover, Figure 16B suggests an episomal amplification of MYCN, already found in medulloblastoma [Surace C. et al. 2008].

4.2 *In vitro* chemotherapeutic treatments

I defined dose-response curves for three compounds on cell lines that have proved to be NMYC amplified: H69, N592 and GLC14. Chemotherapy is currently used in standard protocols and it is characterized by high toxicity due to the incomplete specificity of these drugs to cancer cells. The use of a molecule that does not show toxicity as the PNA in combination with these drugs could then work around this problem by allowing the same therapeutic effect at reduced doses.

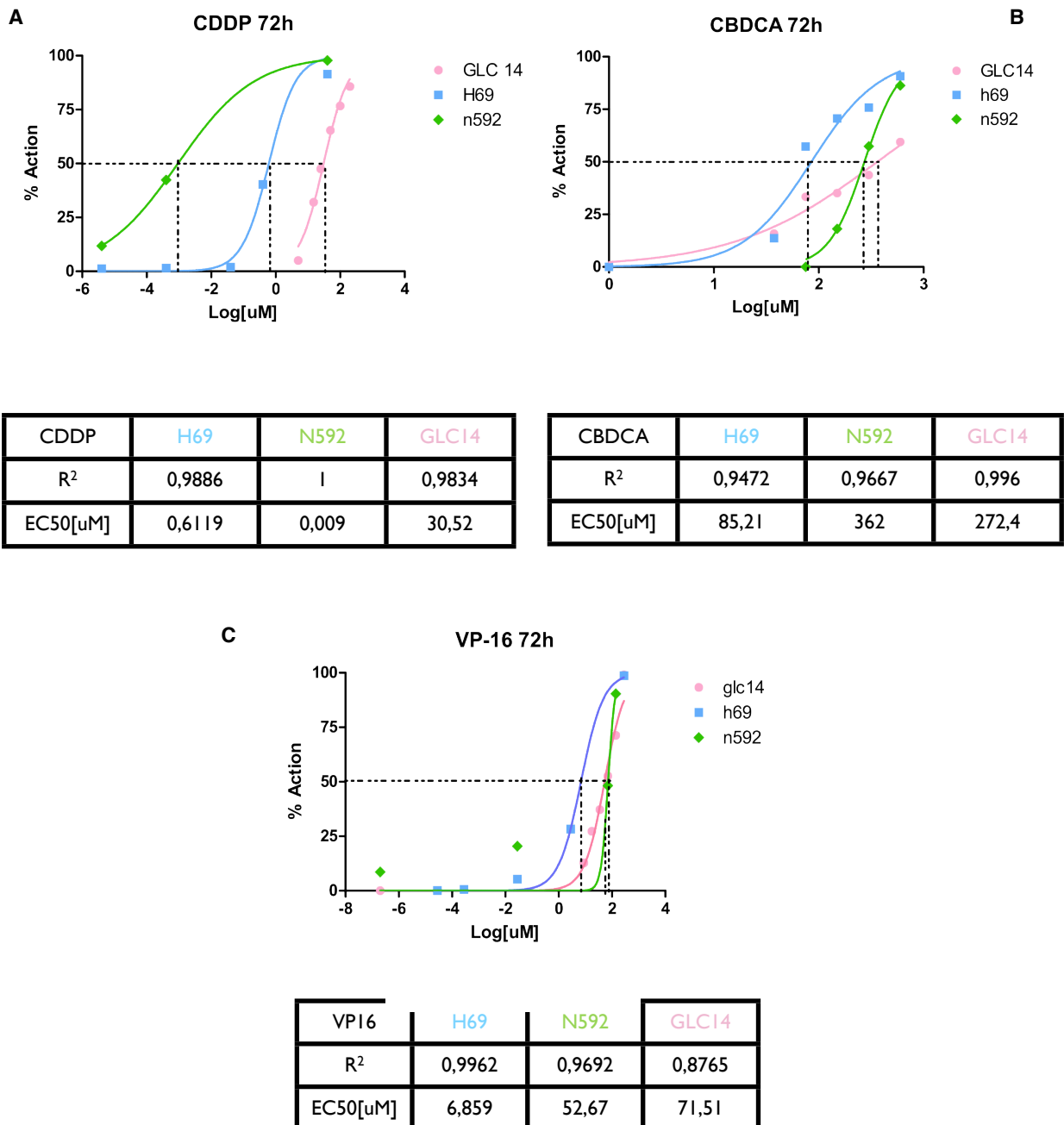


Fig.17 Dose-response curves for three chemotherapy drugs in SCLC cell lines with amplification of MYCN. CDDP = cisplatin, CBDCA = carboplatin; VP-16 = Etoposide EC50 = concentration of drug that defines the 50% cell inhibition. A) CDDP; B) CBDCA and C) VP-16

4.3 In vitro anti-MYCN PNA treatment

Four cell lines, H69, GLC14, N592 and H82 were treated with 20, 15, 10 and 5 μ M anti-MYCN anti-gene PNAs-NLS (PNAwt), for 24 hours and the IC50 (concentration of drug that induces the increase of a cycle of $\Delta\Delta$ Ct or a 0.5 Fold change of MYCN tansgene transcript) was evaluated by semi-quantitative Real-Time PCR, normalizing the values on the β -actin housekeeping gene. The duration of treatment was derived from previously

made experiments. To test the specificity and the possible toxicity of the PNA an anti-gene anti-MYCN PNAmut was used, whose sequence has been altered by three point mutations.

Anti-gene PNAwt significantly inhibits the transcription of MYCN transgene 24 hours after treatment. Figure 18 shows an inhibition by 90% in H69 cell line, 65% in GLC14 and 55% in N592, using PNA at 15uM, with IC50 reported in Table 3. On the contrary, NMYC was not inhibited in H82 cell line, and to obtain an IC50 we used a Compusyn extrapolation method.

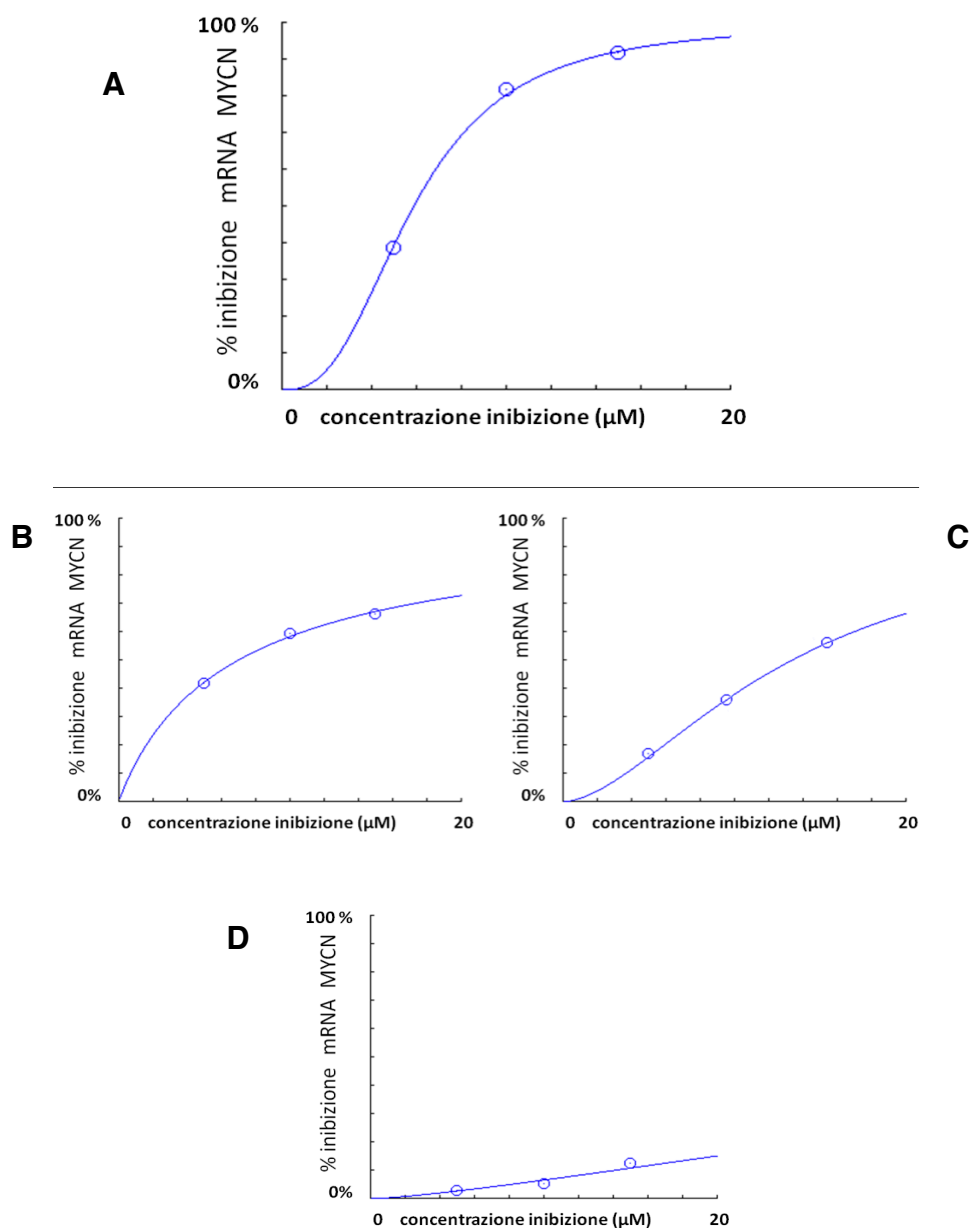


Fig.18 Dose-response curves for A)H69; B)GLC14; C)N592 and D)H82

Cell line	IC50
H69	5.86 μ M
GLC14	6.96 μ M
N592	13.34 μ M
H82	272.8 μ M

Tab.3 IC50 values

The anti-gene PNAmut showed, instead, no significant effects on cell lines characteristics.

4.4 MYCN-amplified SCLC xenograft orthotopic mice models

4.4.1 *In vitro* validation of bioluminescent signal

In this part of my project I developed xenograft orthotopic SCLC murine models for a next pharmacological study. For these models we decided to use a new bioluminescence type of *in vivo* imaging monitoring system. The luminescent imaging system requires the introduction of a reporter gene, the luciferase enzyme gene, that allows real-time monitoring of cell growth *in vivo*. In Figure 19, RLU (Relative Luminescence group) signal graph of the chosen transfected cell lines. All of them stable express the luciferase gene with H69 cell line showing the highest luminescence.

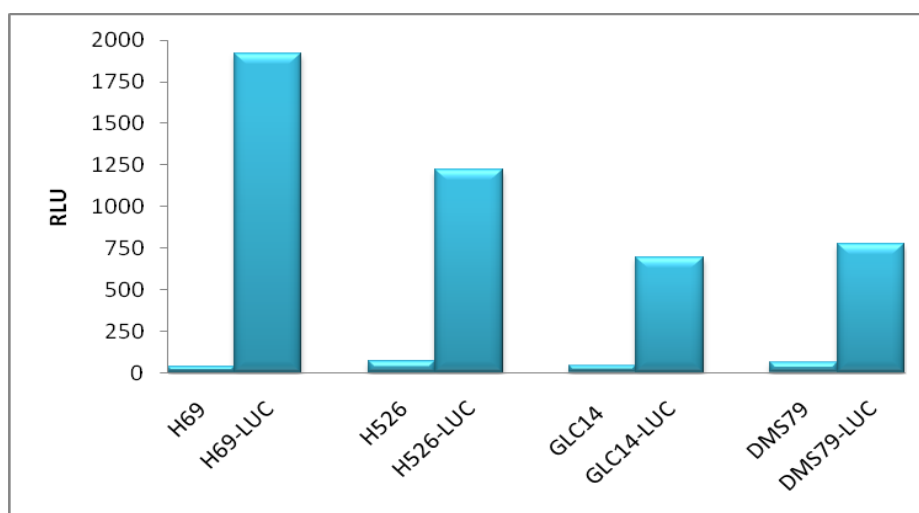


Fig.19 Luciferase assay

Stably transfected H69 cells subsequently used for *in vivo* experiments were analyzed to identify the specific luciferase emission peak (attended on 560 nm) and to identify a

correlation between luciferase expression and cells number. The luciferase emission spectrum analysis was obtained after the addition of D-luciferin at whole living cells. The results showed that the cell line presented a relative luciferase emission peak (560 nm) (Figure 20A) highlighting a perfect linear correlation between number of cells and photons detected (Figure 20B).



Fig. 20A

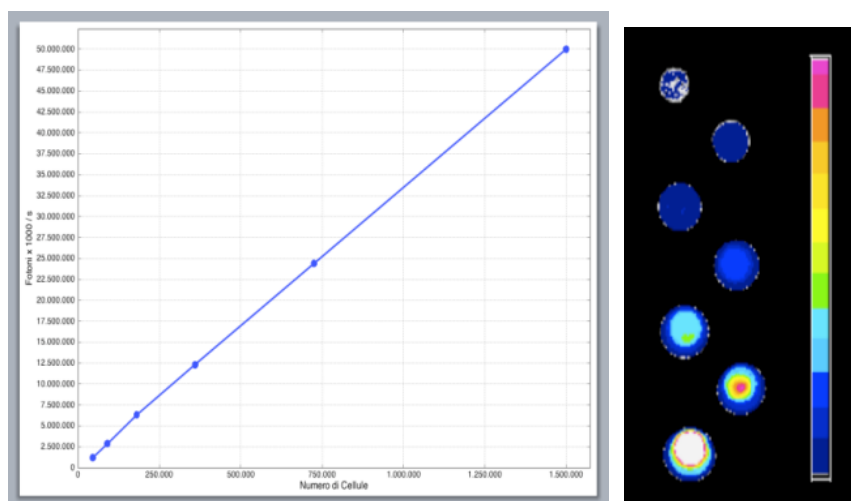


Fig.20B

4.4.2 In vivo bioluminescent imaging

For *in vivo* study twenty mice were used: 10 were inoculated with $1,5 \times 10^6$ H69-luc cells, 5 with $1,5 \times 10^6$ H526-luc and 5 mice constituted the control group. Our previously experiments showed a higher incidence using $1,5 \times 10^6$ compare with 3×10^6 cells (Figure 21).

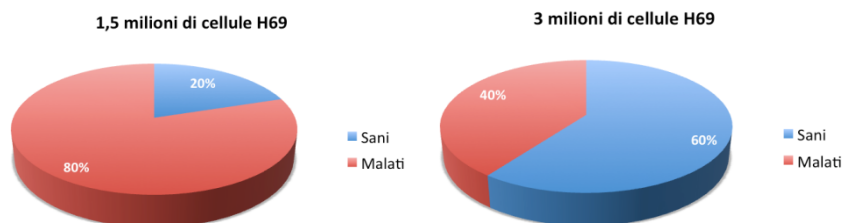


Fig.21 H69 tumor incidence

Mice were monitored weekly by examination of *in vivo* bioluminescence.

The temporal window for *in vivo* analysis was determined by the kinetics of biodistribution of D-luciferin, and it identified the time interval at which the signal is stable and the intensity of the signal is maximum. Figure 22 shows the acquisitions carried out for 1 min, 15 sec intervals for 15 min in total.

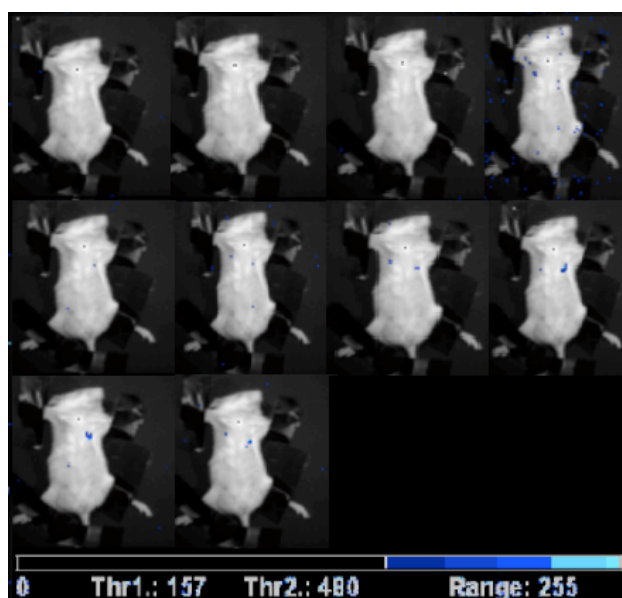


Fig.22 *In vivo* kinetics of bio-distribution of D-luciferin. The acquisitions carried out for 1 minute, 15 second intervals for 15 minutes in total on the same mouse after the somministration of D-luciferin.

The data obtained with the luminometer showed a peak signal from the eighth minute that can be used up to 12 minutes. The range of acquisitions between the 8 to 12 minutes after injection of D-luciferin was used for all orthotopic models to analyze the tumor burden and progression.

After this experiment, each animal was analyzed with NightOwl Berthold LB981 luminometer to detect the presence of the tumor. Under anesthesia each animal was injected with D-Luciferin substrate to a concentration of 150 mg/kg. After 8 minutes it was

scanned for 3 minutes. The animals were monitored every seven days starting one week after inoculation with BLI. Figure 23 shows tumor progression in a mouse for each model, it is clear the evolution of the tumor marked by luminescence signal at different time of recording, covering a time period ranging from 4 weeks post-inoculation (first appearance of the signal) at 10 weeks (endpoint). The xenograft orthotopic model obtained injecting H526luc showed a tumor characterized by a shorter latency (four weeks) and a higher BLI signal compared to xenograft orthotopic model obtained injecting H69luc.

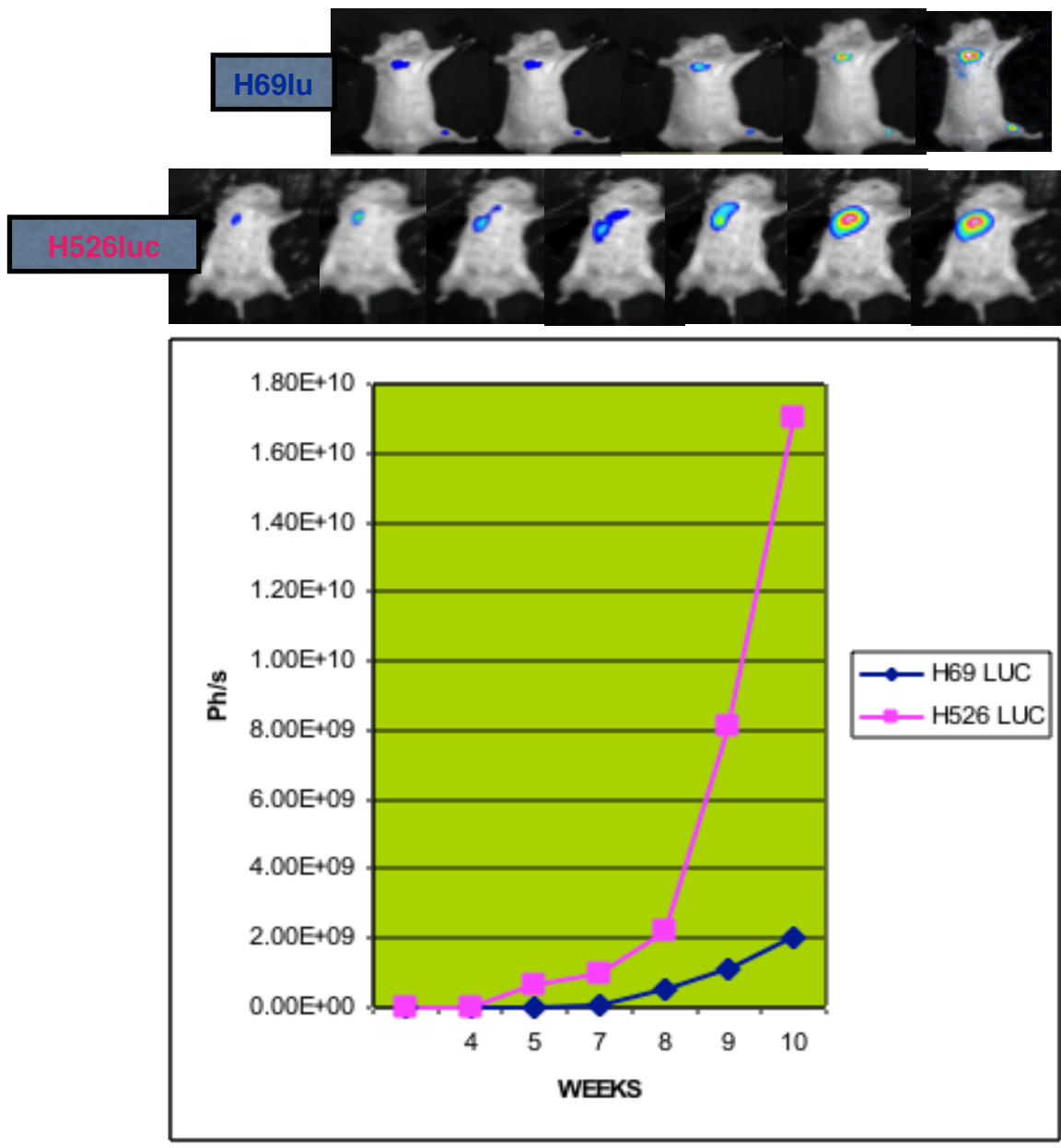


Fig.23 In vivo monitoring of two different SCLC Xenograft Orthotopic mice models. The graph represents of tumor burden onset and progression at different timepoints (left side); signal detected from Berthold luminometer once a week starting one week after day of cells injection (right side).

For one of the 10 mice injected with H69luc cell lines, we report the tumor progression by scan imaging. As shown in Figure 24, it was also possible to detect a bone metastasis and his growth during the weeks.

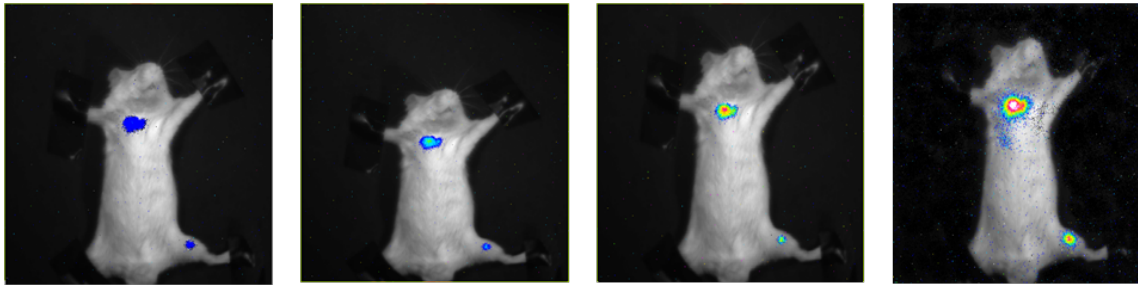


Fig.24 *In vivo* monitoring of tumor burden onset and progression at different timepoints

4.4.3 Mouse model validation

5 mice were inoculated with H69-luc cells and at the first bioluminescent signal they underwent a therapy with Cisplatin and Etoposide. 5 mice were taken as placebo control and received only saline solution.

We analyzed the data from mice become positive for BLI within the fourth and the sixth week. As already reported in Figure 23 they showed a 5 weeks latency and a following quantum growth. The chemotherapy group shows a decrease that starts at the seventh week, after two treatment cycles, and continues to decrease until it gets back to basal levels around the eleventh week.

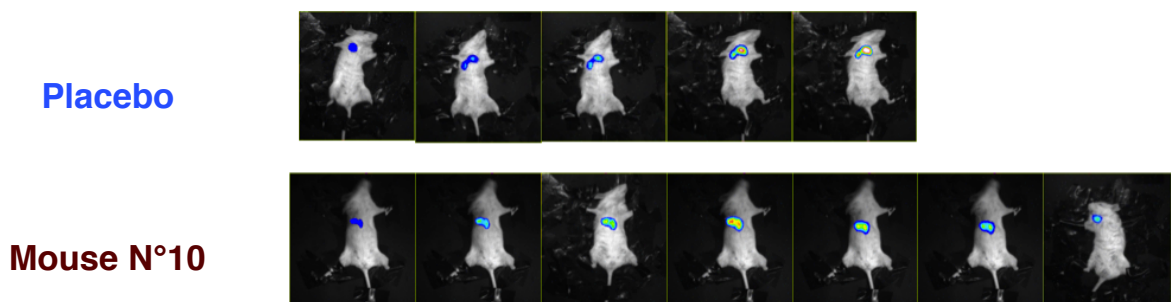
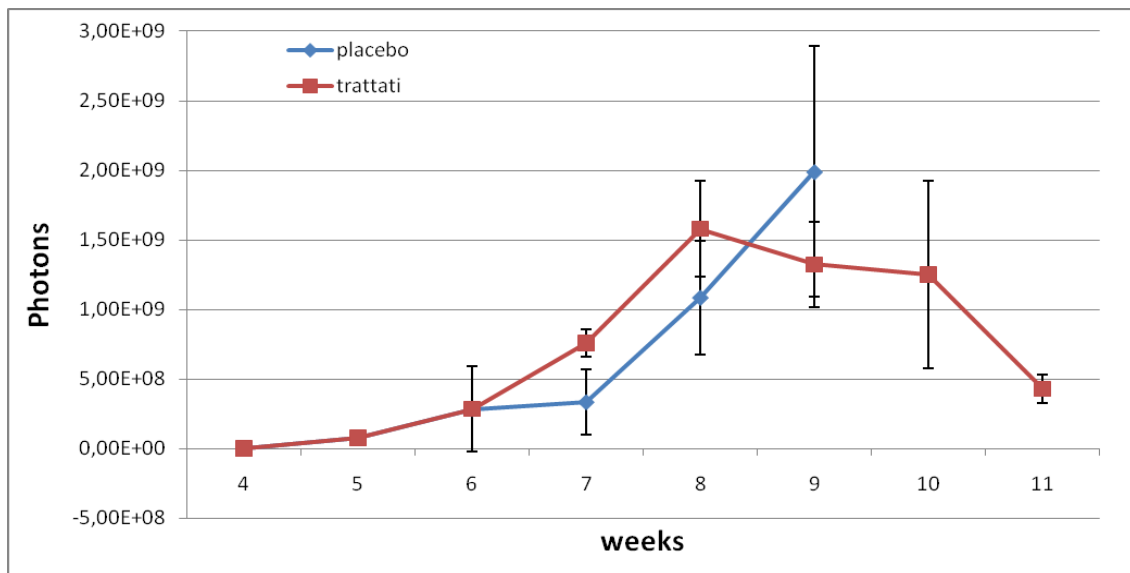


Fig.25 Tumor progression curve of both treated and untreated mice and the related bioluminescent images

This trend becomes even clearer translating the data in survival rate: the average life in the placebo group is 65 days compared to 85 days in the chemotherapy group.

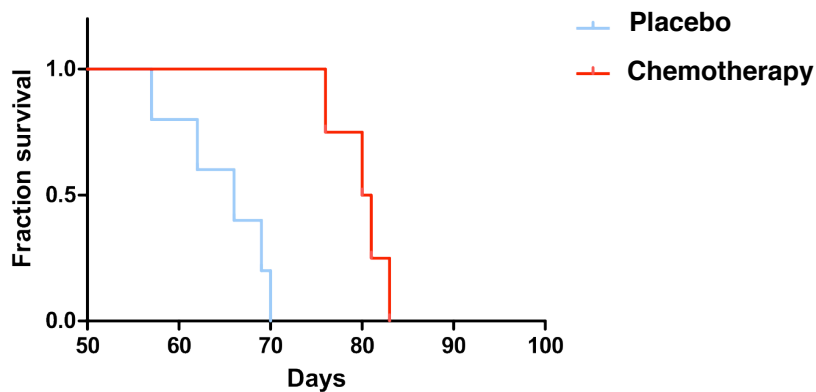


Fig.26 Different survival between Chemotherapy group (red line) and placebo group (blue line). An average survival of 85 days compared with only 65 days for the placebo control.

4.4.4 *Ex vivo* analysis of xenograft orthotopic tumor

The analysis was performed *ex vivo* on the mass removed at late stage of the disease. Figure 27 shows the altered lungs morphology (B) and confirms that photons detected by CCD camera were produced in these organs (C). The luminescence signal *ex vivo* is much sharper, skin, adipose tissue ribcage attenuate the intensity distribution and the photons detected. This analysis has allowed an assessment of the organ specific tumor mass, highlight that right lung, where the cells were implanted, is dramatically deformed.

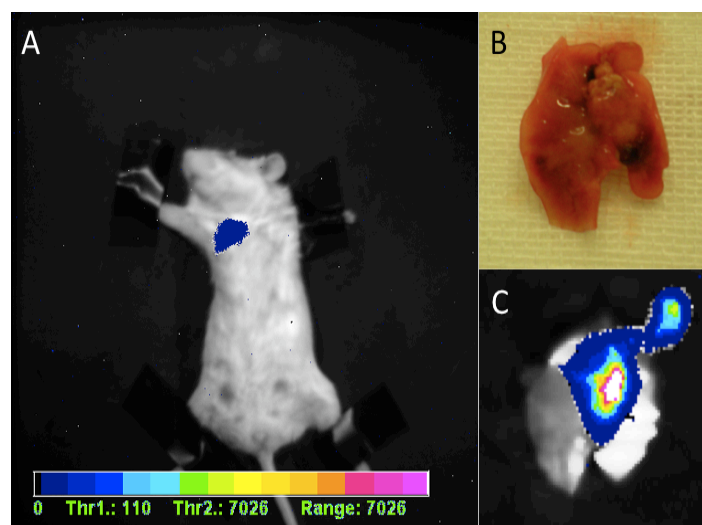


Fig.27 Tumor mass *ex-vivo* analysis

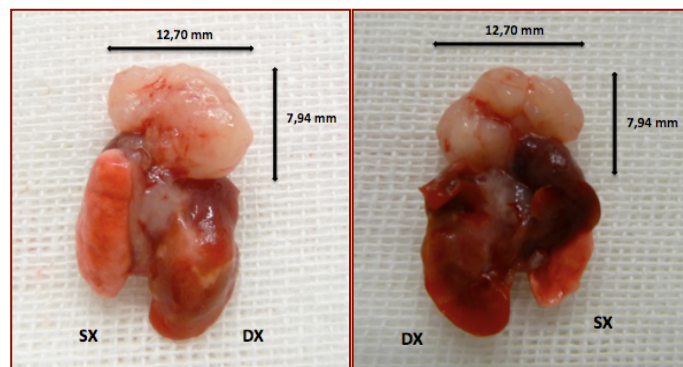


Fig.28

The autopsy allowed collection of tumor samples useful for the histological and molecular evaluation. From the post-mortem examination, all positive animals have a tumor mass located predominantly in the chest region. At advanced stage, the tumor mass alters the structure of surrounding organs, for example it is possible find adhesion part. The tumor masses occur heterogeneous in the samples in which it is possible to distinguish necrotic

regions (Figure 28). It has been found the presence of metastases at bones level. The tumor presence was confirmed with histological analysis and the presence of human MYCN was seen with immunohistochemistry.

Histological data confirm that all samples were SCLCs. In Figure 29, we can see the characteristic structure of healthy lungs (A, B, C): bronchi (Br), bronchioles (Bi) and alveoli (Al). This structure is completely altered in the tumor mass (D, E, F): there are a lot of them (Mt) infiltrating the lung, constituted of non-organized cells. Near the tumor, the alveoli look like crushed. Within the tumor mass we can also notice blood vessel sections.

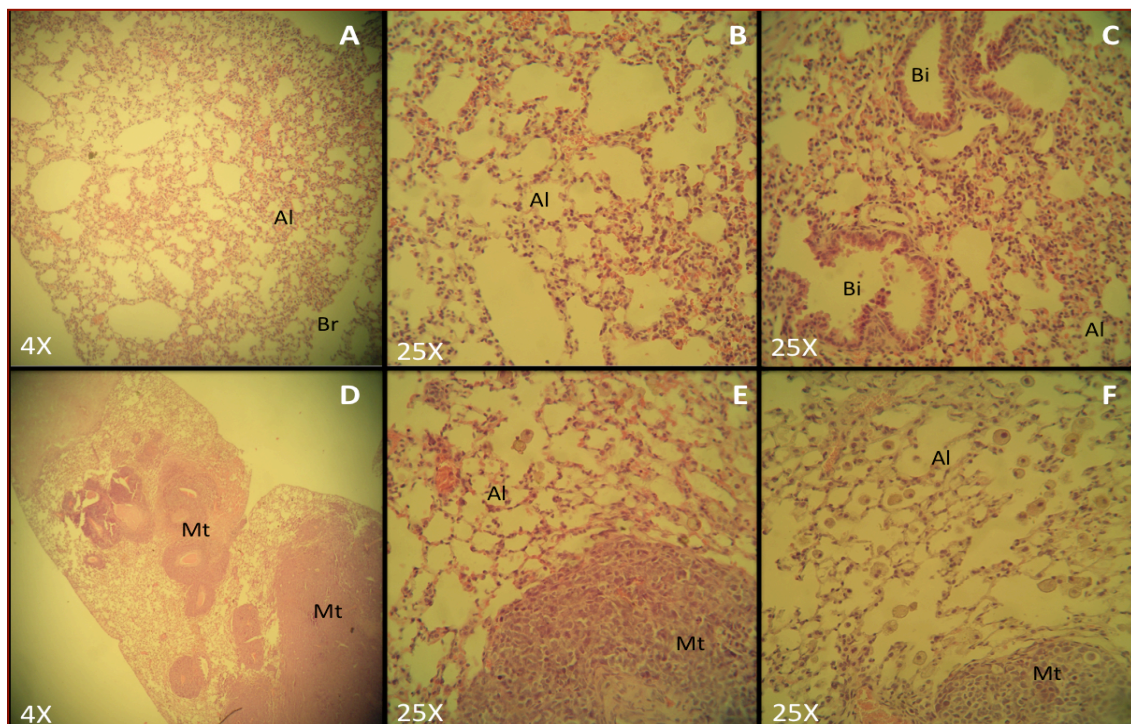


Fig.29 H&E staining of normal tissue (A,B,C) and tumor tissue (D,E,F)

Immunohistochemistry (IHC) stainings evidence the high expression of MYCN oncogene in all samples. The majority of cells in the samples resulted positive for the presence of N-Myc to the detection with the chromogenic DAB that gives brown signal in cells nuclei. IHC was also performed on metastases tissue, confirming the abundance of N-Myc (Figure 30).

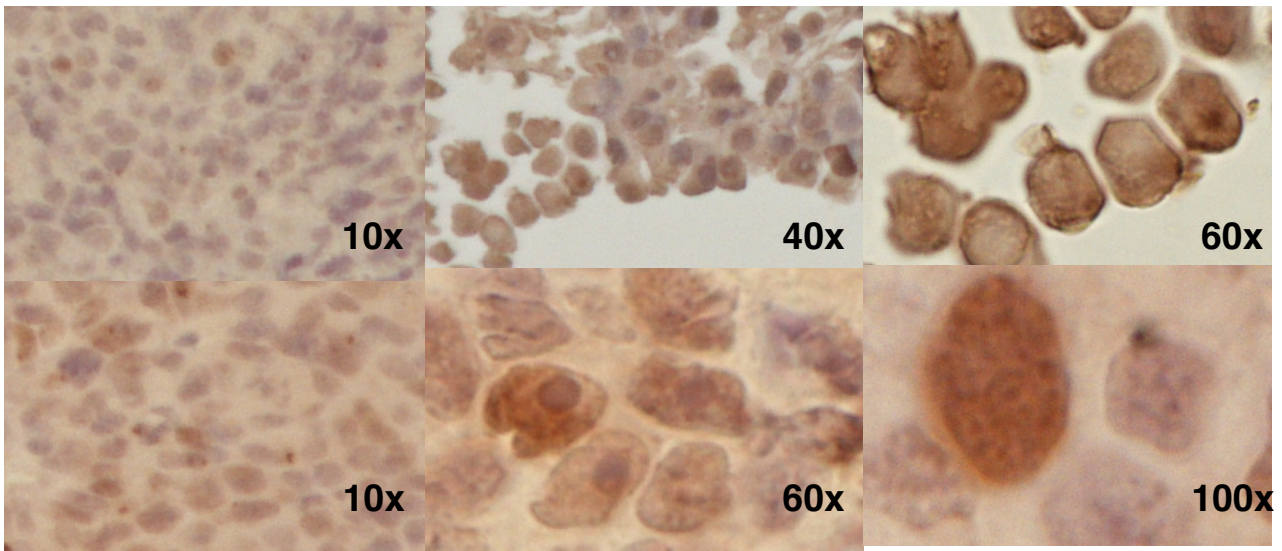


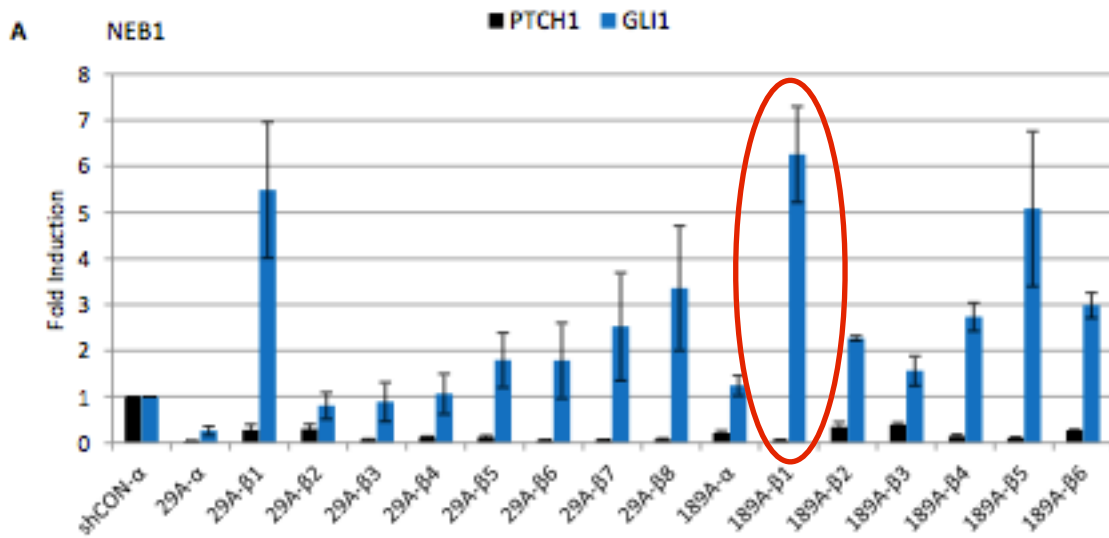
Figure 30 N-Myc IHC on murine SCLC tissue. Tumor and metastases (below)

4.5 *In vitro* and *in vivo* modelling of Basal cell carcinoma

4.5.1 Creation and characterisation of human keratinocyte cell line with stable PTCH1 suppression

The human immortalized cell line NEB1 was chosen for this study as they are widely used in skin research and retain the ability to differentiate [Morley et al., 2003]. In addition, the levels of PTCH1 and the downstream HH signalling component GLI1 were analyzed by qPCR to confirm that these cells were suitable for targeted PTCH1 suppression. Cell line was retrovirally transduced with a construct containing a non-targeting scrambled control (shCON) as well as two constructs targeting exons 3 (termed 29A) and 24 (termed 189A) of the PTCH1 gene respectively. After drug selection with Puromycin, clonal cell lines were derived by single cell seeding from the heterogeneous populations of NEB1-29A, and NEB1-189A. A number of clonal cell lines were derived from 29A and 189A heterogeneous populations based on their compact, BCC-like morphology and the level of PTCH1 suppression was assessed by qPCR (Figure 31A). NEB1-189A- β 1 cells showed the strongest suppression of PTCH1 which correlated with an increase of GLI1 and therefore, most of the studies were conducted on this particular clonal cell line. NEB1-189A- β 1 will now be referred to as NEB1-shPTCH1.

Morphologically, NEB1-shPTCH1 cells displayed a more compact cobblestone-like colony formation compared to NEB1-shCON cells and parental NEB1 cells (Figure 31B).



B

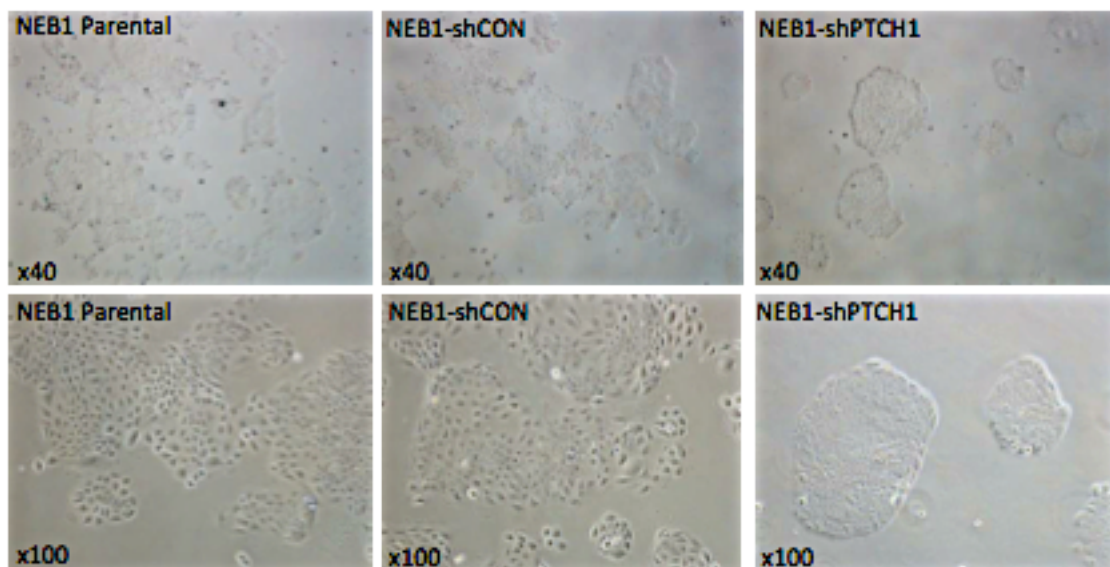
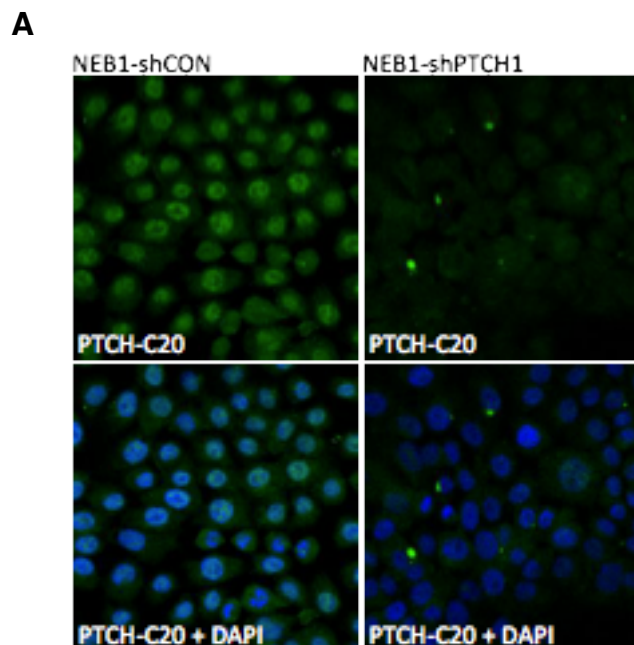


Fig.31: A)qPCR for PTCH1 and GLI1 in shPTCH1 clonal cell lines PTCH1 and GLI1 mRNA expression levels in NEB1-shPTCH1; B)PTCH1 suppression induces a highly compact morphology in human keratinocytes.

To confirm that the increase of GLI1 is specifically due to reduced PTCH1 activity in NEB1-shPTCH1 cells, a rescue experiment was performed by ectopically expressing the PTCH1B isoform and analysing GLI1 expression. As the PTCH1B vector only contains the coding sequence (i.e. START to STOP codons) its mRNA is not subject to degradation by the PTCH1 shRNA as the hairpin targets a region that is downstream of the STOP codon in exon 24. Ectopic PTCH1B suppressed GLI1 to basal levels thus confirming that the increase of the latter is due to reduced PTCH1 function in NEB1-shPTCH1 cells.

4.5.2 Characterisation of Hedgehog signalling components in NEB1-shPTCH1 cells

Having established that PTCH1 is strongly suppressed in NEB1-shPTCH1 cells, further characterisation at the protein level by immunocytochemistry confirmed a reduction of PTCH1 protein which was quantified by Image J software (Figure 32). The commercial (Santa Cruz) PTCH1-C20 antibody is specific to the C-terminus of the protein and this gave a distinct signal in the nucleus of NEB1-shCON cells which was reduced in NEB1-shPTCH1 cells thus helping confirm antibody specificity. PTCH1 is generally considered to be a transmembrane protein however, a recent study showed that the protein is cleaved and that the C-terminus resides in the nucleus where it can regulate GLI1 (Kagawa et al., 2011).



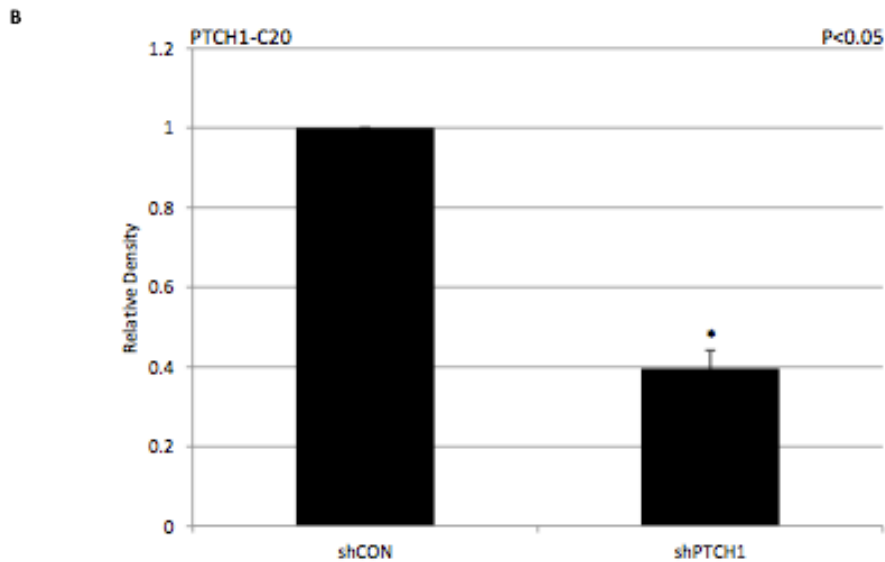
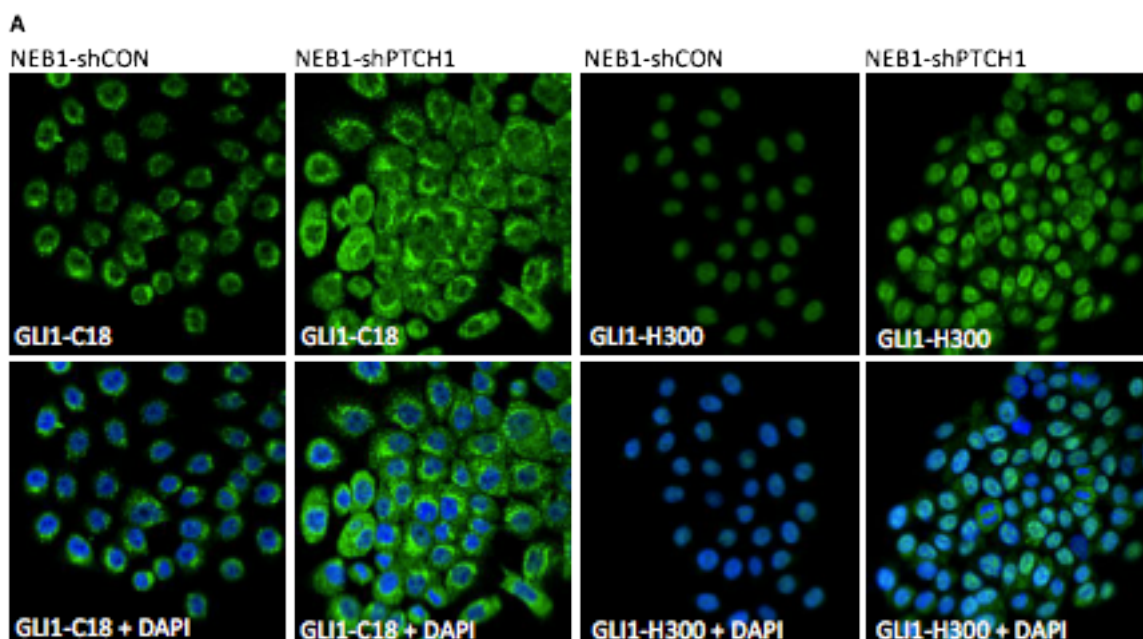


Fig.32: Immunofluorescent analysis of PTCH1 protein expression [A] NEB1-shCON and NEB1-shPTCH1 cells stained for C-terminal PTCH1-C20. [B] Image J quantification for PTCH1 staining. Error bars represent mean \pm standard deviation, student's t-test shows a significant difference with 95% confidence ($p < 0.05$).

Consistent with the results of qPCR analysis (Figure 31 A), GLI1 protein was also found to be increased in NEB1-shPTCH1 cells. Two different antibodies were used with GLI1-C18 detecting cytoplasmic and nuclear protein and GLI1-H300 detecting mainly nuclear protein (Figure 33). The reason for this is unclear but other studies in the laboratory have shown that both antibodies detect ectopic GLI1 by Western blot analysis of keratinocyte protein lysates.



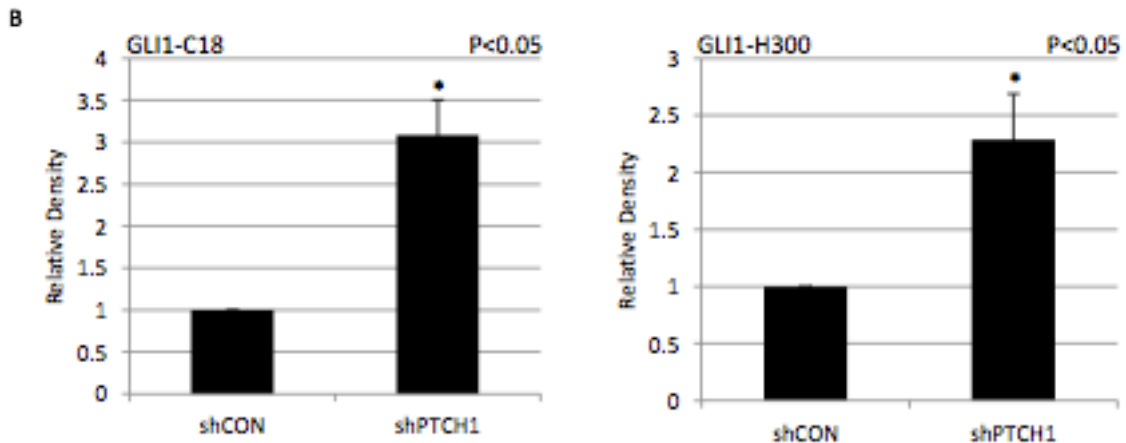


Figure 33: Immunofluorescent analysis of GLI1 protein expression [A] NEB1-shPTCH1 cells stained for cytoplasmic GLI1-C18 and nuclear GLI1-H300. [B] Image J quantification for GLI1 staining. Error bars represent mean \pm standard deviation, student's t-test shows a significant difference with 95% confidence ($P < 0.05$).

Other components of the HH signalling pathway were also investigated in NEB1-shPTCH1 cells. SHH was found to be decreased at the protein and mRNA level. SMO mRNA was also increased two fold in NEB1-shPTCH1 cells (Figure 34).

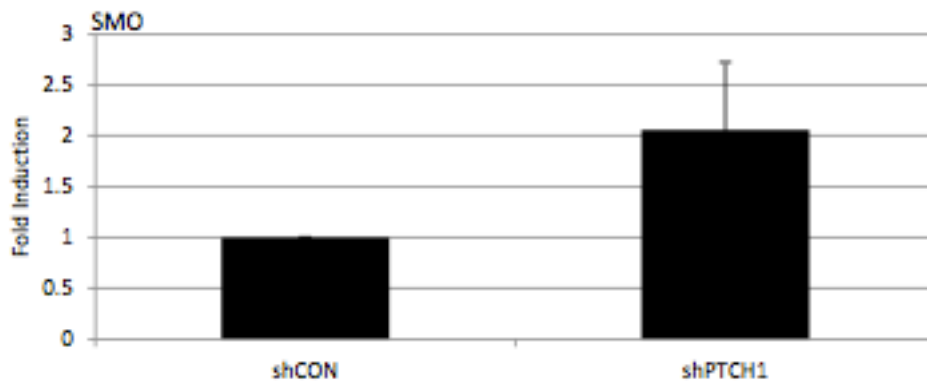


Fig.34: Analysis of HH signalling components in NEB1-shPTCH1 cells. qPCR for SMO. Error bars represent mean \pm standard deviation.

4.5.3 Non-canonical GLI1 signalling in NEB1-shPTCH1 cells

To determine if the increase of GLI1 expression in NEB1-shPTCH1 cells is mediated through SMO (i.e. canonical HH signalling), NEB1-shPTCH1 cells were exposed to the SMO antagonist Cyclopamine-KAAD. As shown by qPCR and IF, over a period of 24 hours GLI1 expression was strongly suppressed in NEB1-shCON cells whereas it was not significantly altered in NEB1-shPTCH1 cells (Figure 35).

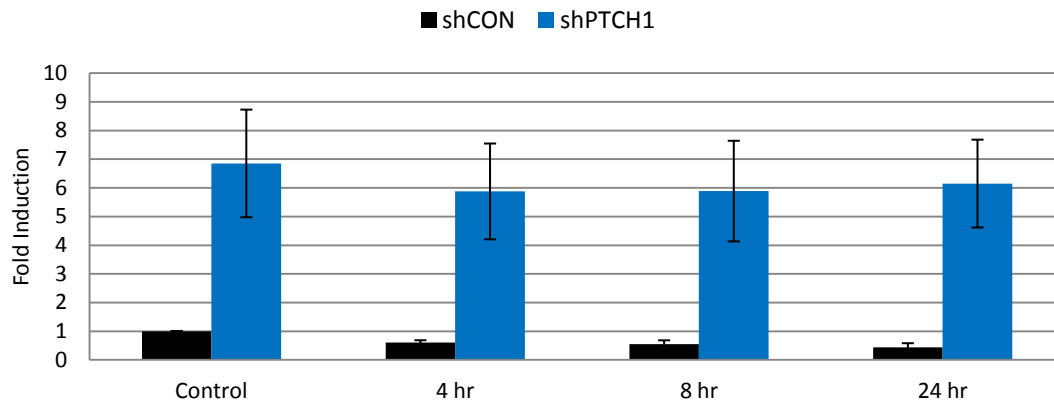


Figure 35: GLI1 expression is not influenced by SMO pharmacological inhibition in NEB1-shPTCH1 cells; qPCR for GLI1 in NEB1 cells treated with 100 nM Cyclopamine-KAAD for up to 24 hours. Error bars represent mean \pm standard deviation.

In summary, shPTCH1 cell lines that were treated with the SMO inhibitors retained a higher GLI1 expression level (compared to shCON cells) which suggests that PTCH1 regulates GLI1 via a SMO-independent mechanism. NEB1 cells exposed to SMO inhibitors was analysed for GLI2 mRNA levels which were lower in NEB1-shPTCH1 cells compared to NEB1-shCON. GLI2 mRNA expression in both cell lines were suppressed by Cyclopamine-KAAD which suggests that GLI2 signalling occurs via canonical HH signalling. Taken together, these data suggest that there is a canonical SMO-GLI1/GLI2 signalling axis in shCON cells and a canonical SMO-GLI2 signalling axis in shPTCH1 cells, but they also indicate the presence of a non-canonical PTCH1-GLI1 signalling axis that is independent of SMO activity in shPTCH1 cells (Figure 36).

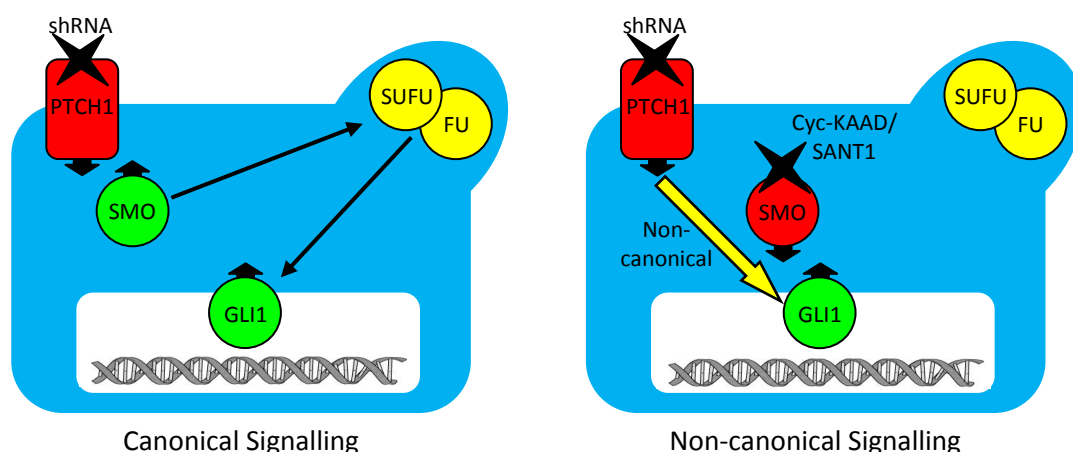


Fig.36: Schematic diagram depicting a novel non-canonical PTCH1-GLI signalling pathway in shPTCH1 cells (right panel)

4.5.4 Functional studies of NEB1-shPTCH1 cells

As well as investigating the HH signalling pathway, the *in vitro* BCC model was established to investigate specifically the effects of PTCH1 suppression upon certain aspects of keratinocyte biology including proliferation, invasion and anchorage-independent growth.

With regards, to proliferation rate, there was a slight but consistent decrease in NEB1-shPTCH1 cells (29A and 189A) compared to the control. In contrast, NEB1-shPTCH1 cells were hyperproliferative when seeded onto a Matrigel based organotypic culture system although there was no evidence of invasion into the artificial dermis characteristic of superficial BCC or compact colony formation characteristic of nodular BCC (Figure 37).

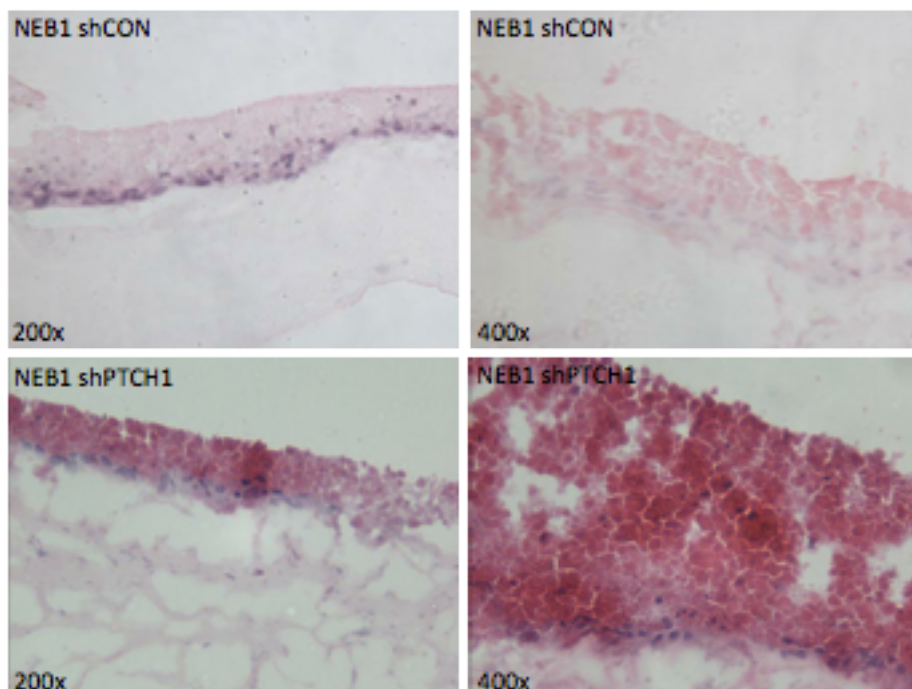


Fig.37: Organotypic skin model of NEB1 cells

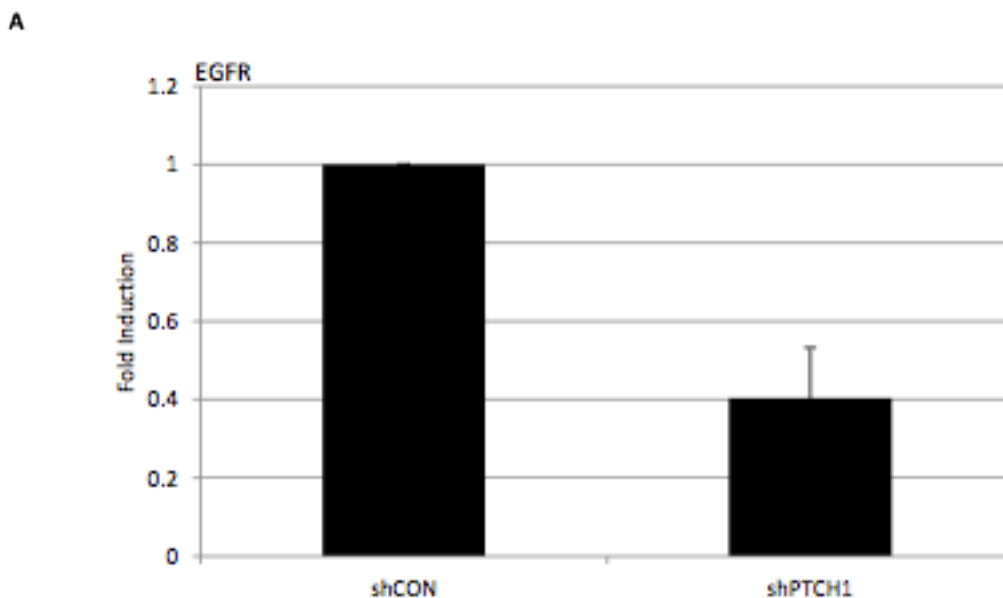
4.5.5 EGFR signalling in NEB1-shPTCH1 cells

Microarray analysis of NEB1-shPTCH1 cells revealed that a number of major signalling pathways are affected by the suppression of PTCH1. One significant pathway that was highlighted was the MEK/ERK pathway downstream of EGFR signalling. It has been shown that EGFR signalling modulates the expression of GLI1 in N/Tert keratinocytes and that a number of genes could be induced synergistically by GLI1 and EGF treatment. Furthermore, the GLI1 target genes were modulated by EGFR signalling via MEK/ERK pathways (Kasper et al., 2006). Other studies have demonstrated that GLI1 and GLI2

expression is induced by EGFR mediated MEK/ERK signalling and that mouse BCCs treated with EGFR and GLI inhibitors reduced tumour growth (Schnidar et al., 2009).

In contrast, the Neill group has previously shown that the over expression of GLI1 in N/Tert cells reduces EGFR expression and that ERK activity is also repressed. Furthermore, pERK protein was not expressed in 13/14 BCC tumours whereas it was expressed in the epidermis indicating that the loss of pERK may be important for tumour formation (Neill GW. et al. 2008). These contradictions in the literature warrant further investigation to determine if MEK/ERK signalling is a viable therapeutic target for BCC treatment. As such, NEB1-shPTCH1 cells were analysed for the expression of EGFR signalling and downstream MEK/ERK components.

EGFR expression was shown to be reduced at the mRNA level and also by western blotting (Figure 38 A and B). Downstream of EGFR, pMEK and pERK protein levels were also reduced in NEB1-shPTCH1 cells compared to NEB1-shCON cells (Figure 38 C). To confirm if MEK/ERK signalling expression was reduced in NEB1-shPTCH1 cells, the expression of several target genes known to be activated by MEK/ERK signalling including FOS, JUN and MYC were investigated by qPCR in NEB1 cells (Figure 37). The expression of all these genes was increased in NEB1-shPTCH1 cells (189A) and this was additionally confirmed in NEB1-29A cells.



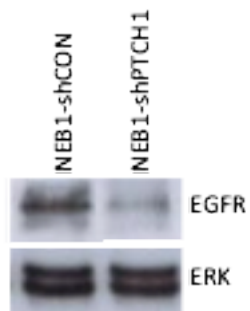
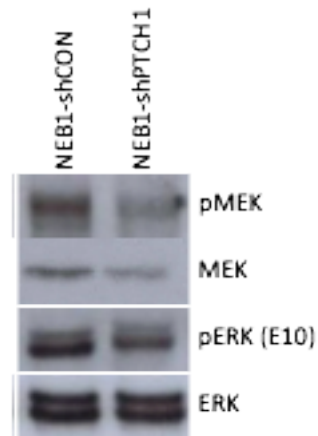
B**C**

Fig.38: EGFR pathway expression in NEB1 cells: EGFR analysis by [A] qPCR; [B] western blotting; [C] Western blot for EGFR downstream targets pERK (E10), pMEK, MEK with ERK loading control.

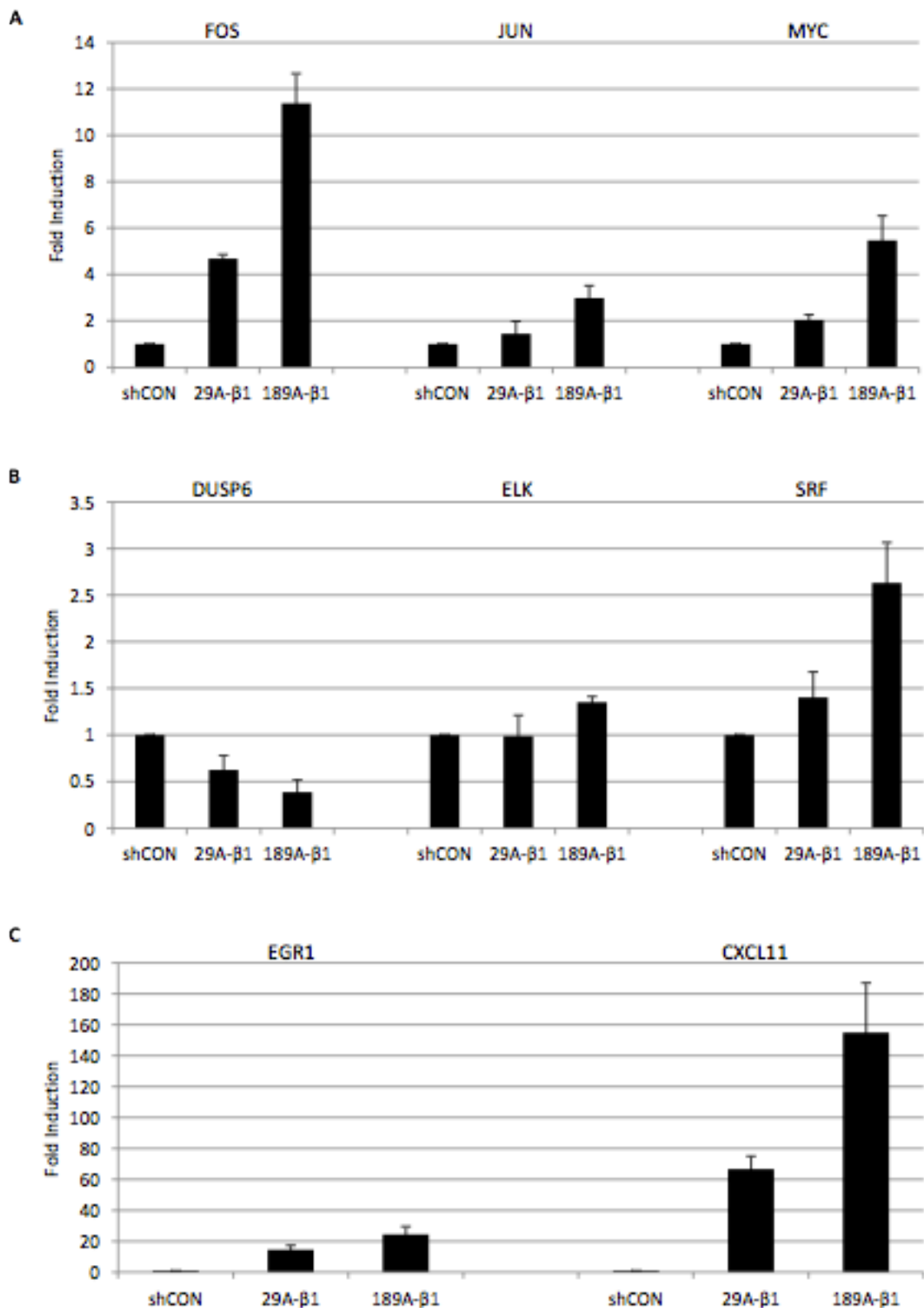
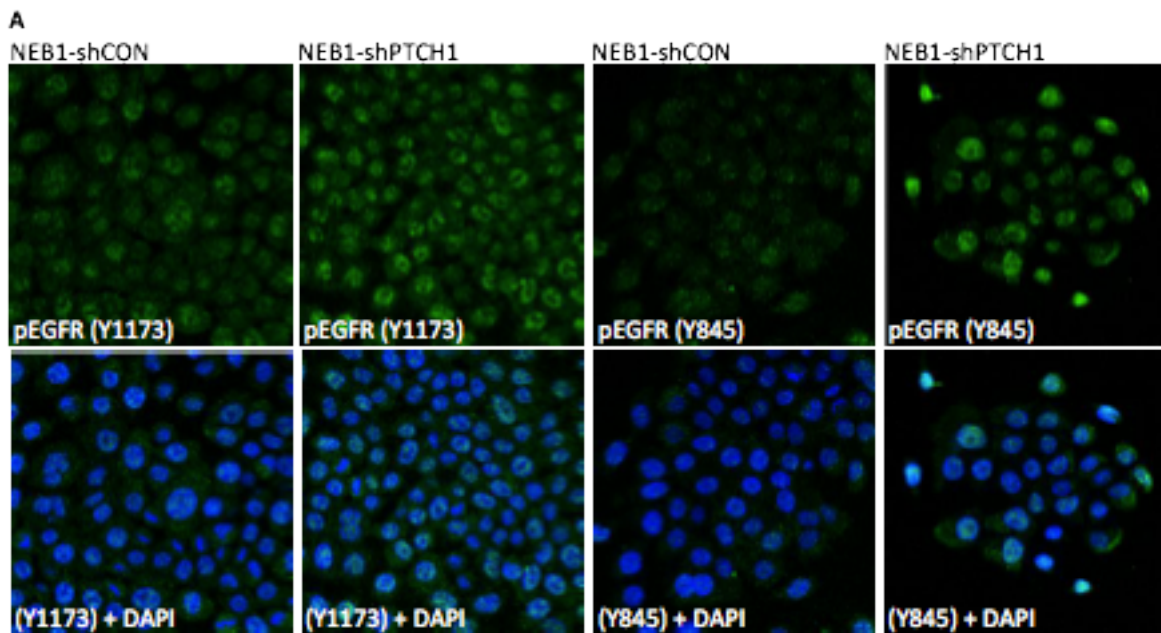


Fig.39: qPCR for ERK target genes in NEB1 cells [A] FOS, JUN, MYC, [B] DUSP6, ELK, SRF, [C] EGR1 and CXCL11 mRNA expression in NEB1 cells.

At the mRNA level, there is evidence that the ERK signalling pathway is active however western blotting revealed that protein levels of MEK, pMEK and pERK were decreased in NEB1-shPTCH1 cells compared to NEB1-shCON cells. This correlates with the finding that EGFR protein expression was reduced in NEB1-shPTCH1 cells however it does not

explain why ERK target genes would be increased. Intriguingly, immunocytochemical analysis of pEGFR revealed an increase of nuclear localization in NEB1-shPTCH1 cells (Figure 40 A). The reason for this is unclear but it could account for reduced MEK/ERK signalling due to weaker signals emanating from the outer cell membrane. Nuclear EGFR translocation is induced in cultured cells exposed to DNA damaging agents (including UVB irradiation) where it is linked with DNA repair and suppression of the apoptotic response (Xu et al., 2009).

Further analysis by immunocytochemistry revealed that pERK was more localised in the nucleus in NEB1-shPTCH1 cells which could account for the increase of the pERK target genes (Figure 40B). Also, immunocytochemical analysis of pMEK localisation was inconclusive although there was some evidence of nuclear pMEK in NEB1-shPTCH1 cells that was not observed in NEB1-shCON cells (Figure 40C).



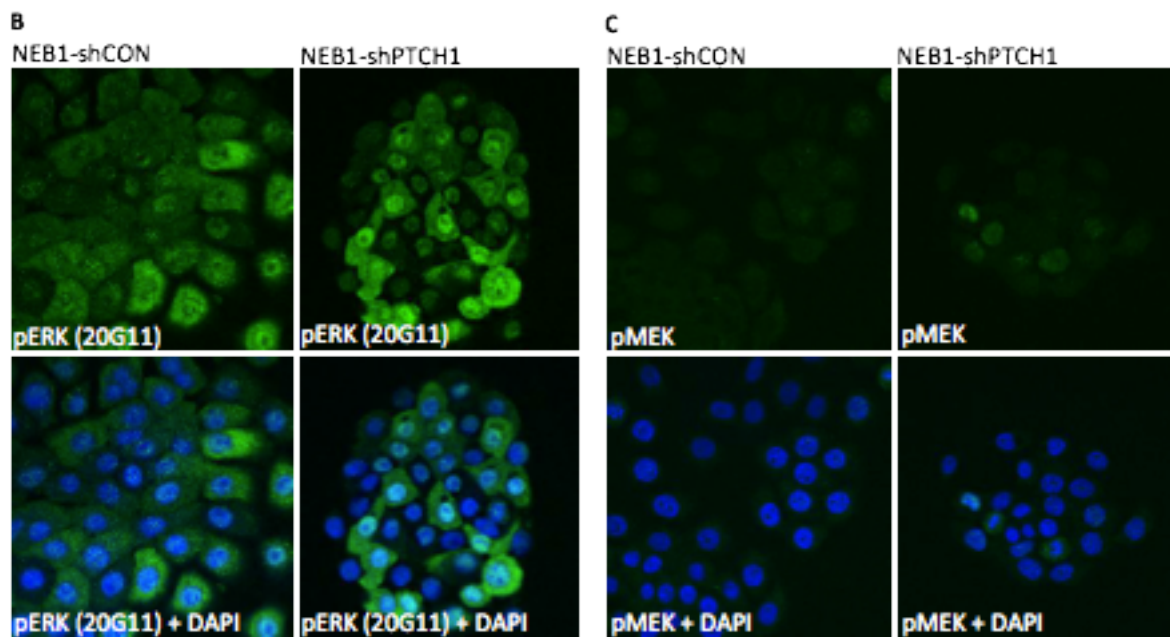


Fig.40: pEGFR, pERK and pMEK protein expression in NEB1 cells. Immunofluorescence staining of [A] pEGFR (Y1173 and Y845), [B] pERK (20G11) and [C] pMEK in NEB1- shCON and NEB1-shPTCH1 cells.

4.5.6 EGFR signalling and control of GLI expression in shPTCH1 cells

Several studies have shown that GLI1 transcriptional activity is increased by MEK/ERK signalling and it has also been shown that GLI1 expression is actually induced by MEK/ERK signalling (Schnidar et al., 2009). To determine if MEK/ERK signalling regulates the increase of GLI1 in NEB1-shPTCH1 cells, cultures were exposed to the MEK inhibitor U0126 as well as the EGFR inhibitor AG1478. The expression of GLI1 returned to basal levels in the presence of both U0126 and AG1478 indicating that the increase of GLI1 is mediated by EGFR/MEK/ERK signalling (Figure 41). Intriguingly, inhibition of EGFR, led to an increase of GLI2 mRNA levels which raises concerns about the use of anti-EGFR compounds for the treatment of BCC and possibly other tumours.

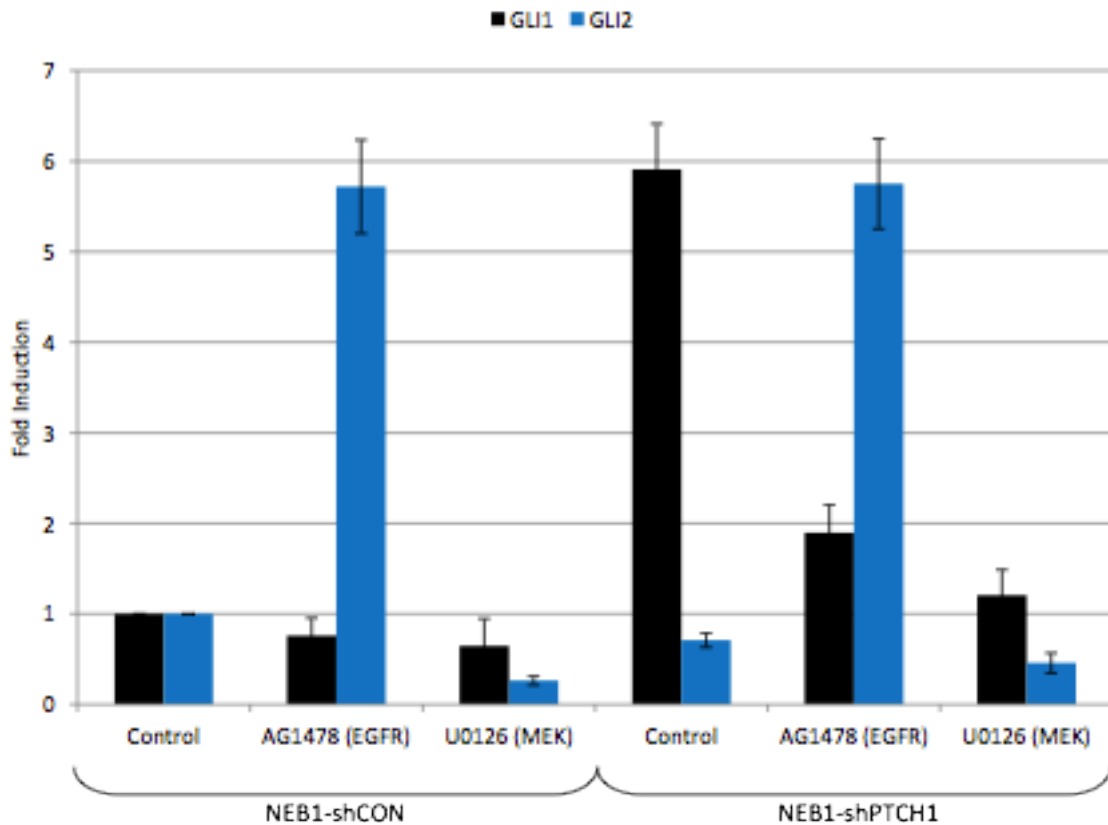


Fig.41: NEB1 cells treated with EGFR and MEK inhibitors

4.7 EGFR signalling pathway in human and murine BCCs

Despite demonstrating that the ERK pathway is more active in NEB1 due to the suppression of PTCH1, this does not correlate in BCC tissue. Immunohistological studies of pERK and pAKT in BCC tissue show that neither protein is active in BCC (Neill et al., 2008; Hafner et al., 2012). My group in London has done extensive analysis of EGFR signalling in BCCs and confirmed that pERK is not expressed in non-aggressive human BCCs (Figure 42). Interestingly, our group has also shown that human BCCs express pMEK so why it does not phosphorylate its principal target ERK (the un-phosphorylated protein is expressed in the tumours) is surprising and under further investigation. Moreover, we have also shown that pERK is not expressed in mouse BCCs whereas pMEK is abundant (unpublished data) (Figure 43).

The expression of pEGFR, pERK and pMEK was examined in 15 non-invasive and 14 invasive human BCCs (Figure 44). All phospho-proteins were expressed in normal and tumour associated epidermis (nuclear/cytoplasmic) but whereas pEGFR and pMEK were also present in all tumours (albeit at varying levels and with no apparent correlation), pERK was consistently absent in non-invasive BCCs; pERK staining was slightly higher in

invasive tumour islands but the main feature of these samples was that pERK was often localized to the stroma. pERK (but not pMEK) was dramatically absent compared to the epidermis. Conversely, pERK (but not pMEK) was expressed in the stromal cells of a more aggressive BCC-like variant which correlates with the presence of stromal pERK in invasive human BCC.

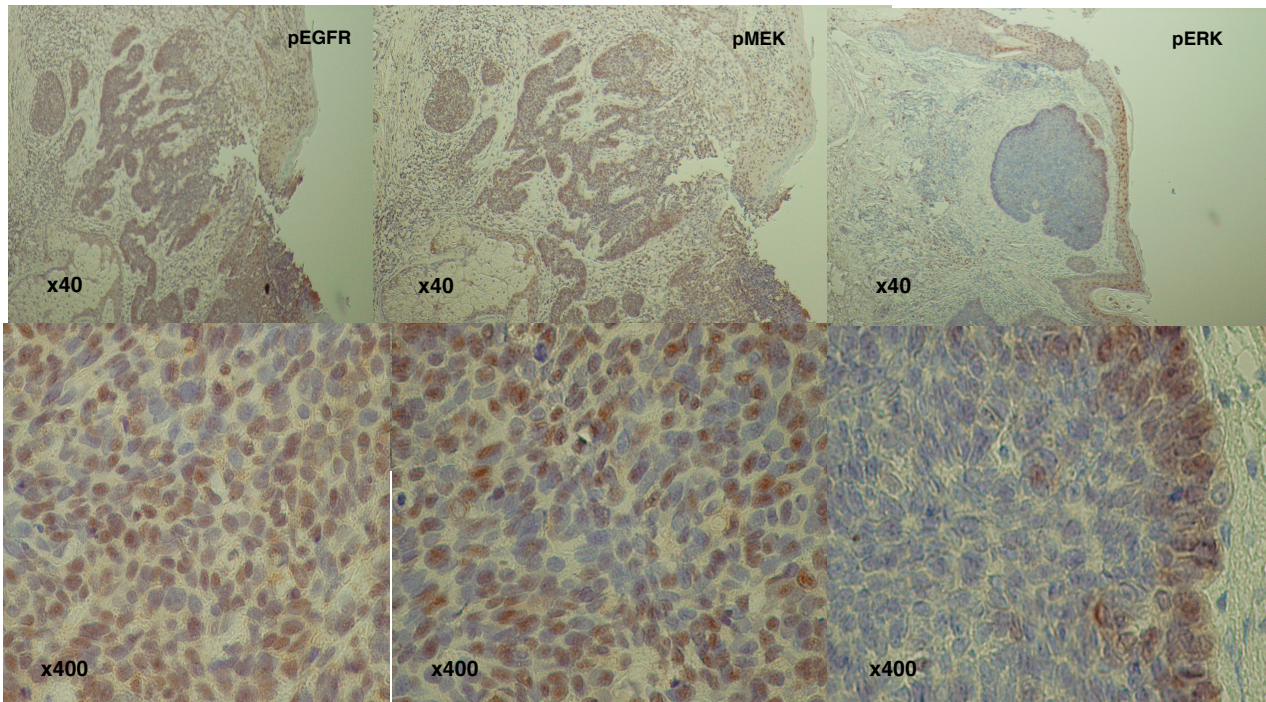


Fig.42 pEGFR, pMEK and pERK expression in non-infiltrative BCC

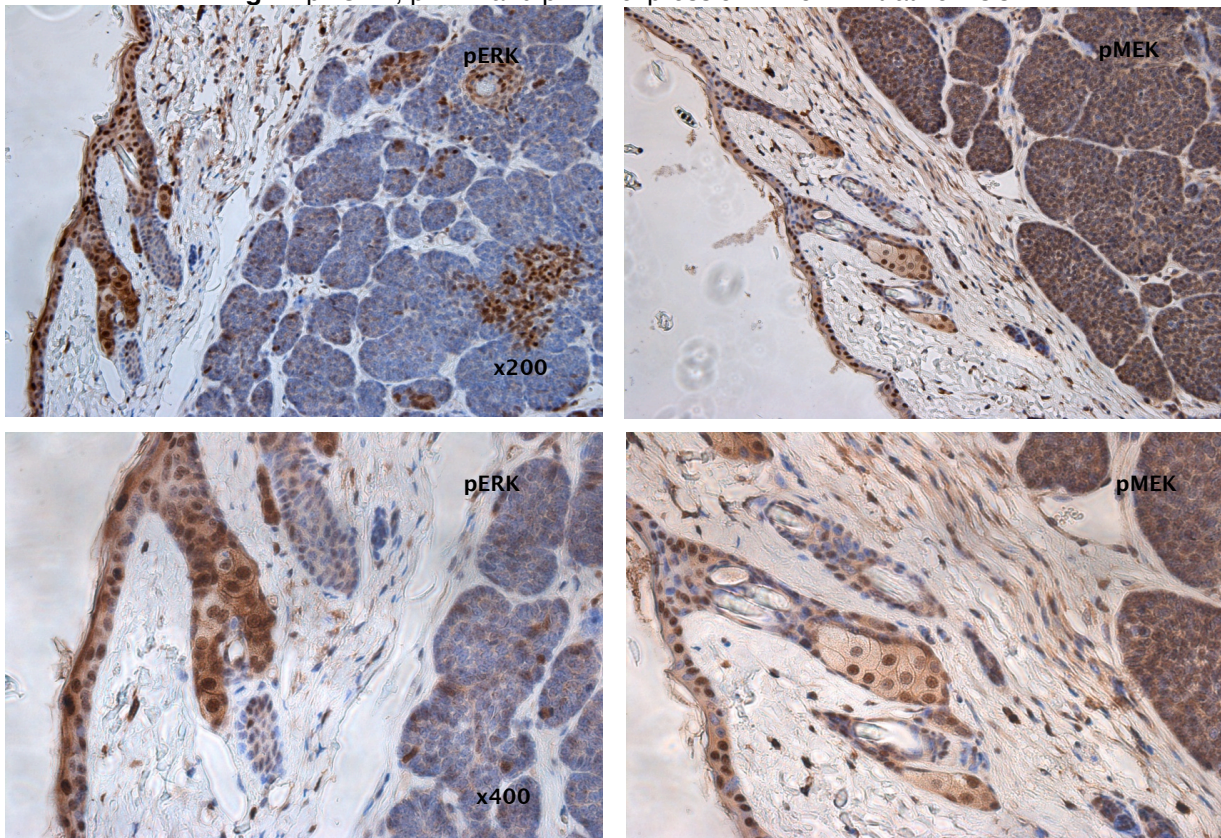


Fig.43 pMEK and pERK expression in murine BCC-like tumors

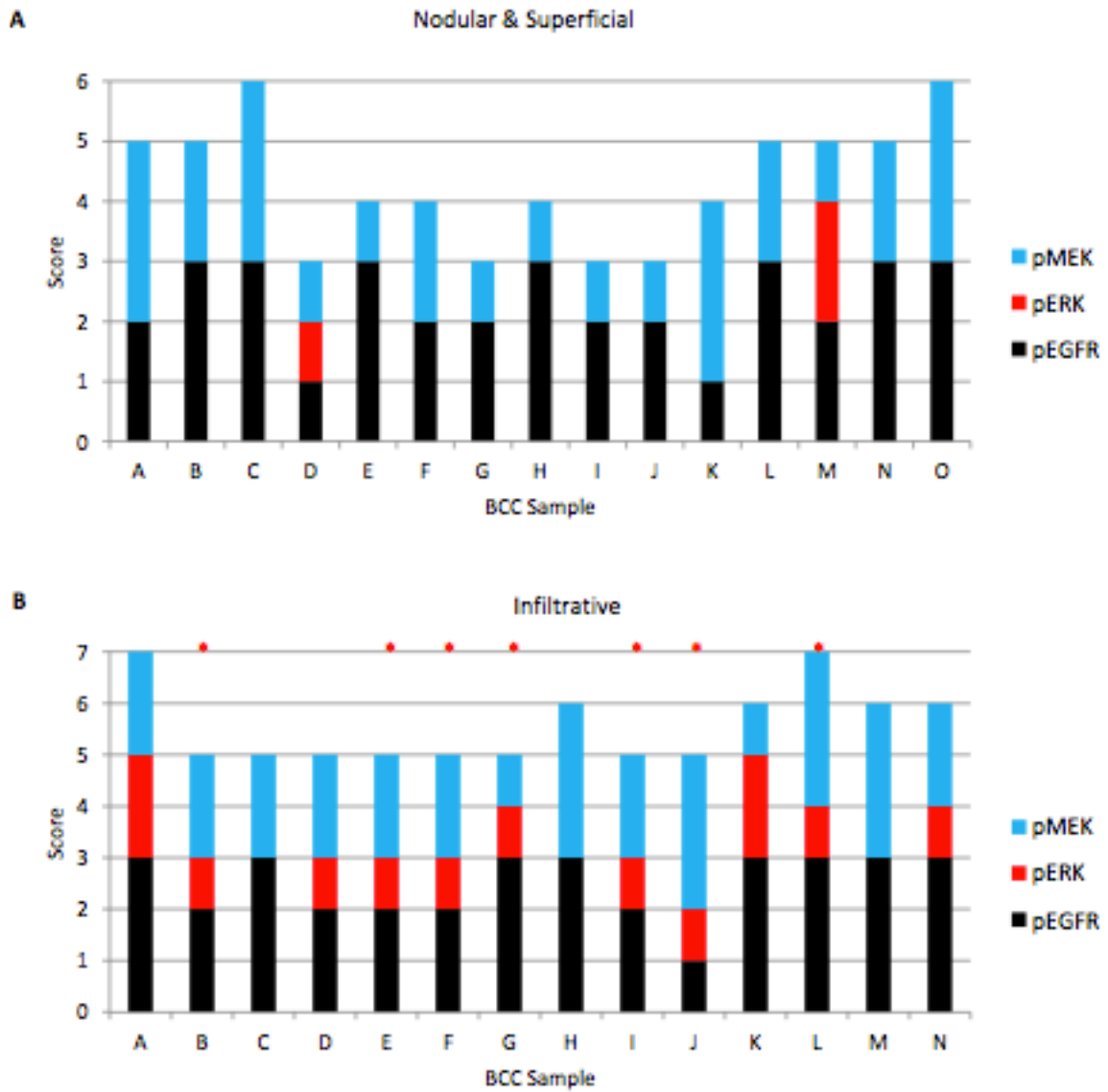


Figure 44: pEGFR, pERK and pMEK immunohistochemistry scoring in BCC tissue: [A] pEGFR, pERK and pMEK scoring in non-invasive BCCs. [B] pEGFR, pERK and pMEK scoring in invasive BCCs
 Scoring: 0 = 0%, 1 = 1-29%, 2 = 30-59%, 3 = 60-100% * denotes presence stromal pERK staining

CHAPTER 5

DISCUSSION

Prediction of human tumor response from preclinical data could reduce failure rates of clinical development of new anticancer drugs. The crucial question is therefore to define whether established preclinical models, in vitro and in vivo, retain the characteristics of the human tumors from which they are derived.

I focused my PhD course on development of preclinical models of two of the most common and aggressive malignancies: Small cell lung cancer (SCLC) and Basal cell carcinoma (BCC).

SCLC accounts for approximately 15% of bronchogenic carcinoma. SCLC is more responsive to chemotherapy and radiation therapy than other cell types of lung cancer; however, a cure is difficult to achieve because SCLC very frequently relapses and has a greater tendency to be widely disseminated by the time of diagnosis.

BCC, a slow-growing form of skin cancer, is the most common form of cancer in the Western World. Although BCC is a malignant neoplasm, it rarely metastasizes. The incidence of metastatic BCC is estimated to be less than 0.1%. Nevertheless, after treatment, which is curative in more than 95% of cases, BCC may develop in new sites.

Although quite different, these two pathologies share important features:

- Lack of effective and decisive treatments;
- Need for new experimental models to test novel therapies.

The poor therapeutic efficacy achieved to date is a direct consequence of the lack of knowledge of molecular mechanisms underlying these diseases.

In our previous studies at the Laboratory of Pediatric Oncology of the University of Bologna, we characterized the anti-tumor activity of a specific anti-MYCN PNA inhibitor able to silence human MYCN gene expression (Tonelli R. et al, 2005) in MYCN-amplified NB cells: a potent and specific anti-tumor activity as well as an apoptosis induction were demonstrated. Following MYCN silencing also MDM2 protein level was reduced, rescuing p53 levels and inducing apoptosis in MA-NB cells (Slack A. et al, 2005). In a preliminary study, anti-

MYCN PNA did not show toxicity in no-expressing MYCN cells (Tonelli R. et al, 2005).

MYCN amplification and overexpression have been found in both SCLC and BCC. In particular three of the members of the MYC family, c-MYC, MYCN and LMYC, have been shown to be amplified in tumors and tumor cell lines from patients with SCLC [Gazzeri et al. 1991]. MYC amplification is associated with a variant form of SCLC that has a more rapid growth rate than the classic type [Johnson BE et al. 1986].

The first part of the project has been dedicated to set up appropriate preclinical in vitro and in vivo model to evaluate the potential therapeutic role of targeting MYCN in SCLC.

Thirteen SCLC cell lines have been characterized at the molecular level, by qPCR, WB and FISH to evaluate respectively mRNAs, proteins and DNA amplifications of c-MYC, MYCN and LMYC. Surprisingly in each cell line, only one member of the MYC family genes has been found to be predominant. WB confirmed the expression of N-Myc protein in H69, N592 and GLC14 cell lines, and FISH confirmed the DNA amplification.

The same cell lines have been employed to test the antitumor activity of three chemotherapy compounds largely administered in clinical protocols: Cisplatin, Carboplatin and Etoposide.

Cisplatin showed the highest efficacy in all the cell lines tested, probably due to its covalent binding to DNA and the consequent formation of cruciate ligaments between complementary strands, regardless of the cell cycle stage. Therefore the cytotoxic action indiscriminately affects all cells. Moreover Etoposide results to be very effective on cells, although EC50 values are higher than Cisplatin. Etoposide is a cycle-specific compound and, by inhibiting the topoisomerase II enzyme, blocks the cells exclusively during their proliferative phase; this particular mechanism, more selective for cancer cells (rapidly proliferating compared to healthy cells) allows the drug to have a lower toxicity and limited adverse effects compared to Cisplatin.

Among the antineoplastic drugs tested, Carboplatin is the least effective: higher concentrations are required to achieve the same effect obtained with Cisplatin or Etoposide. These results confirm literature data, in which elderly patients with

renal impairment capacity tolerate better oral administration of Carboplatin [Puglisi M. et al 2010], due to the favorable toxicity profile of this drug.

In vitro studies performed on SCLC cell lines using anti-MYCN PNAwt showed cell growth inhibition activity only in the H69, N592 and GLC14 cell line, carrying MYCN amplification, while no inhibition was observed in H82 cell line. This result correlates with Real Time PCR assays, showing a significant change of expression in response to PNA treatment only in MYCN amplified cell lines. To evaluate the specificity of the molecule, we conducted a test with a mutated PNA that has confirmed that the effect is sequence specific. Therefore the data obtained, besides highlighting the critical role of MYCN amplification in this disease, can also be considered valid basis for a preclinical study.

All cell lines have been engineered to insert a stable expression of the luciferase gene; the transfection is rather complicated and each step presents several variables that could result in errors; for this reason the percentage of success of the method is not very high, and among all, only H69, H526, GLC14 and DMS-79 cell lines passed positively the antibiotic selection phase.

Following completion of in vitro experiments, in vivo studies have been started. As it's well known, transgenic murine models better summarize the clinical development of pathologies. Currently only a mouse model of small cell lung carcinoma have been developed [Berns A. et al. 2005]. The lack of models is due to a poor knowledge of the molecular mechanisms leading to carcinogenesis in this pathology and the role of pulmonary neuroendocrine cells from which SCLC originates.

Therefore, we created two orthotopic xenograft mouse models using H69-Luc and H526-Luc cell lines and in vivo bioluminescence imaging as a strategy.

Bioluminescence in vivo represents a method with no aspecific signal, widely used in preclinical oncology. It allows to monitor the presence of tumoral cells in internal organs, quantify tumor growth in real-time without animal sacrifice and identify metastases.

By intrapulmonary inoculation we created two models injecting H69 and H526 luminescent cells respectively: tumor progression over time was monitored in both models.

We established excellent preclinical models; small cell lung cancer cells are able in vivo to organize and develop, generating a tumor mass recognized by histological analysis as Small Cell Lung Carcinoma. The described models

allow to monitor early development and tumor mass growth, which is very important since the only visible symptoms occur late. Not of secondary importance, the model created, compared to transgenic models and others based on PET analysis, can be developed in a relatively short time, requires a low level of specialization and utilizes inexpensive reagents and equipment.

By definition, an animal model for preclinical studies must be able to mimic accurately the pathology, to assume with confidence that any positive result obtained in animals is also translatable to men.

Since one of the main features of Small cell lung cancer is the immediate response to chemotherapy, one of the two mouse models has been validated using standard chemotherapy (Cisplatin plus Etoposide).

As in clinical treatments, this model shows a decrease of BLI signal after two weeks of chemotherapy cycles. In addition, chemotherapy is well tolerated and does not affect drastically the vital functions. The results are quite encouraging both in terms of efficacy and safety. Finally, the treated animals have an extension of survival of 20 days compared to the control and the placebo groups.

All these features make our preclinical models of Small cell lung carcinoma ideal for drug screening and for a better evaluation of potential new therapeutic agents against this disease. In the future it is expected to complete the development of these models by increasing the number of mice studied to improve the statistics and to define more precisely the chemotherapy protocols to improve the toxicological profile.

In addition, other mouse models will be created using stabilized xenograft cells derived from patients relapsed or refractory to treatment, and the different models will be compared to one another.

Considering that the cell lines used (H69 and H526) were characterized in details and showed a pattern of substantial genetic alterations, the models developed may be used to evaluate the efficacy of target-specific molecules with the ultimate goal of being able to use in humans for personalized treatments based on the altered genes in each individual patient.

In the second part of the project, pre-existing preclinical in vitro and in vivo models of BCCs were used to find new targets for customized therapies. Moreover this was a chance to study the Hedgehog signalling pathway, one of

the most investigated pathway for its implications in the pathogenesis of certain types of cancer.

In vitro BCC model was developed by the suppression of PTCH1 in human keratinocytes using shRNA and the HH signalling pathway was characterized.

The validity of suppressing PTCH1 to create an in vitro model of BCC was first supported by the observation that in two-dimensional culture some clonal NEB1-shPTCH1 cell lines cultured as more compact colonies compared to parental or control cells, thus showing a morphology similar to nodular BCC.

It is difficult to determine which form of BCC NEB1-shPTCH1 cells are modeling: in two-dimensional culture the morphology of the cells would suggest a nodular BCC while in organotypic culture they more likely resemble superficial BCC.

Matrigel based organotypic culture of NEB1-shPTCH1 cells did not result in BCC formation, as there might be the need of a certain level of PTCH1 suppression to initiate tumour formation, whereas shRNA does not fully suppress PTCH1. However, there was evidence of a hyperproliferation of the epidermal layer and since NEB1-shPTCH1 cells present a high grade of PTCH1 suppression, a separate event might be needed to occur before BCCs could develop. This could be obtained through UV irradiation as seen in mice studies or via other pathways that are linked to HH signalling.

Most clonal cell lines also displayed increased levels of GLI1. The induction of GLI1 via PTCH1 suppression was confirmed by the fact that the increase of endogenous GLI1 was suppressed upon ectopic expression of the PTCH1B isoform which is not targeted by the PTCH1 shRNA construct.

We also noticed that SMO and GLI1 expression is not suppressed upon exposure to SMO pharmacological inhibitors in NEB1-shPTCH1 and it is worth noting that no studies have convincingly shown that GLI1 expression is actually reduced in BCCs using clinical compounds such as GDC-0449 (Erivedge®). Various SMO inhibitors have been described including GDC-0449 however, many patients do not respond to these treatments and the levels of GLI1 have not been reported in non-responding tumours (Van Hoff et al., 2009). Indeed, having demonstrated that GLI1 is not suppressed by Cyclopamine-KAAD or SANT1 in shPTCH1 cells, the effects of anti-SMO inhibitors upon GLI1 expression in BCCs requires further evaluation.

This mode of non-canonical GLI1 signalling may occur through other pathways. The idea that HH signalling can occur non-canonically has been explored and is not entirely a new concept. GLI1 was over expressed in NIH-3T3 cells and the increase of its activity was confirmed with a GLI1 reporter construct. Cells treated with Cyclopamine did not repress GLI1 reporter activity which only returned to basal levels when the cells were transfected with PTCH (3:1 ratio of PTCH:GLI1) (Rahnama et al., 2006). This shows that GLI1 is controlled by PTCH but signals independently of SMO. Also, if the HH pathway was linear (i.e. PTCH1 signals through to GLI1 without the influence of any other pathway), a lower amount of PTCH would need to be transfected into NIH-3T3 cells to suppress GLI1. Since three times the amount of PTCH to GLI1 is required, GLI1 may be expressed thorough other non-conventional modes.

Analysis of the SMO protein sequence reveals a bipartite N-terminal nuclear localization sequence (NLS) which provides evidence that SMO has the capacity to localize to the nucleus. As NEB1 cells display nuclear expression of PTCH1, SMO and GLI1, then potentially this could explain why, despite the presence of a SMO inhibitor, GLI1 is activated.

The effectiveness of new SMO inhibitors to treat BCCs might depend upon the method by which the tumour was initiated (e.g. through PTCH1 mutations, SMO activation or UV associated DNA damage).

Thus, one more time, it is extremely important to select the right animal model. In this study we employed *Ptch*^{+/-} mice that upon X-ray irradiation lost the wt allele and started to develop BCCs. As already mentioned, if the mice have been irradiated during the telogen phase BCCs will be superficial; in contrast they will be more aggressive/infiltrative if the X-ray irradiation is administered during the anagen phase.

On this model we performed extensively IHC analysis to address the possibility for HH and EGFR to cooperate in BCC tumorigenesis.

The EGFR signalling pathway and its downstream targets are altered in NEB1-shPTCH1 cells due to the suppression of PTCH1. Neill and colleagues have previously shown that EGFR signalling influences GLI1 target genes in human keratinocytes and they demonstrated how a strong GLI1 activity negatively regulates EGFR/ERK signalling (Neill et al., 2008).

In the previous study a higher GLI1 overexpression in N/Tert keratinocytes was obtained through an EGFP-GLI1 fusion protein whereas NEB1-shPTCH1 cells,

with a modest increase of GLI1 levels, were used in the present study. However there was a reduction in EGFR mRNA expression in NEB1-shPTCH1 cells compared to NEB1-shCON cells. Interestingly, analysis of pEGFR (Y1173 and Y845) showed increased nuclear expression in NEB1-shPTCH1 cells compared to NEB1-shCON cells. Phosphorylation of Y845 has been implicated in maintaining activation of EGFR (Hubbard et al., 1994) while Y1173 phosphorylation has been linked to ERK activation (Hsu et al., 2011). Despite a decrease in EGFR protein and mRNA expression in NEB1-shPTCH1 cells, downstream ERK and its target genes are more active.

Western blot analysis of EGFR downstream targets pERK and pMEK showed that there was reduced expression in NEB1-shPTCH1 cells compared to NEB1-shCON cells. Similar to pEGFR expression, there was increased nuclear staining for pERK and pMEK in NEB1-shPTCH1 cells compared to NEB1-shCON cells. Again, this suggests that pERK and pMEK are more active in NEB1-shPTCH1 due to nuclear protein localization. However, without a MEK/ERK reporter construct, it would be difficult to determine if ERK is more active in the cells. NEB1 cells were difficult to lyse when attempting to perform a Luciferase assay therefore ERK target genes were analyzed.

Based on the data obtained from the microarray that suggests EGFR signalling is differentially regulated, ERK target genes were analyzed by qPCR in NEB1 cells. Downstream targets of ERK were increased in NEB1-shPTCH1 cells compared to NEB1-shCON cells. As ERK is phosphorylated and translocates to the nucleus, it acts upon FOS, JUN, MYC and ELK transcription factors (Kerkhoff and Rapp, 1998). FOS and SRF are known to bind to each other to regulate DNA binding activity (Prywes et al., 1988). Also, active ERK has been shown to induce phosphorylation of ELK (Cruzalequi et al., 1999). EGR1 expression in PC3 prostate cell lines has been shown to be mediated through the EGF induced ERK signalling pathway (Gregg and Fraizer, 2011). This along with the nuclear expression of pEGFR that may lead to increased expression of pERK and pMEK supports the idea that ERK signalling is more active in NEB1-shPTCH1 cells compared to NEB1-shCON cells.

As mentioned earlier, the EGFR and HH signalling pathways are likely to be linked and that the over expression of GLI1 leads to differential expression of EGFR components in keratinocyte cell lines. The tight colony formation observed in NEB1-shPTCH1 cells was also observed when GLI1 was over

expressed in N/Tert keratinocytes (Neill et al., 2008). In contrast, studies have shown that the EGFR and HH pathways are synergistically linked as demonstrated in N/Tert keratinocytes where 19 genes were found to be induced synergistically by GLI1 and EGF treatment also; GLI1 target genes were shown to be modulated by EGFR signalling through MEK/ERK pathways (Kasper et al., 2006). This is further supported by the study of mouse BCC cell lines ASZ001 and BSZ2 (Ptc^{-/-}) as well as CSZ1 (p53^{-/-}). These cell lines express higher levels of EGFR mRNA compared to keratinocytes. By inhibiting both EGFR with gefitinib and GLI signalling with GANT61 there is a reduction of BCC growth which suggests that both are a good target for BCC therapy (Schnidar et al., 2009). Conversely, this suggests that the dysregulation of both pathways may lead to BCC formation or development.

The study also demonstrated that EGFR/MEK/ERK pathways increase GLI1 and GLI2 expression (Schnidar et al., 2009) In agreement with this, the expression of GLI1 was reduced in NEB1-shCON and NEB1-shPTCH1 cells that were treated with the EGFR inhibitor AG1478 and both GLI1 and GLI2 were suppressed with the MEK inhibitor U0126. However, inhibition of EGFR, led to an increase of GLI2 mRNA levels which suggests that EGFR and HH signalling do not act in synergy with regards to control of GLI2 in human keratinocytes.

These data also shows that the inhibition of MEK/ERK effectively suppresses both GLI1 (canonical as well as non-canonical GLI1 that is not suppressed by SMO inhibitors) and GLI2 in NEB1-shPTCH1 cells which could be a good therapeutic target. In NIH-3T3 cell, MEK and ERK were able to stimulate GLI reporter activity and when MEK/ERK combined with either GLI1 or GLI2, there was a much greater induction of GLI reporter activity (Riobo et al., 2006 B). Based on this and the data generated that show activation of ERK signalling, GLI1 induction in NEB1-shPTCH1 cells may be mediated through ERK rather than the canonical HH pathway. The question then arises as to whether the loss of PTCH1 leads to MEK/ERK mediated GLI expression in a signalling mode that may not require SMO. This would explain why NEB1-shPTCH1 cells do not respond to SMO inhibitors to a certain extent but not why SMO siRNA represses GLI1.

Treatment of NEB1 cells with EGFR inhibitor increased GLI2 expression despite GLI1 expression being reduced. This is interesting as GLI1 and GLI2 are part of a feedback loop therefore if GLI1 is suppressed then GLI2 should also be

suppressed (Regl et al., 2002). The induction of GLI2 may occur to compensate for the suppression of GLI1. Also, the data suggest that GLI1 and GLI2 can be expressed independently of each other i.e. GLI2 expression does not depend on GLI1 expression. To use such inhibitors for therapy may therefore induce GLI2 which in turn could facilitate BCC growth. A study where the targeting of both the EGFR and HH pathways reduced mouse BCC growth (Schnidar et al., 2009) could therefore be interpreted as the EGFR inhibitor reducing GLI1 and the HH inhibitor repressing GLI2. If the MEK/ERK cascade is disrupted by the EGFR inhibitor, it is likely that both GLI1 and GLI2 are reduced.

Despite demonstrating that the ERK pathway is more active in NEB1 and N/Tert cells due to the suppression of PTCH1, this does not correlate in BCC tissue. Immunohistological studies of pERK and pAKT in BCC tissue show that neither protein is active in BCC (Neill et al., 2008; Hafner et al., 2012). We have done extensive analysis of EGFR signalling in BCCs and confirmed that pERK is not expressed in non-aggressive human BCCs. Interestingly, we have also shown that human BCCs express pMEK so why it does not phosphorylate its principal target ERK (the un-phosphorylated protein is expressed in the tumours) is surprising and under further investigation. Moreover, pERK is not expressed in mouse BCCs whereas pMEK is abundant (unpublished data).

The expression of pEGFR, pERK and pMEK was examined in 15 non-invasive and 14 invasive human BCCs. All phospho-proteins were expressed in normal and tumour associated epidermis (nuclear/cytoplasmic) but whereas pEGFR and pMEK were also present in all tumours (albeit at varying levels and with no apparent correlation), pERK was consistently absent in non-invasive BCCs; pERK staining was slightly higher in invasive tumour islands but the main feature of these samples was that pERK was often localized to the stroma. pERK (but not pMEK) was dramatically absent compared to the epidermis. Conversely, pERK (but not pMEK) was expressed in the stromal cells of a more aggressive BCC-like variant which correlates with the presence of stromal pERK in invasive human BCC.

As pEGFR was localized in the nucleus in nodular BCCs and in NEB1-shPTCH1 cells, it is possible that this could account for the global reduction of pERK due to reduced EGFR activity at the cell membrane. Analysis of the EGFR signalling in human tumors reveals that the canonical pathway is not fully

active in BCC and that further work is required to determine if and how components of the pathway warrant therapeutic attention.

Indeed, whether or not loss of ERK activity is important for tumour formation these data reveal that the nature of EGFR signalling(including how it interacts with HH signalling) in BCC biology is complex and that further reserach is required to determine the suitability of components of this pathway thearapeutic intervention.

Moreover, we are currently setting up the *Ptch*^{+/-} colony to continue these experiments and to bear out that NMYC oncogene is a Shh downstream effector and high expression of N-Myc protein is a frequent event in BCC predominantly in more aggressive subtypes. If these findings were confirmed novel systemic antigene inhibition strategies could be a promising option for therapy-refractory BCC.

CHAPTER 6

REFERENCES

ADOLPHE C. et al. Patched1 functions as a gatekeeper by promoting cell cycle progression. *Cancer Res.* 2006;66(4);2081-8.

ADRIANSEN et al. Evidence for a role of neuroepithelial bodies as complex airway sensor: comparison with smooth muscle-associated airway receptor. 2006 *J Appl Physiol*;101:960-970.

AMATI B. et al. Myc-Max-Mad: a transcription factor network controlling cell cycle progression, differentiation and death. *Curr Opin Genet Dev.* 1994 Feb; 4(1):102-8.

ASZTERBAUM M. et al. Ultraviolet and ionizing radiation enhance the growth of BCCs and trichoblastomas in patched heterozygous knockout mice. *Nat Med.* 1999 Nov;5(11):1285-91.

BEACHY PA. et al. Tissue repair and stem cell renewal in carcinogenesis. 2004 *Nature.* 432:324-31.

BECK W.T. et al. Cytotoxic signalling by inhibitors of DNA topoisomerase II. *Biochem Soc Trans.* 2001 Nov;29(Pt 6):702-3.

BERTHOLD F. et al., The current contribution of molecular factors to risk estimation in neuroblastoma patients. *Eur J Cancer,* 1997. 33(12): p. 2092-7.

BINNS W. A congenital cyclopi-an-type malformation in lambs induced by maternal ingestion of a range plant, *Veratrum californicum*. *Am. J. Vet. Res.* 24, 1164–1175 (1963).

BLACKWOOD E.M. et al. Max: a helix-loop-helix zipper protein that forms a sequence-specific DNA-binding complex with Myc. *Science,* 1991. 251(4998): p. 1211-7.

BLESH A. et al. Lentiviral and MLV based retroviral vectors ex vivo and in vivo gene transfer. *Methods* 2003;33:164-172

BOFFA L.C. et al. Dihydrotestosterone as a selective cellular/nuclear localization vector for anti-gene peptide nucleic acid in prostatic carcinoma cells. *Cancer Res.* 2000 Apr 15;60(8):2258-62

BONVINI P. et al. In vivo degradation of N-myc in neuroblastoma cells is mediated by the 26S proteasome. 1998 *Oncogene*, 16(9): p. 1131-9.

BRAMBILLA E. et al. Apoptosis-related factors p53, Bcl2, and Bax in neuroendocrine lung tumors. 1996 *Am.J. Pathol.* 149: 1941–1952

BREMNES R.M. et al. The E-cadherin cell–cell adhesion complex and lung cancer invasion, metastasis, and prognosis. 2002 *Lung Cancer* 36: 115–124.

CHAMBERS A.F. et al. Changing views of the role of matrix metalloproteinases in metastasis. 1997 *J. Natl. Cancer Inst.* 89: 1260–1270.

CHEN J. K. Inhibition of Hedgehog signaling by direct binding of cyclopamine to Smoothened. *Genes Dev.* 16, 2743–2748 (2002).

CHIKAKO K., OHNO Y. Sex differences in lung cancer susceptibility: a review. 2010 *Gend Med* Oct;7(5):381-401

COLLINS TJ. ImageJ for microscopy. 2007 *Biotechniques.* 43(1 Suppl):25-30.

CRETNIK M. et al. Involvement of p16 and PTCH in pathogenesis of melanoma and basal cell carcinoma. *Int J Oncol.* 2009;34; 1045-1050.

CROWSON AN. Basal cell carcinoma: biology, morphology and clinical implications. 2006 *Mod Pathol.* 19 Suppl 2:S127-47.

CUTRONA G. et al. Inhibition of the translocated c-myc in Burkitt's lymphoma by a PNA complementary to the E μ enhancer. *Cancer Res.* 2003 Oct 1;63(19): 6144-8

CUTZ E. et al. Pulmonary neuroendocrine cell system in pediatric lung disease-recent advances. 2007 *Pediatr Dev Pathol*;10:419-435126:545-553.

DALLA-FAVERA R. et al. Oncogene amplification in promyelocytic leukaemia cell line HL- 60 and primary leukaemic cells of the same patient. 1982 *Nature*, 299(5878): p. 61-3.

DAVIS R.L. et al., The MyoD DNA binding domain contains a recognition code for muscle-specific gene activation. 1990. *Cell*, 60(5): p. 733-46.

DEMIDOV V.V. et al., Stability of peptide nucleic acids in human serum and cellular extracts. *Biochem Pharmacol*,1994. 48(6): p.1310-3.

DENEF N. et al. Hedgehog induces opposite changes in turnover and subcellular localization of patched and smoothed. 2000 *Cell*. 102:521–31.

D'ERRICO M. p53 Mutations and Chromosome Instability in Basal Cell Carcinomas Developed at an Early or Late Age. 1997 *Can Res.* 57; 747-752.

DOHOLEN G. et al. Antioxidant Activity in the Newborn Brain: A Luciferase Mouse Model. *Neonatology* 2008;93:125-131

DONOVAN J. Review of the Hair Follicle Origin Hypothesis for Basal Cell Carcinoma. 2009 *Dermatol Surg.* 35(9):1311-23

EGHOLM M. et al., PNA hybridizes to complementary oligonucleotides obeying the Watson-Crick hydrogen-bonding rules. *Nature*, 1993. 365(6446): p. 566-8.

EILERS M. et al. The MYC protein activates transcription of the alpha-prothymosin gene.1991 *Embo J*, 10(1): p. 133-41

FISHER B. et al. Current status of clinical trials for small cell lung cancer. 2008 *Rev Recent Clin Trials* 3: 40–61

FOX W., SCADDING JG. Medical Research Council comparative trial of surgery and radiotherapy for primary treatment of small-celled or oat-celled carcinoma of bronchus. Ten-year follow-up. *Lancet* 1973 2:63–65

FREIER K. et al. Recurrent NMYC copy number gain and high protein expression in basal cell carcinoma. *Oncol Rep.* 2006 May;15(5):1141-5.

FRESE KK. et al. Maximizing mouse cancer models *Nat Rev Cancer.* 2007 Sep;7(9):645-58.

GAILANI MR. Developmental genes and cancer: role of patched in basal cell carcinoma of the skin. 1997 *J Natl Cancer Inst.* 89(15):1103-9.

GHALI L. et al. Gli1 protein is expressed in basal cell carcinomas, outer root sheath keratinocytes and a subpopulation of mesenchymal cells in normal human skin. 1999 *J Invest Dermatol.* 113(4):595-9.

GONZALEZ V.M. et al. Is cisplatin-induced cell death always produced by apoptosis? *Mol Pharmacol.* 2001 Apr;59(4):657-63

GORDON J.W. et al. Integration and stable germline transmission of genes injected into mouse pronuclei. *Science*, 1981. 214(4526): p. 1244-6.

GORLIN RJ. et al. Multiple nevoid basal-cell epithelioma, jaw cysts and bifid rib. A syndrome. 1960 *N Engl J Med.* 262:908–912

GOSNEY JR. Neuroendocrine cell population in postnatal human lungs: minimal variation from childhood to old age. 1993 *Anat Rec.* 236:117-180

GOVINDAN R. et al. Changing epidemiology of small-cell lung cancer in the United States over the last 30 years: analysis of the surveillance, epidemiologic, and end results database. 2006 *J Clin Oncol.* Oct 1;24(28):4539-44

GRALLA RJ. et al. Quality-of-life considerations in patients with advanced lung cancer: effect of topotecan on symptom palliation and quality of life. 2004 *Oncologist* 9 (Suppl 6): 14–24

GRANDORI C. et al., Myc target genes. *Trends Biochem Sci*, 1997. 22(5): p. 177-81.

GRANDORI C. et al. The Myc/Max/Mad network and the transcriptional control of cell behavior.2000 *Annu Rev Cell Dev Biol*. 16: p. 653-99.

GRACHTCHOUK M. et al. Basal cell carcinomas in mice overexpressing Gli2 in skin. *Nature Genet*. 24, 216–217 (2000).

GRACHTCHOUK V. et al. The magnitude of hedgehog signaling activity defines skin tumor phenotype. *EMBO J*. 22, 2741–2751 (2003).

GUSTAFSSON B.I. et al. Bronchopulmonary Neuroendocrine Tumors. 2008 *Cancer* Volume 113-1

HAHN H. et al. Mutations of the human homolog of Drosophila patched in the nevoid basal cell carcinoma syndrome. 1996 *Cell*. 85(6):841-51.

HEINE VM. et al. Dexamethasone destabilizes Nmyc to inhibit the growth of hedgehog-associated medulloblastoma. *Cancer Res*. 2010 Jul 1;70(13):5220-5

HERBST RS. "Review of epidermal growth factor receptor biology". 2004 *Int. J. Radiat. Oncol. Biol. Phys*. 59 (2 Suppl): 21–6

HIRATA T. et al. Expression of E-cadherin and lymph node metastasis in resected non small-cell lung cancer. 2001 *Clin. Lung Cancer* 3: 134–140

HOUGHTON PJ. et al. Stage 2 Combination Testing of Rapamycin with Cytotoxic Agents by the Pediatric Preclinical Testing Program, *Mol Cancer Ther* 2010;9:101-112.

HYRUP B. et al., Peptide nucleic acids (PNA): synthesis, properties and potential applications. *Bioorg Med Chem*, 1996. 4(1): p. 5-23.

ITO T. et al. Development of pulmonary neuroendocrine cell of fetal hamster in explant culture. 1997 *Lab Invest* ;77:449:453

JIANG S.X. et al. Expression of bcl-2 oncogene protein is prevalent in small cell lung carcinomas.1995 *J. Pathol.* 177: 135–138.

JOHNSON BE. et al. MYC family DNA amplification in 126 tumor cell lines from patients with small cell lung cancer. 1996 *J. Cell Biochem Suppl.* 24: 210–217

JOHNSON BE. et al. Farnesyl transferase inhibitors for patients with lung cancer. *Clin Cancer Res.* 2004

JOHNSON RL. et al. Human homolog of patched, a candidate gene for the basal cell nevus syndrome. 1996 *Science.* 272(5268):1668-71.

JOPLING C.L. et al. N-myc translation is initiated via an internal ribosome entry segment that displays enhanced activity in neuronal cells. 2001 *Oncogene*, 20(21): p. 2664-70.

KALOGERAKI A. et al. E-cadherin expression on fine-needle aspiration biopsies in primary lung adenocarcinomas is related to tumor differentiation and invasion. 2003 *Anticancer Res.* 23: 3367–3371

KASPER M. Selective modulation of Hedgehog/GLI target gene expression by epidermal growth factor signaling in human keratinocytes. 2006 *Mol Cell Biol.* 26(16):6283-98.

KHANNA K.K. et al. DNA double-strand breaks: Signaling, repair and the cancer connection. 2001 *Nat Genet* 27: 247–254.

KILLION J.J. et al. Orthotopic models are necessary to predict therapy of transplantable tumors in mice. *Cancer Metastasis Rev.* 1998-1999;17(3): 279-84. Review.

KIM MY. et al. Mutations of the p53 and PTCH gene in basal cell carcinomas: UV mutation signature and strand bias. 2002 *J Dermatol Sci.* 29(1):1-9.

KIM YH. et al. Combined microarray analysis of small cell lung cancer reveals altered apoptotic balance and distinct expression signatures of MYC family gene amplification. *Oncogene* (2006) 25, 130–138

KOHL N.E. et al., Transposition and amplification of oncogene-related sequences in human neuroblastomas. 1983 *Cell*, 35(2 Pt 1): p. 359-67.

KRYSTAL GW et al. The selective tyrosine kinase inhibitor STI571 inhibits small cell lung cancer growth. *Clin Cancer Res.* 2000;6(8):3319-3326

KRYSTAL GW. et al. The insulin-like growth factor I receptor kinase inhibitor, NVP-ADW742, sensitizes small cancer cell lines to the effect of chemotherapy. *Clin Cancer Res.* 2005;11(4):1563-1571

KUHN H. et al. Kinetic sequence discrimination of cationic bis-PNAs upon targeting of double-stranded DNA. *Nucleic Acids Res*, 1998. 26(2): p. 582-7.

LAD T. et al. A prospective randomized trial to determine the benefit of surgical resection of residual disease following response of small cell lung cancer to combination chemotherapy. 1994 *Chest* 106: 320S–323S

LALLY BE. et al. Small cell lung cancer: have we made any progress over the last 25 years? 2007 *Oncologist* 12: 1096–1104

LANDSCHULZ W.H. et al. The leucine zipper: a hypothetical structure common to a new class of DNA binding proteins. 1988 *Science*, 240(4860): p. 1759-64.

LI T.K. et al. Tumor cell death induced by topoisomerase-targeting drugs. *Annu Rev Pharmacol Toxicol.* 2001;41:53-77. Review.

LIEN MH. et al. Nonsurgical treatment options for Basal cell carcinoma. *J Skin Cancer* 2011:571734.

LIM E. et al. Surgery as primary treatment for limited disease small cell lung cancer: time to re-evaluate. 2008 **J Clin Oncol** 25. Abstract 7719

MAGRATH I. et al. The pathogenesis of Burkitt's lymphoma. 1990 *Adv Cancer Res*, 1990. 55: p. 133-270.

MANCUSO M. et al. Basal cell carcinoma and its development: insights from radiation induced tumors in Ptch1 deficient mice. *Cancer Res* 2004;64:934-41

MARCIL I. et al. Risk of developing a subsequent nonmelanoma skin cancer in patients with a history of nonmelanoma skin cancer: a critical review of the literature and meta-analysis. *Arch Dermatol.* 2000 Dec;136(12):1524-30

MEUWISSEN R. et al. Mouse models for human lung cancer. 2005 *Genes Dev* 19: 643-664

MICKE P. et al. Staging small cell lung cancer: Veterans Administration Lung Study Group versus International Association for the study of lung cancer - what limits limited disease? 2002 *Lung Cancer* 37: 271-276.

MORLEY SM. et al. Generation and characterization of epidermolysis bullosa simplex cell lines: scratch assays show faster migration with disruptive keratin mutations. 2003 *Br J Dermatol.* 149(1):46-58.

MURRE C. et al. Interactions between heterologous helix-loop-helix proteins generate complexes that bind specifically to a common DNA sequence. 1989. *Cell*, 58(3): p. 537- 44.

NAU M.M. et al., L-myc, a new myc-related gene amplified and expressed in human small cell lung cancer. 1985 *Nature*, 318(6041): p. 69-73.

NEGRONI A. et al. Decrease of proliferation rate and induction of differentiation by a MYCN antisense DNA oligomer in a human neuroblastoma cell line. *Cell Growth Differ*, 1991. 2(10): p. 511-8.

NEIL J.C. et al. The role of feline leukaemia virus in naturally occurring leukaemias. 1987 *Cancer Surv*, 6(1): p. 117-37.

NEILL G. W. et al. GIL1 repression of ERK activity correlates with colony formation and impaired migration in human epidermal keratinocytes. *Carcinogenesis* 2008. 29(4):738-46.

NELSON A.R. et al. Matrix metalloproteinases: Biologic activity and clinical implications. 2000 *J. Clin. Oncol.* 18: 1135–1149

NEMATI F. et al. Distinctive potentiating effects of cisplatin and/or ifosfamide combined with etoposide in human small cell lung carcinoma xenografts. 2000 *Clin Cancer Res*;6(5):2075-86

NESBIT C.E. et al. MYC oncogenes and human neoplastic disease. 1999 *Oncogene*, 18(19): p. 3004-16

NICUM SJ. et al. Topotecan for the treatment of small-cell lung cancer. 2007 *Expert Rev Anticancer Ther* 7: 795– 801

NIELSEN P.E. et al., Sequence-selective recognition of DNA by strand displacement with a thymine-substituted polyamide. *Science*, 1991. 254(5037): p. 1497-500.

NIELSEN P.E. et al. Peptide nucleic acids (PNAs): potential antisense and anti-gene agents. *Anticancer Drug Des*, 1993. 8(1): p. 53-63.

NIKLIŃSKA W. et al. Expression of vascular endothelial growth factor (VEGF) in non-small cell lung cancer (NSCLC): Association with p53 gene mutation and prognosis. 2001 *Lung Cancer* 34 Suppl 2: S59–S64.

NILSSON M. et al. Induction of basal cell carcinomas and trichoepitheliomas in mice overexpressing GLI-1. *Proc. Natl Acad. Sci. USA* 97, 3438–3443 (2000)

ODA K. A comprehensive pathway map of epidermal growth factor receptor signaling. 2005 *Mol Syst Biol.* 1(1):2005.0010.

OKAMOTO H. et al. Randomised phase III trial of carboplatin plus etoposide vs split doses of cisplatin plus etoposide in elderly or poor-risk patients with extensive disease small cell lung cancer: JCOG 9702. 2007 *Br J Cancer* 97: 162–169.

ONN A. et al. Development of an orthotopic model to study the biology and therapy of primary human lung cancer in nude mice. 2003 *Clin. Cancer Res.* 9: 5532–5539.

PAN J. et al. Mechanical stretch-induced serotonin release from pulmonary neuroendocrine cells: implication for lung development. 2006 *Am J Physiol Lung Cel Mol Physiol* ;290:185-193 2005.

PARK KS. et al. A crucial requirement for Hedgehog signaling in small cell lung cancer. *Nat Med.* 2011 Oct 9;17(11):1504-8

PAYNE G.S. et al., Multiple arrangements of viral DNA and an activated host oncogene in bursal lymphomas. 1982 *Nature*, 295(5846): p. 209-14.

PESSION A. et al. Targeted inhibition of NMYC by peptide nucleic acid in N-myc amplified human neuroblastoma cells: cell-cycle inhibition with induction of neuronal cell differentiation and apoptosis. *Int J Oncol*, 2004. 24(2): p. 265-72

PESSION A. et al. The MYCN oncogene as a specific and selective drug target for peripheral and central nervous system tumors. 2005 *Curr Cancer Drug Targets*. Jun;5(4):273-83.

PUGLISI M. et al. Treatment options for small cell lung cancer – do we have more choice? *British Journal of Cancer* (2010) 102, 629 – 638

RADY P. et al. p53 mutations in basal cell carcinomas. 1992 *Cancer Res*. 1;52(13):3804-6.

RAY A. et al. Peptide nucleic acid (PNA): its medical and biotechnical applications and promise for the future. *Faseb J*, 2000. 14(9): p. 1041-60

REGL G., NEILL G. W. et al. Human GLI2 and GLI1 are part of a positive feedback mechanism in Basal Cell Carcinoma. *Oncogene*. 21(36):5529-39

REISSMANN P.T. et al. Inactivation of the retinoblastoma susceptibility gene in non-small-cell lung cancer. 1993 The Lung Cancer Study Group. *Oncogene* 8: 1913–1919

RUIZ I ALTABA A. et al. Hedgehog-Gli signalling and the growth of the brain. 2002 *Nat Rev Neurosci*. 3(1):24-33

SADIKOT R. et al. Bioluminescence Imaging. *Proc Am Thorac Soc* 2005;2:537-540

SALDANHA G. Basal cell carcinoma: a dermatopathological and molecular biological update. 2003 *Br J Dermatol*. 148(2):195-202.

SANSONE R. et al., Age-dependent prognostic significance of N-myc amplification in neuroblastoma. The Italian experience. *Cancer Genet Cytogenet*, 1991. 54(2): p. 253-7

SARAN A. Basal cell carcinoma and the carcinogenic role of aberrant Hedgehog signaling. 2010 *Future Oncol*. 6(6):1003-14.

SCHMIDT M.L. et al., The biological effects of antisense N-myc expression in human neuroblastoma. *Cell Growth Differ*, 1994. 5(2): p. 171-8.

SCHNIDAR H. Epidermal growth factor receptor signaling synergizes with Hedgehog/GLI in oncogenic transformation via activation of the MEK/ERK/JUN pathway. 2009 *Cancer Res*. 69(4):1284-92.

SCHWAB M. et al. Amplified DNA with limited homology to myc cellular oncogene is shared by human neuroblastoma cell lines and a neuroblastoma tumour. 1983 *Nature*, 305(5931): p. 245-8.

SCHWAB M. et al. Chromosome localization in normal human cells and neuroblastomas of a gene related to c-myc. 1984 *Nature*, 308(5956): p. 288-91.

SCHWAB M. et al. Human N-myc gene contributes to neoplastic transformation of mammalian cells in culture. *Nature*, 1985. 316(6024): p. 160-2.

SCHWAB M. et al., Sustained expression of the human protooncogene MYCN rescues rat embryo cells from senescence. *Proc Natl Acad Sci U S A*, 1988. 85(24): p. 9585-9.

SEEP-LORENZINO et al. A peptidomimetic inhibitor of farnesyl-proteintransferase blocks the anchorage dependent and independent growth of human tumor cell lines. *Cancer Res*. 1995;55(22):5302-5309.

SHNEIDER B. et al. Phase II trial of imatinib maintenance therapy after irinotecan and cisplatin in patient with c-kit positive extensive stage small cell lung cancer (ES SCLC) [abstract 17089]. *J Clin Oncol*. 2006;24(18S)(suppl)

SIMON C. et al. Small-cell lung cancer. 2001 *Chest Surg Clin N Am* 11:165 -188

SMALL M.B. et al. Neoplastic transformation by the human gene N-myc. *Mol Cell Biol*, 1987. 7(5): p. 1638-45.

SMITH PK. et al. Measurement of protein using bicinchoninic acid. *Anal. Biochem.* 1985 150, 76–85.

SOCINSKI MA. et al. Duration of first-line chemotherapy in advanced non small-cell lung cancer: less is more in the era of effective subsequent therapies. 2007 *J Clin Oncol* 25: 5155–5157

SOLETI R. et al. Microparticles harboring Sonic Hedgehog promote angiogenesis through the upregulation of adhesion proteins and proangiogenic factors. *Carcinogenesis.* 30(4):580- 588.

SOLOMON D.L. et al., Distinct DNA binding preferences for the c-Myc/Max and Max/Max dimers. *Nucleic Acids Res*, 1993. 21(23): p. 5372-6.

SORDET O. et al. Apoptotic topoisomerase1-DNA complexes induced by oxygen radicals and mitochondrial dysfunction. *Cell Cycle.* 2004 Sep;3(9): 1095-7. Epub 2004 Sep 12. Review

SPIGEL DR. et al. Irinotecan, carboplatin and imatinib in untreated extensive stage small cell lung cancer: a phase II trial of the Minnie Pearl Cancer Research Network. *J thorac Oncol.* 2007;2(9):854-861

STANTON L.W. et al., Alternative processing of RNA transcribed from NMYC. *Mol Cell Biol*, 1987. 7(12): p. 4266-72

STECICA B. et al. Melanomas require HEDGEHOG-GLI signalling regulated by interactions between GLI1 and the RAS-MEK/AKT pathways. 2007 *Proc Natl Acad Sci USA.* 104, 5895–5900.

STRIEDER V. et al. Regulation of N-myc expression in development and disease. *Cancer Lett*, 2002. 180(2): p. 107-19.

SUN L. et al. Antisense peptide nucleic acids conjugated to somatostatin analogs and targeted at the n-myc oncogene display enhanced cytotoxicity to

human neuroblastoma IMR32 cells expressing somatostatin receptors. *Peptides*. 2002 Sep;23(9):1557-65.

SUNDSTROM S. et al. Cisplatin and etoposide regimen is superior to cyclophosphamide, epirubicin, and vincristine regimen in small-cell lung cancer: results from a randomized phase III trial with 5 years' follow-up. 2002 *J Clin Oncol* 20:4665– 4672

SVARD J. et al. Genetic elimination of Suppressor of fused reveals an essential repressor function in the mammalian Hedgehog signaling pathway. *Dev. Cell* 10, 187–197 (2006).

TAI KY. Axl promotes cell invasion by inducing MMP-9 activity through activation of NF-kappaB and Brg-1. 2008 *Oncogene*. 27(29):4044-55.

TAIPALE J. et al. Effects of oncogenic mutations in Smoothed and Patched can be reversed by cyclopamine. *Nature* 406, 1005–1009 (2000).

TANG JY. et al. Emerging Treatments and Signaling Pathway Inhibitors Semin *Cutan Med Surg*. 2011 Dec;30(4 Suppl):S14-8.

TANG JY. et al. Inhibiting the Hedgehog Pathway in Patients with the Basal-Cell Nevus Syndrome. *N Engl J Med*. 2012 Jun 7;366(23):2180-8.

TONELLI R. et al. Antigene peptide nucleic acid specifically inhibits MYCN expression in human neuroblastoma cells leading to cell growth inhibition and apoptosis. *Molecular Cancer Therapy*. 2005;4(5)

TSURUTANI J. et al. Inhibition of the phosphatidylinositol 3-kinase/Akt/mammalian target of rapamycin pathway but not the MEK/ERK pathway attenuates laminin mediated small cell lung cancer cellular and resistance to imatinib mesylate or chemotherapy. *Cancer Res* 2005;65(18):8423-8432.

VENNSTROM B. et al. Isolation and characterization of c-myc, a cellular homolog of the oncogene (v-myc) of avian myelocytomatosis virus strain 29.1982 *J Virol*, 42(3): p. 773- 9.

VAN HOFF DD. et al. Efficacy data of GDC-0449, a systemic Hedgehog (Hh) pathway antagonist, in a first-in-human, first-in-class, phase I study with locally advanced, multifocal or metastatic basal cell carcinoma patients. Proc. 99th Annu. Meeting Am. Assoc. Cancer Res. abstract LB-138 (2008).

VON HOFF DD. et al. Inhibition of the hedgehog pathway in advanced basal-cell carcinoma. 2009 *N Engl J Med*. 361(12):1164-72.

WAKAMATSU Y. et al. Regulation of the neural crest cell fate by N-myc: promotion of ventral migration and neuronal differentiation. *Development*, 1997. 124(10): p. 1953- 62.

WANG D. et al. Cellular processing of platinum anticancer drugs. *Nat Rev Drug Discov*. 2005 Apr;4(4):307-20. Review.

WEISS W.A. et al., Targeted expression of MYCN causes neuroblastoma in transgenic mice. *Embo J*, 1997. 16(11): p. 2985-95.

WETMORE C. et al. Loss of p53 but not ARF accelerates medulloblastoma in mice heterozygous for patched. *Cancer Res*. 61, 513–516 (2001).

WICKING C. The role of hedgehog signalling in tumorigenesis. 2001 *Cancer Lett*. 2001:173; 1–7.

WISTUBA II. et al. Molecular genetics of small cell lung carcinoma. *Semin Oncol*. 2001 Apr;28(2 Suppl 4):3-13.

YANCOPOULOS G.D. et al., N-myc can cooperate with ras to transform normal cells in culture. 1985. *Proc Natl Acad Sci U S A*, 82(16): p. 5455-9.

XIE J. et al. Activating Smoothed mutations in sporadic basal-cell carcinoma. *Nature* 391, 90–92 (1998).

ZHANG H. et al. Role of PTCH and p53 in Early- onset Basal Cell Carcinomas. *Am J Pathol.* 2001;158;381-85.

ZHANG H. et al. ErbB receptors: from oncogenes to targeted cancer therapies. 2007 *J Clin Invest.* Aug;117(8):2051-8.

ZOCHBAUER-MULLER S. et al. Molecular Pathogenesis of lung cancer. 2002 *Annu. Rev. Physiol* 64:681-708.